INVESTIGATING BACTERIAL OUTER MEMRANE POLYMERS AND BACTERIAL INTERACTIONS WITH ORGANIC MOLECULES USING ATOMIC FORCE MICROSCOPY

BY

ARZU ATABEK

A THESIS SUMITTED TO THE FACULTY OF

WORCESTER POLYTECHNIC INSTITUTE

IN PARTIAL FULFILLMENT OF THE REQUIREMENTS FOR THE

DEGREE OF MASTER OF SCIENCE

IN

CHEMICAL ENGINEERING

----
23 AUGUST, 2006

APPROVED:

TERRI A. CAMESANO, PH.D., MAJOR ADVISOR
ASSOCIATE PROFESSOR OF CHEMICAL ENGINEERING
WORCESTER POLYTECHNIC INSTITUTE

APPROVED:

DAVID DIBIASIO, PH.D., H.O.D.
ASSOCIATE PROFESSOR OF CHEMICAL ENGINEERING
WORCESTER POLYTECHNIC INSTITUTE

Contents

List of Tables

List of Figures

Acknowledgements

First, I would like to thank my advisor, Professor Terri A. Camesano, for her support, guidance, understanding, and for giving me this opportunity. You are a very special person. Thanks for everything.

Further, I would like to thank my coworkers in the lab, Dr. Ray Emerson, Laila Abu-lail, Yatao Liu, Paola Pinzon-Arango and Joshua Strauss for their help, valuable discussions and ideas.

Next, the Department of Chemical Engineering for providing me this opportunity, National Science Foundation grant, BES-0238627, for funding this project, also Professor David S. Adams and Dr. JoAnn Whitefleet-Smith, Professor Jochen Weiss and Thrandur Helgason, and Professor William G. McGimpsey for their help and valuable discussions.

I would also like to thank my friends, Ameesha Shetty, M. Engin Ayturk, M. Didem Ayturk, Dr. Caitlin A. Callaghan, Alpna Saini, Xiaoshu Dai, Mariana Jbantova, James Liu, Jean-Roland Pascault and Dr. Amparo M. Gallardo-Moreno.

Finally, I would like to thank my parents, Huri and Saffet Atabek, my sister, Zeynep Atabek, and Mert Turksel for supporting me throughout the past two year.

1- Introduction

The adhesion of bacteria to surfaces has been analyzed in terms of surface charge, surface energy, and the characteristics of polymers on bacteria, to understand the factors that control bacterial adhesion [12,13]. Even though some properties of bacteria such as hydrophobicity, DLVO calculations, and surface charge have been used to explain bacterial adhesion to a surface, a molecular level understanding of the initial bacterial adhesion process is still lacking [6,14]. Over the past few years, force measurement techniques such as atomic force microscopy (AFM) have made it possible to examine interactions between colloidal particles and surfaces [14,15]. Extrapolymeric substances (EPS) and lipopolysaccharides (LPS) are important for the study of bacterial adhesion and transport, as they exist on all Gram-negative bacteria, which include the majority of cells found in aquatic environments [6]. LPS also plays a role in cell interactions with different surfaces such as epithelial cells and medical implants. Irreversible bacterial adhesion occurs because of short-range molecular interactions like hydrogen, ionic, and covalent bonding [16], as well interactions involving extracellular structures including LPS, pili, and fimbriae [17]. Bacterial cell surface molecules contain a variety of functional groups, exhibit repulsive and attractive interactions with the surface, and mediate bacterial adhesion [18].

Pseudomonas aeruginosa has received a great deal of interest because it is responsible for a variety of chronic bacterial infections. *P. aeruginosa* is a Gram-negative and rod shaped opportunistic pathogen. There are many *Pseudomonas* strains with different LPS

structures [19]. They can easily be isolated from water or soil environments because they are able to colonize multiple environmental niches, using natural compounds as energy sources [20]. Infections caused by opportunistic pathogens can migrate to locations within the body and can easily contaminate medical implants because of the fragments of biofilms [21]. Some of the important diseases that are caused by *P. aeruginosa* are airway infections in cystic fibrosis patients and ulcerative bacterial keratitis in soft contact lens users [20]. Recently, researchers have focused on identifying the factors that initiate bacterial adhesion to tissues and biomedical implants, and increase antibiotic resistance. For example, blood contacting biomaterials such as catheters, and kidney dialyzers, trigger adsorption of numerous plasma proteins [22]. Plasma proteins such as serum albumin, fibrinogen, fibrin, and fibronection, which can competitively adsorb on biomaterials, and various type of polymers [22-26]. They prepare a vulnerable environment for bacterial adhesion. Many proteins have carbohydrate binding sites at their surface [27]. They play an important role in bacterial adhesion and recognition of pathogens [27]. Some proteins on the epithelial cells are found to be responsible for bacterial adhesion to the corneal epithelial cells [28]. Once the initial cell attachment occurs, the bacteria grow into a biofilm and can cause serious infections.

In the natural environment, the fate of many organic compounds and contaminants in groundwater can be influenced by the activity of bacteria attached to soil particles [29]. Better understanding of bacterial interactions with organic molecules is essential to develop an effective bioremediation approach for soils contaminated with organic compounds. Natural organic materials in soils can be classified in two groups:

unrecognizable polymeric compounds which are highly organized structures and called humic materials, and recognizable compounds such as sugars, proteins and organic acids which are originating from organisms [30]. Fabiano et al. reported that the proteins are the second most abundant material in the natural organic matter from the ancient port of Genoa [31]. Therefore, it is important to understand the role of proteins in bacterial adhesion. Reducing bacterial adhesion can increase the success of bioremediation of contaminated soils and aquifers [30,32].

AFM has been used to study interactions between bacteria and different surfaces such as biomaterials [11,14]. AFM is an advanced technique, which can be used to understand nanocale interactions of microbial cells with different surfaces such as protein coated materials, and to identify the role of attractive and repulsive forces between bacteria and surfaces. In the present study, the AFM was used to study the interactions between each of two *Pseudomonas aeruginosa* strains with proteins. Topographical images and force cycles of bacterial cells and proteins were analyzed. Bovine serum albumin (BSA) and concanavalin A (Con A) were the model proteins chosen to represent protein molecules that might affect bacterial adhesion. In addition, the role of LPS structure in bacterial adhesion was investigated.

2 - Literature Review

Adhesion of bacteria to different substrates such as soil particles, medical implants and human epithelial cells is important for many environmental and biomedical applications. In this chapter, factors that affect bacterial adhesion, biofilms, environmental and biomedical impacts of bacterial adhesion, and the importance of *P. aeruginosa* for different applications will be presented.

2.1 Bacterial Adhesion

Bacterial adhesion has been described as the balance of attractive and repulsive physicochemical interactions between bacteria and surfaces. The adhesive nature of bacteria is due to various outer membrane features such as pili, flagella, proteins, and lipopolysaccharides (LPSs) [6,12]. Adhesion of bacteria is governed not only by long range forces such as steric and electrostatic interactions, but also by short range forces such as van der Waals, acid-base, hydrogen bonding and biospecific interactions [2,33]. Bacterial adhesion and subsequent cell growth on a surface have important roles in a variety of systems including biomaterial development and bacterial delivery systems used for bioremediation [34,35]. Biofilms that develop from deposited cells can have important effects on the transport of some organic compounds and the quality of groundwater, and also make it hard to treat bacterial infections [15,29,36]. Reducing bacterial adhesion can increase the success of bioremediation of contaminated soils and

aquifers [30,32]. Alternatively, increasing the adhesion of bacteria can be used to limit the migration of pathogenic bacteria in groundwater aquifers [37].

Several interactions must be taken into account in studying bacterial adhesion events which depend on the bacterial cell, the substrate surface, and the solution environment [16,38]. Bacterial, environmental and solid surface properties such as roughness, solid surface chemical structure, ionic strength [39], hydrophobicity [40-42], and surface charge [43] govern the initial adhesion phase of bacteria to a surface and affect bacterial retention [32,33,37]. Interfacial interactions such as Lifshitz-van der Waals (LW) and Lewis acid-base (AB) interactions are considered important for the initial attachment of bacteria [2]. Lifshitz-van der Waals interactions are apolar whereas Lewis acid-base interactions are polar and comprise all electron-acceptor and electron donor interactions [44]. The apolar and polar components of the interfacial free energy are additive (Equation 2.1) [44].

$$\gamma_i = \gamma_i^{LW} + \gamma_i^{AB} \qquad 2.1$$

$$\gamma_i^{AB} = 2\sqrt{\gamma_i^+ \gamma_i^-} \qquad 2.2$$

where γ_i is total surface free energy of component i, γ_i^{LW} is Lifshitz - van der Waals energy component, γ_i^{AB} is Lewis acid - base energy component, and γ_i^+ and γ_i^- are the electron donor and acceptor components, respectively.

In 1804, Thomas Young developed an expression to describe the connection between adhesion and the surface tension of a solid (γ_S) and liquid (γ_L) by using the interfacial tension between solid and liquid (γ_{SL}) and the contact angle (θ) made by a drop of liquid L [44] (Equation 2.3). The Dupré equation (Equation 2.4) expresses the relation between the work of adhesion between a solid and a liquid.

$$\gamma_L . \cos\theta = \gamma_S - \gamma_{SL} \qquad\qquad 2.3$$

$$\Delta G_{SL} = \gamma_{SL} - \gamma_S - \gamma_L \qquad\qquad 2.4$$

Inserting the Dupré equation into the Young equation, and combining them with the expressions for apolar and polar interactions, a more precise expression, the Young-Dupré equation (Equation 2.5), can be obtained.

$$\gamma_L . (1 + \cos) = 2(\sqrt{\gamma_S^{LW} . \gamma_L^{LW}} + \sqrt{\gamma_S^+ . \gamma_L^-} + \sqrt{\gamma_S^- . \gamma_L^+}) \qquad\qquad 2.5$$

The contact angle values of three liquids with known surface tension components have to be determined in order to calculate the surface free energy components of bacterial cells deposited on a solid surface (Figure 2.1).
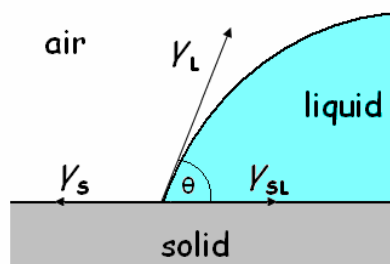
Figure 2.1 Contact angle and surface free energy components on a solid surface. Typically, the liquids used are water, diiodomethane and formamide (Adapted from [1]).

Electrostatic interactions are also important in influencing bacterial attachment. The electrostatic potential can be measured by electrokinetic models such as electrophoresis and zeta potential. Electrostatic forces are usually due to charged groups on the bacteria and substrate such as phosphates, lipopolysaccharides or carboxyls [45]. The electrostatic and van der Waals forces have been combined in the Derjaguin-Landau-Verwey-Overbeek (DLVO) theory of colloid stability, giving the interaction energy as a function of separation distance (Figure 2.2) [46]. Some researchers have helped explain the adhesion of bacteria to surfaces using the classical DLVO theory [13,16].

DLVO theory has been extended by the inclusion of acid-base interactions (XDLVO) which accounts for the hydrophobicity of the surfaces involved [44]. In addition to DLVO and XDLVO theories, bacterial properties such as water contact angles [2,47] and zeta potentials [43] are incorporated into these models about cell surface hydrophobicity, surface free energy and adhesive behavior. van Loosedrecht et al. showed that the percentage of bacteria attaching to a solid surface such as glass was related to both the hydrophobicity of the bacterium and its charge [1,48]. Nevertheless, they were not able to

use the model to explain bacterial adhesion based on bacterial surface polymers, which interfere with the other interactions [49]. Therefore, microbial cell surface characteristics and bacterial adhesion are studied by using different techniques such as transmission electron microscopy (TEM) [50] and atomic force microscopy (AFM) [38] to better understand microscopic scale interactions.
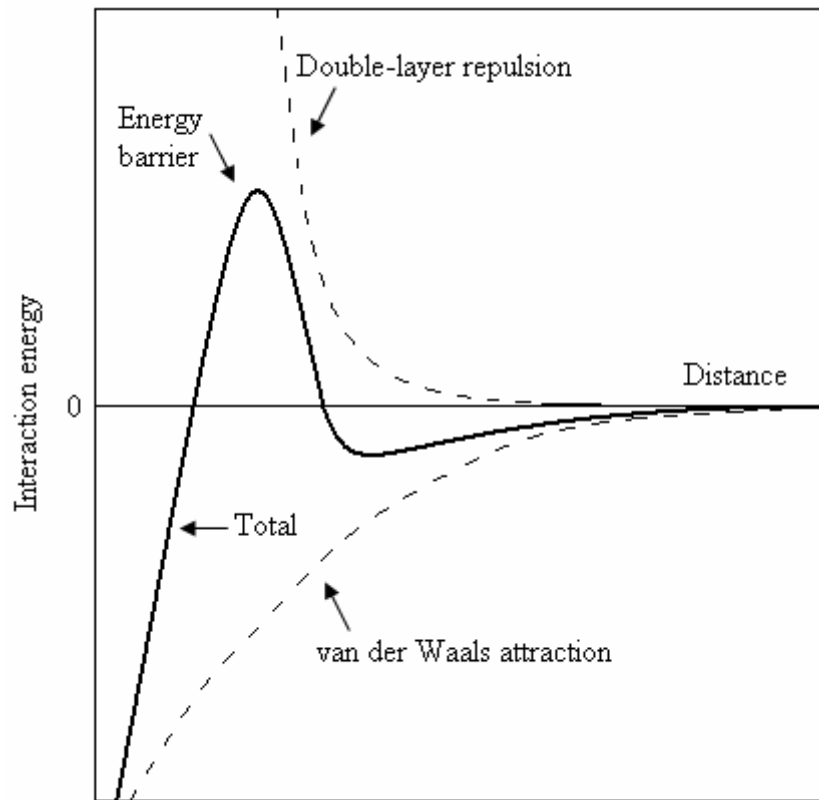
Figure 2.2 Schematic energy profiles of DLVO interactions (Adapted from [2]).

It has been postulated that an increase in adhesion may be explained by outer membrane polymer adsorption to surfaces [49]. Polymer repulsion has been known to arise from higher affinity of the bacterial polymers for the aqueous medium than solid surface or the rigidity of the polymers preventing the cell from reaching the DLVO energy maxima

[49]. However, polymers that are long enough to bridge the distance between cells and the surface may cause adhesion even when the cells do not experience short term attraction [49,51]. In addition, the DLVO and XDLVO models have not been tested in a single study using a wide range of bacteria and surfaces, and are often not sufficient to explain bacterial adhesion due to complexities of biological surfaces [16]. These complexities modify the DLVO forces and add steric, hydrophobic, and bridging effects [12,34]. Also, surface roughness may affect bacterial adhesion and is not typically included in DLVO theory [37,52]. Therefore, bacterial adhesion is a complicated process and of significant interest to researchers, since control of bacterial adhesion is important in many environmental, biomedical and industrial applications.

2.2 Biofilms

A biofilm is a population of cells growing on a surface surrounded with an extracellular polysaccharide matrix. They are mushroom-like structures with polysaccharide-enclosed microorganisms [53]. The study of biofilms has been of significant interest in the last decade [21]. Biofilm cells are more complex and have different characteristics compared to planktonic cells [54]. One of the most important features of biofilms is their resistance to antimicrobials and components of the host immune tissue [55]. Since biofilms offer an optimum surrounding for the cells, bacteria prefer being in a closely integrated community over a planktonic state.

2.2.1 Biofilm Development

Research has demonstrated that environmental conditions play an important role for biofilm development [56]. Biofilm development is a complex process and can be regulated by different factors such as cell surface structure, growth medium, oxygen limitation and substratum [36]. Planktonic bacteria initially form a reversible attachment on the surface within minutes. After the initial attachment, other chemical and physical interactions transform the reversible attachment to enduring irreversible adsorption.

After the irreversible attachment, bacteria produce extracellular polymeric substances (EPS) containing sugars, such as glucose and fructose, which create a protective environment and help the bacteria develop antibiotic resistance [54]. EPS is mainly composed of polysaccharides and can be considered as the primary component of biofilms. Because of its dynamic nature, it is hard to explain the structure and characterize the composition of the heterogeneous EPS matrix. Different strains use different mechanisms to develop mature biofilms. For example, *P. aeruginosa* isolated from cystic fibrosis patients produces large amounts of alginate which has been thought to be the major polysaccharide polymer in EPS for *P. aeruginosa* [21]. However, Wozniak et al. showed that alginate is not a major component of the extracellular matrix of *P. aeruginosa* PAO1 and PA14 biofilms [57]. Alginate is not important for biofilms of nonmucoid strains of *P. aeruginosa*, but alginate production influences biofilm architecture in mucoid strains of *P. aeruginosa* [57]. Furthermore, mannose and glucose were suggested to be the polysaccharides which are produced by biosynthetic genes in

this organism [54]. Acyl homoserine lactones (Acyl-HSLs) are also required for the maturation of *P. aeruginosa* biofilms [54]. EPS can link to metal ions and other macromolecules such as proteins, DNA and humic substances. EPS may also have an important role on antibiotic resistance by slowing down the diffusion of antibiotics into the biofilm [58,59]. The detachment of individual cells from a mature biofilm completes the developmental cycle and it may be defined as the transport of bacterial cells from the attached biofilm phase to the fluid phase.

2.2.2 Quorum Sensing

The structure of biofilms provides an ideal environment for gene transfer and cell-to-cell interactions. Cell-to-cell signaling, termed quorum sensing, has been shown to play an important role in virulence factors, biofilm differentiation, cell attachment and detachment [60]. Bacteria can monitor environmental conditions and organize the expression of different genes which specify extracellular products and virulence factors in a cell density-dependent behavior by using intercellular communication [61]. At high cellular densities, diffusible signal molecules can activate specific transcriptional regulators and reach concentrations required for activation of genes involved in biofilm differentiation. For example, the production of cell associated extracellular virulence factors, which are regulated by quorum sensing, is responsible for pathogenicity in the opportunistic pathogen *P. aeruginosa* [61]. Quorum sensing has also been shown to control expression of genes coding for extracellular enzymes, secondary metabolites such as the pigment pyocyanin and toxins [62,63]. As can be seen in Figure 2.3, *P.*

aeruginosa has two different signaling systems, *lasR-lasI* and *rhlR-rhlI*, for biofilm

formation [54,61]. The *las* cell-to-cell signaling system is positively controlled by Vfr, a

cyclic AMP receptor protein (CRP), which is required for the transcription of *lasR* [3,64].
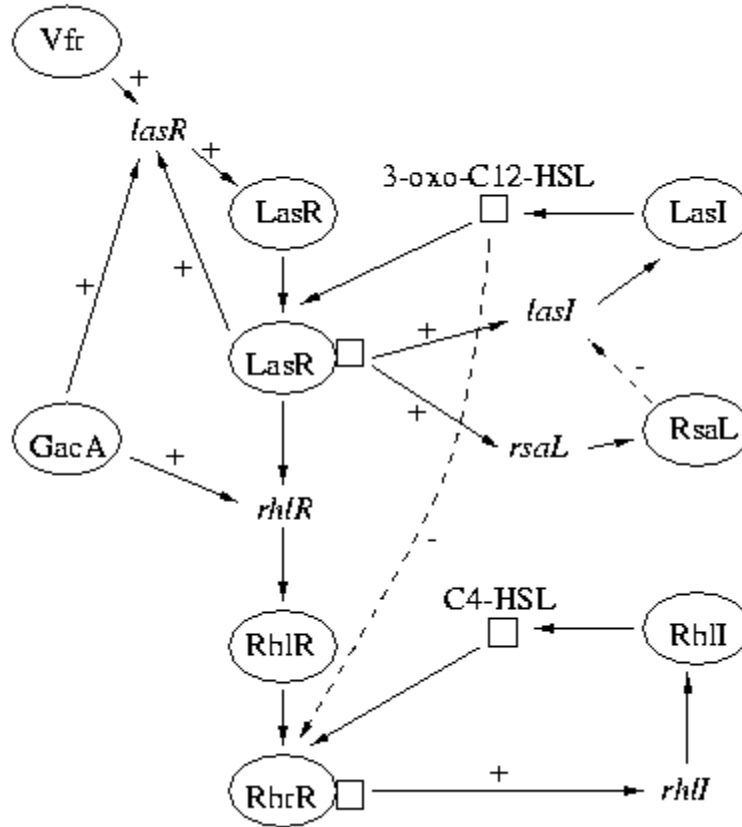
Figure 2.3 Quorum sensing in *P. aeruginosa* [3].

In the *lasRI* system, biosynthesis of N-(3-oxododecanoyl)-L-homoserine lactone

(OdDHL) is catalyzed by LasI synthase, and LasR-OdDHL complex controls the

production of virulence factors such as exotoxin A, elastases, hydrogen cyanide and

induces the development of an autoinduction loop [61]. In the global regulatory network,

the quorum sensing mechanism is regulated by LasR and RhlR. The *las* system is

dominant in the quorum sensing hierarchy. The *rhlRI* system is the secondary

autoinducer system which also develops the expression of extracellular products. Blue-green pigment pyocyanin production is induced by the *rhl* system [62]. Recently, it was revealed that an alternative sigma factor, σ^{54} (*rpoN*), is important for several models such as infections in burn victims and cystic fibrosis cases [61]. The *rpoN* function is required for expression of pili and flagella, and the virulence of *P. aeruginosa* is reduced in *rpoN* mutants [54]. Other mutants unable to produce both signals were able to produce a biofilm, but their biofilms were much thinner compared to wild type, and the typical biofilm architecture was lacking (Figure 2.4) [4]. However, addition of homoserine lactones to the media of mutant biofilms resulted in biofilms similar to the wild type with respect to structure and thickness [54]. Therefore, the quorum sensing mechanism has important roles on behavior bacteria and biofilm formation. A better understanding of regulatory systems could help to identify virulence factors and provide information for vaccine and antibiotic development [65].
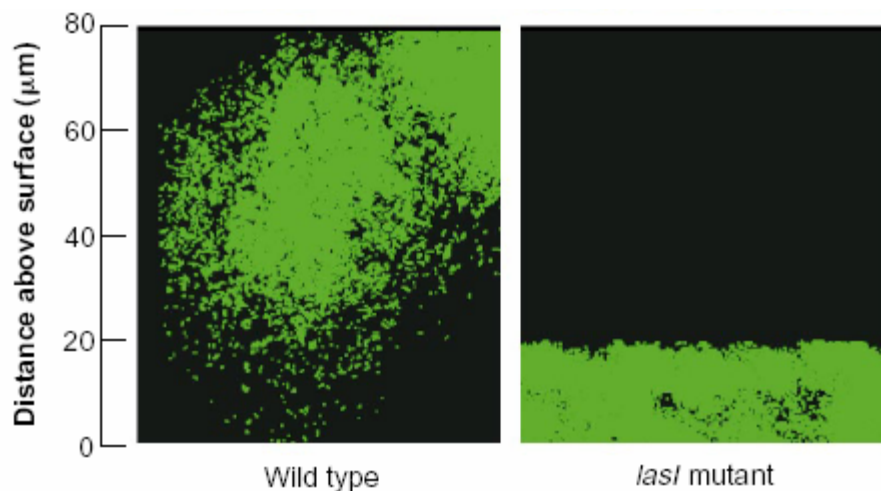
Figure 2.4 Epifluorescence and scanning confocal photomicrographs of the WT and the *lasI* mutant *P. aeruginosa* biofilms containing the GFP expression vector pMRP9-1 (Taken from [4]).

2.3 Importance of *Pseudomonas aeruginosa* Adhesion in Biomedical and Environmental Applications

Better understanding of *P. aeruginosa* adhesion can be useful for different biomedical and environmental applications. For example, a variety of chronic bacterial infections are caused by *P. aeruginosa* and new ways to eradicate these infections are being investigated. This organism can also be used as an effective isolate in biodegradation of petroleum hydrocarbons [66].

2.3.1 Biomedical Infections

Pseudomonas aeruginosa has received a great deal of interest because it is responsible for a variety of chronic bacterial infections. Infections caused by opportunistic pathogens can migrate to locations within the body and can easily contaminate medical implants because of the fragments of biofilms [21]. Recently, researchers have focused on identifying the factors that initiate bacterial adhesion to tissues and biomedical implants, and increase antibiotic resistance. Some of the important diseases that are caused by *P. aeruginosa* are airway infections in cystic fibrosis patients and ulcerative bacterial keratitis in soft contact lens users [20].

2.3.1.1 Lung Infections in Cystic Fibrosis

Cystic fibrosis (CF) is a genetic disease, an autosomal recessive disorder, which causes respiratory failure [67]. A defective gene causes the mutation of the cyclic AMP regulated chloride ion channel protein known as the cystic fibrosis transmembrane conductance regulator (CFTR) [20]. This mutation causes the human body to produce thick, dehydrated and sticky mucus that clogs the lungs and leads to life-threatening lung infections [67]. There are also other abnormal protein secretion and accumulation in CF epithelia [67]. CF patients' lungs show a particular susceptibility to infections with the common opportunistic bacterium *P. aeruginosa*. CF infections are chronic and extremely hard to treat with antibiotics [68]. *P. aeruginosa* present in CF sputum produces acyl-HSL signals in fractions similar to those produced by laboratory biofilms [21,69]. The bacterial phenotype that is isolated from CF infections is LPS-rough and highly mucoid [70]. Mucoid layer in CF was shown to be due to the overproduction of alginate [71]. One hypothesis is that oxygen stress in CF airways is very low and *P. aeruginosa* relies on anaerobic metabolism to grow as a biofilm [21]. According to this hypothesis, *P. aeruginosa* grows on mucous plugs in the lung and alginate production is induced in this environment. Recent studies suggest that the CFTR protein may influence *P. aeruginosa* lung infection directly through its role as an epithelial cell receptor for this organism [20].

2.3.1.2 Bacterial Keratitis

Bacterial keratitis is an ocular infection which is an inflammatory response of the cornea to bacterial infection and requires appropriate treatment to limit corneal morbidity and vision loss [20,72]. The number of people that experience ulcerative keratitis is estimated to be 12,000 to 15,000 patients per year in the United States [73]. *Staphylococuccus* species and *Pseudomonas aeruginosa* are responsible for bacterial keratitis in soft contact lens wear [72]. Disposable contact lens wear is the most common risk factor for bacterial keratitis although there are other reasons such as blepharitis (chronic inflammation of the eyelids), dry eye syndrome and corneal surgery [72].

Normally the tear film, lids and an intact corneal epithelium provide an effective barrier against most infections. *P. aeruginosa* do not adhere to undamaged cornea [33]. Extended contact lens wear and adherence of the microorganisms to the lens serve as a risk factor for ulcerative bacterial keratitis because it has a direct effect on the pre-corneal tear film and epithelial surface [20,73]. Pathogenicity is directly related to the ability of the organism to adhere to the edge of the epithelial defect and initiate infection. Some corneal epithelial glycoproteins exhibit receptor activity for *P. aeruginosa* binding [74]. The factors such as pili, flagella, LPS and glycocalyx facilitate adherence and biofilm formation that resist phagocytosis [20,73,75]. *Pseudomonas* biofilms produce exotoxin A which inhibits cellular protein synthesis and a corneal destroying proteoglyanase [75]. Particularly, proteases are also thought to be responsible for many features of the pathogenesis of *Pseudomonas* in the eye [20]. The amount of visual loss produced by

16

microbial keratitis is directly related to the extent of inflammatory cell infiltration, cell death, and damage to the endothelium [73]. Even though bacterial resistance remains a problem, fluoroquinolones are found to be an effective antibiotic treatment in bacterial keratitis, providing a broad spectrum of antibacterial activity and good tissue penetration [72]. Surface properties of the contact lenses [76] and lens care solutions [77] can also be improved to prevent bacterial contact with the corneal epithelial cells.

2.3.2 Environmental Impact: Bioremediation

Bioremediation can be defined as a process which requires the inoculation of a contaminated environment with a specific microorganism to remove contaminants from polluted soil or groundwater by using the degradative capacity of bacteria [30]. Microorganisms can degrade contaminants into nontoxic compounds. They already exist naturally in the environment, so bioremediation is a natural degradation which leads to harmless removal of hazardous substances with the advantage of low environmental impact [78]. Undesirable substances such as oil spills, petroleum hydrocarbons [66], pesticides, phenolic [79], and chlorinated and nitroaromatic compounds [80] can be degraded by specific bacterial strains. For example, *Pseudomonas aeruginosa* is an effective isolate in biodegradation of petroleum hydrocarbons such as phenolic compounds [79], benzene, toluene [66], bioreduction of hexavalent chromium [81,82], and decolorizing crystal violet, which is a biohazardous substance and usually comes from textile and dye industrial wastes [83]. *P. aeruginosa* strains are also active

17

denitrifiers and produce biosurfactants (rhamnolipids) which are advantageous for bioremediation, as they solubilize and mobilize hydrocarbons [84].

Physical and chemical characteristics of soil have important impacts on bioremediation. Soil particles form aggregates with organic and inorganic materials [30]. Inorganic soil compounds are usually crystalline materials in the form of layered silicates. Natural organic materials in soils can be classified in two groups: unrecognizable polymeric compounds which are highly organized structures and called humic materials, and recognizable compounds such as sugars, proteins and organic acids which are originating from organisms [30]. Large amounts of organic materials are known to accumulate in areas where the water exchange is limited. Fabiano et al. analyzed biochemical composition of the organic matter in the natural sediments of the Ancient Port of Genoa and found that carbohydrates were the first and proteins were the second dominant components of the organic materials [31]. Differences in soil properties change reactions between the soil and the contaminant, and the soil and microorganisms. Transport of contaminants and bacteria can be facilitated by organic matter or humic substances, so the biochemical composition of organic substrates and the interactions with the microorganisms during bioremediation can provide useful information about the pathways for recovering an organic matter contaminated site [31,32]. It is also important to understand the influence of soil properties on microbial survival and activity [30]. Therefore, the role of organic and inorganic materials on bacterial adhesion and transport is crucial to understand because the efficiency of bioremediation may differ from one location to another depending on the soil characteristics.

2.4 Specific Molecules Responsible for *P. aeruginosa* Adhesion and Pathogenicity

Pseudomonas aeruginosa is a Gram-negative and rod shaped opportunistic pathogen. It can easily be isolated from water or soil environments because it is able to colonize multiple environmental niches by using natural compounds as energy sources [20]. *P. aeruginosa* has virulence genes which allow the organism to proliferate in response to given environmental demands. In addition, some *P. aeruginosa* strains produce a blue-green pigment, pyocyanin, which is a virulence factor in this organism [85,86]. *Pseudomonas* species are aerobic but they can also adapt to anaerobic conditions. They are motile, express pili, flagella and lipopolysaccharides (LPS), and extracellular polymeric substances (EPS) [33].

P. aeruginosa has a large genome size and genetic complexity, which help it to adapt to different ecological niches, transport, and grow on organic substances [87]. Moreover, it has the greatest ratio of genes devoted to command and control systems such as transcriptional regulators which modulate biochemical abilities of this organism in changing environmental conditions and contribute to its resistance to antibiotics [87]. Its genome contains a large family of genes which encodes outer membrane proteins (OMPs) [87]. OMPs are important in release of extracellular virulence factors, transport of antibiotics, and cell surface related properties such as adhesion and motility [87]. Development of new vaccines and antimicrobial agents can be achieved by the identification of OMP families. Because of its genetic properties, *P. aeruginosa* can adapt to environmental stresses such as lack of nutrients, phagocytes [33], temperature [88,89]

19

and oxygen limitation [40]. Different adhesins and heterogeneity in its surface structure enable the bacterium to attach to various surfaces and avoid immune system components of the host [33].

P. aeruginosa strains are effective isolates in biodegradation of hazardous contaminants in the environment, so they can be used for bioremediation of contaminated soils or wastewater [79,84]. On the other hand, they cause serious infections, especially in immunocompromised patients, such as bacteremia in burn victims, bacterial keratitis in soft contact lens users and chronic lung infections in cystic fibrosis patiens [20,33]. These bacteria find receptors on epithelial cells and use different ligands to attach to various substrates [33]. For example, *P. aeruginosa* associated with chronic lung infections were found to have no pili, rough LPS and more alginate (a heterogeneous exopolysaccharide composed of D-mannuronic acid and L-guluronic acid) production [33,90].

2.4.1 Lipopolysaccharides (LPS)

Roughly 3.5 million LPS molecules are present on the outer membrane of Gram-negative bacteria with significant variations in coverage thickness and local distribution [6]. The exact size and composition of LPS is strain-specific. The characteristics of LPS such as the three-dimensional structure and the number of repeating units, which may govern its overall flexibility, contribute to bacterial adhesion [12]. LPS is also related to the patogenicity of bacterial strains. For example, the injection of purified LPS into

experimental animals causes a wide spectrum of nonspecific pathophysiological reactions related to inflammation [91].

LPS contains three components: Lipid A, a core polysaccharide, and a large O-antigen (Figure 2.5) [92]. Lipid A molecules extend from the bacterial membrane and link to Kdo of the core oligosaccharides. The most common lipid A consists of fatty acids which typically have 10-16 carbon atoms although longer chains exist, for example, C_{18} fatty acids in *Helicobacter pylori* lipid A, and C_{18} and C_{21} in *Chlamudia trachomatis* [5]. Unsaturated fatty acids rarely present in lipid A but there are some examples such as in *Rhodopsudomonas sphaeroides* species. Lipid A portion of LPS is less heterogeneous than the polysaccharide region. The 3-D structures of lipid A depend on the presence of different fatty acids.
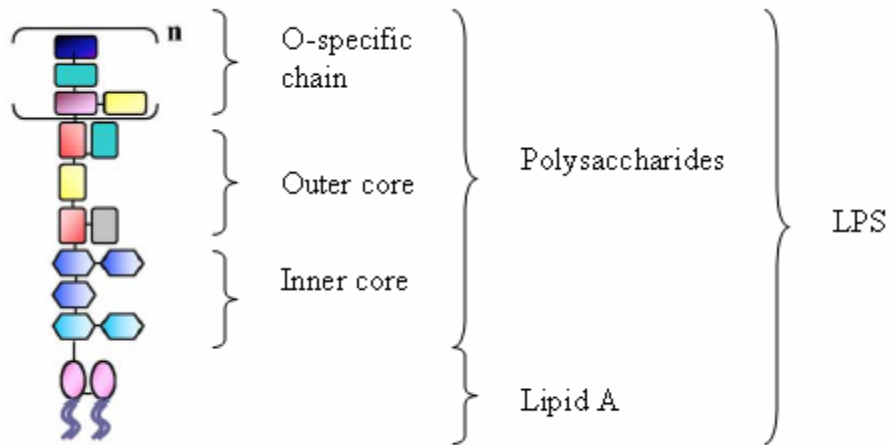
Figure 2.5 Schemetic of LPS structure of Gram-negative bacteria (Adapted from [5]).

The core structure of LPS can be divided into two parts: the inner and outer core. The inner core usually has heptose residues while the outer core generally consists of an

21

oligosaccharide (up to six sugar units) [5]. The outermost portion of the LPS linked to the core polysaccharide region is referred to as the O-specific chains which are antigenic and form the basis for serotype classification. If the bacteria do not have O-specific chains, they are considered rough-type strains. Only smooth-type Gram-negative bacteria have O-antigens. O-specific chains may be necessary for the initial attachment to hydrophilic surfaces [40] and can protect the bacteria from numerous antibiotics [5]. On the other hand, negatively charged O-antigens can bind to specific polycationic antibiotics and increase antibiotic permeability [93,94]. Besides the importance of O-antigens, it also proposed that the negatively charged phosphoryl groups in the core-Lipid A region of LPS are the most important sites involved in metal binding by *P. aeruginosa* [50].

The physiological activities of endotoxins are mediated mainly by the Lipid A component of LPS [91]. O-antigen of LPS may also act as a determinant of virulence in Gram-negative bacteria. The O polysaccharide is hydrophilic and may allow diffusion or delivery of the toxic lipid in the hydrophilic (in vivo) environment. The O polysaccharide may supply a bacterium with its specific ligands for colonization which is essential for expression of virulence [91].

2.4.2 LPS structure of *P. aeruginosa*

P. aeruginosa has a complicated LPS structure. General LPS structure has lipid A, core oligosaccharides and O-antigens. At the nanoscale, LPS molecules are constantly in motion and O-side chains are flexing back and forth driven entirely by entropy [19].

Their rapid motion can affect the strength of their interactions with surfaces. The LPS of *P. aeruginosa* is anionic at physiological pH because of exposed phosphoryl and carboxyl groups [19]. There are many *Pseudomonas* strains with different LPS structures. For example, a genetically well characterized [33,87] serotype O5 wild-type strain is called *P. aeruginosa* PAO1. It is a smooth strain because it expresses two O-antigens, A-band and B-band antigens ($A^+ B^+$). The rough strains such as rd7513 ($A^- B^-$) do not have O-antigens on their surface and the strains with one repeating O-antigen unit are semi-rough, such as AK1401 ($A^+ B^-$). Strain AK1401 and rd7513 are mutants of smooth strain PAO1 [95,96].

It was shown by NMR and chemical analysis that the core region of the LPS from wild type strain PAO1 and mutant strain AK1401 were identical [97]. The core oligosaccharides are linked to lipid A and consist of D-glucose, L-α-D-heptose, and 2-keto-3-deoxyoctonate (KDO) [98]. Carboxyl and phosphoryl groups in the core region are important charge sites. They are available for salt-bridging and contribute strongly to outer membrane integrity [98]. Rivera et al. showed that the components of O-antigen, A- and B-bands, from PAO1 strain are antigenically and chemically distinct (Figure 2.6) [99,100]. Less than 8% of the LPS molecules had long O-antigens in strain PAO1, indicating that a significant amount of the LPS must be A-bands [99].

A-band, common antigen, is expressed by most of the *P. aeruginosa* strains and is comprised of 10 to 20 repeating α-D-rhamnose units [98,101]. A-bands show a lack of reactive amino sugars and phosphate but contain mainly repeating trisaccharide of α-D-

rhamnose, with small amounts of 3-O-methylrhamnose, ribose, mannose, glucose and 3-O-methylhexose [102], and also some heptose, sulfate groups and 2-keto-3-deoxyoctulosonic acid [99]. The lack of phosphate constituents in A-band makes the molecules less negatively charged than the B-band fractions which are high in phosphate groups [99].
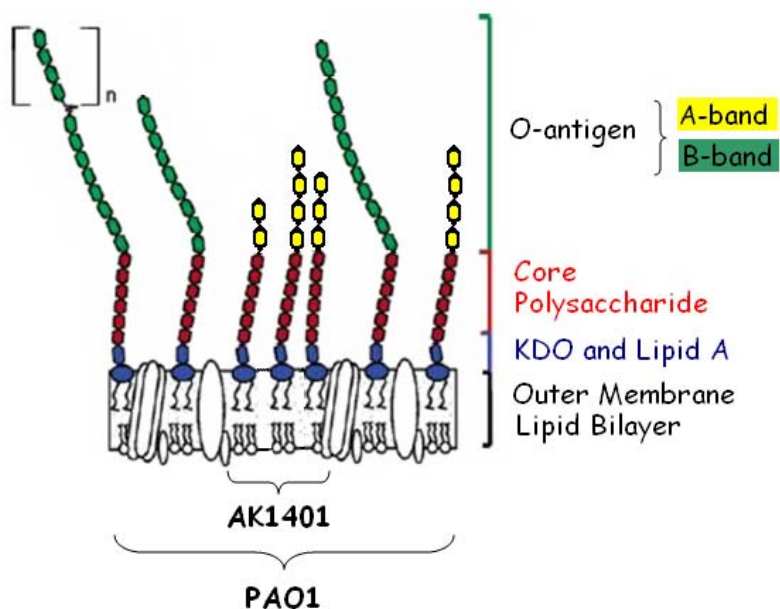
Figure 2.6 Schematic of outer membrane structure of *P. aeruginosa* strains (Adapted from [6]).

B-band is the serotype specific antigen composed of di- to pentasaccharide repeats [101]. B-bands contain much longer polysaccharides than A-bands, and they are high in phosphate content and amino sugars but low in sulfate and rhamnose [100]. Lam et al. showed that strain PAO1 expresses 30 to 50 O-repeating units, with an approximate length of 39 to 65 nm, but they were not able to determine if the LPS polymers were coiled or fully extended [103]. Moreover, freeze substitution has shown that B-band LPS can extend up to 40 nm from the outer membrane [103]. The O-antigen of PAO1 is

composed of residues of amino derivatives of uronic acid with a trisaccharide repeating unit of the β-D-manno configuration and N-acetyl-D-fucosamine [103,104]. The longer B-band LPS extend from the surface and constitute the main antigenic structure exposed on the cell for the strains with both A- and B-bands [100]. Moreover, the shorter A-bands may be covered by the B-band polysaccharides [100]. $A^+ B^+$ LPS bilayers imaged by AFM were typically 500 nm or more across and 10 nm in height [105].

LPS-rough *Pseudomonas* strains are mucoid and express neutral polysaccharides. LPS-rough type phenotypes produce mucoid exopolysaccharides such as alginate [40,90]. Protective efficiency of antibodies to neutral polysaccharides against mucoid strains is lacking [90]. The LPS of strain AK1401, which expresses only neutral A-band antigen, had a lower molecular weight than that of the LPS of strain PAO1 [103]. Hatano et al. suggested that the largest polymers of neutral polysaccharides would be <6 kDa, whereas smooth type O-side chains range up to 30 kDa and project out from the cell surface further than the neutral ones [90].

Kropinski et al. showed that temperature plays a significant role in the chemistry of the outer and inner membranes of *P. aeruginosa* PAO1 [88]. Cells grown at lower temperatures (15 to 45°C) expressed more long chain LPS molecules [88]. In addition, Makin and Beveridge showed that cells cultured at 45°C did not express any B-band LPS on the outer membrane surface [89]. *P. aeruginosa* PAO1 also produces membrane vesicles that are easily removed from cell surface and only contain B-band LPS, at

temperatures of less than 45°C. Sabra et al. showed that the expression of B-band LPS under oxygen-limited conditions is lower than that of oxidative conditions [40].

B-band LPS plays an important role for initial attachment to hydrophilic surfaces. *P. aeruginosa* PAO1 grown at high O_2 levels has increased capacity to adhere to hydrophilic surfaces because of increased B-band production [40]. Moreover, increased formation of MVs is related to enhanced formation of B-band LPS under oxidative conditions. Therefore, the expression of B-band LPS may be reduced because of microaerobic conditions in the biofilms formed in chronic lung infections.

P. aeruginosa is able to pool B-band LPS into small regions on its outer membrane, forms blebs and releases membranous structures which are called membrane vesicles (MVs) [106]. MVs possess OMPs, LPS, phospholipids and periplasmic constituents and they can be 50 to 250 nm in diameter [19]. Stoica et al. imaged these MVs using contact mode AFM and concluded that the MV patches ranged in diameter from 25 nm to several hundred nanometers [105]. Their measurements showed that considerable amounts of periplasmic material are trapped inside MVs [105]. MVs could play important roles in the delivery of virulence factors. They are strongly antigenic structures and can be considered as new vaccine candidates [19]. All of the MVs of the different LPS types (A^+ B^+, A^+B^-, A^-B^+ and A^-B^-) are spherical and contain internal periplasmic material [98]. A and B band LPS are detected in PAO1 MVs whereas AK1401 MVs only had A band LPS [98]. It has also been suggested that since rough mutants are leaky because they have less saccharide molecules and secrete more mucoid substances, they may have a higher

amount of protein, not only because of MVs, but also from cellular proteins that have leaked from cells in the EPS [98].

The distribution of A- band and B-band on the cell surface is still not known clearly, as to whether the LPS types are randomly distributed or distinct domains have A- or B-band [107]. Makin and Beveridge have shown that the surface hydrophobicity of *P. aeruginosa* strains is as follows: $A^+ B^- > A^- B^- > A^+ B^+ > A^- B^+$ [107]. Even though it is not fully understood, the cells lacking B-band LPS demonstrated the highest surface electronegativity when a positively charged resin was used for electrostatic interaction chromatography [107]. This result suggests that the main surface charge determining groups are located in the core region of LPS molecule [107]. Langley and Beveridge also proposed that the negatively charged phosphoryl groups in the core-Lipid A region of LPS are the most important sites involved in metal binding by *P. aeruginosa* [50].

2.4.3 Role of *Pseudomonas* LPS in Bacterial Infections

In a group of 250 clinical isolates of *Pseudomonas aeruginosa* from cystic fibrosis patients, 68% had A-band and did not express B-band O-antigen [108]. Serotypeable O-antigen was replaced with A-band as major antigen during the infection [108]. Knirel et al. investigated the LPS of a rough cystic fibrosis isolate and found that the LPS structure had 3-deoxy-D-manno-actulosonic acid and L-glycero-D-manno-heptose [109]. They proposed that the clinical rough strain has the same core-lipid A backbone of the smooth strain *P. aeruginosa* PAO1, and the core oligosaccharide of LPS is the bacterial ligand

for cystic fibrosis transmembrane regulator (CFTR) which is not functional in CF patients [99,109]. Strain AK1401 and clinical CF strains have similar LPS structures, considering O-antigens [99,109]. The lack of B-band LPS in clinical CF isolates can be explained with the effect of oxygen-limited conditions [40].

Polycationic antibiotics displace the cations such as Mg^{2+} and Ca^{2+} which can bind or cross-bridge LPS molecules [93,94]. Lam et al. have shown that anionic groups of B-band LPS are natural reservoirs for metal ions such as Ca^{2+} and Mg^{2+} [103]. They also showed that strains expressing both A- and B-band LPS bound more gentamicin than the LPS defective strains [93]. Cells with only A-band also interacted with gentamicin but possessed lower affinity [93]. This indicates that the accessibility of ionic binding sites is different between the two types of LPS molecules [93] since uptake of aminoglycoside antibiotics such as gentamicin into *P. aeruginosa* involves ionic interactions [110]. It might also explain the resistance that is caused by poor permeability of antibiotics among clinical strains [93]. Even though A-band is less negatively charged compared to B-band, the charge of core oligosaccharides or lipid A portion in AK1401 may be substituting the charge of B-band LPS since they are closer to the surface in AK1401 than that of PAO1 [93]. Bryan et al. [110] proposed that the decreased number of repeating side chain sugars results in reduced overall LPS length, increased aminoglycoside resistance and makes the bacterium less hydrophobic. A-band is present in many standard serotype and clinical strains so it appears to be a common *Pseudomonas* antigen. Vaccines used against pathogenic Gram-negative bacteria consist of a mixture of O-antigens from different

serotypes of the same species [102]. Therefore, A-band polysaccharide can be considered as a potential vaccine candidate for CF infections [108].

2.5 Proteins

Proteins are organic compounds that consist of 20 common amino acids joined by peptide bonds [111]. All amino acids have a central carbon atom to which a hydrogen atom, an amino group (NH_2) and a carboxyl group (COOH) are attached in common (Figure 2.7) [112]. Sequences of amino acids fold to generate compact domains (three dimensional structures; secondary, tertiary and quaternary) from linear chains (primary structure) [112]. Electrostatic interactions, van der Waals forces, hydrogen bonds and hydrophobic interactions play an important role in defining and stabilizing the three dimensional structure and adsorption of protein molecules [111,113].
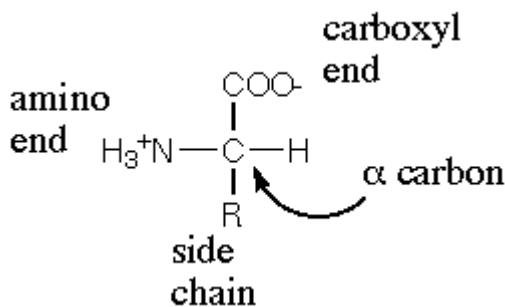
Figure 2.7 General structure of amino acids [7].

Material surfaces adsorb proteins or other organic molecules when exposed to a fluid environment. For example, blood contains hundreds of proteins such as serum albumin, fibrinogen, fibrin, and fibronection, which can competitively adsorb on biomaterials [22-26]. Blood contacting biomaterials such as catheters, and kidney dialyzers trigger

adsorption of numerous plasma proteins [22]. Plasma proteins adsorb on various type of polymers [22]. They prepare a vulnerable environment for bacterial adhesion. S*taphylococcus aureus* attachment to catheters can be given as an example [25].

Many proteins have carbohydrate binding sites at their surface [27]. They play an important role in bacterial adhesion and recognition of pathogens by specific surface carbohydrates of the immune system [27]. Some proteins on the epithelial cells are found to be responsible for bacterial adhesion to the corneal epithelial cells. One of the LPS binding proteins is galectin-3, which is critical for *P. aeruginosa* LPS binding to the eye [28]. Once the initial cell attachment occurs, the bacteria grow into a biofilm and can cause serious infections.

In addition, proteins are one group of recognizable organic matter from the environment. For example, Fabiano et al. reported that the proteins are the second most abundant material in the natural organic matter from the ancient port of Genoa [31]. Proteins play an important role in bacterial transport in natural environments. Therefore, it is important to understand the role of proteins in bacterial adhesion. In the present study, bovine serum albumin (BSA) and concanavalin A (Con A) are the model proteins chosen to represent protein molecules that might affect bacterial adhesion.

2.5.1 Bovine Serum Albumin

Serum albumin is one of the most widely studied and most abundant plasma proteins with a typical concentration of 50 mg·mL^{-1} in plasma [8,113]. The physico-chemical

characteristics of serum albumin are well characterized [24]. The natural environment of serum proteins contains much sodium chloride (NaCl), so it is preferred to use a buffer solution with NaCl when studying BSA in the laboratory.

Bovine serum albumin (BSA) is a globular protein with the shape of a prolate spheroid of dimensions 4 x 4 x 14 nm (Figure 2.8) [114,115]. BSA contains 583 amino acid residues [114]. It can represent the proteins in the human body and environment. It is made up of three homologous domains (I, II, III) which are divided into nine loops by 17 disulfide bonds [8]. The disulfide bonds in albumin are protected at physiological pH from reducing agents [8]. The three domains with varying charge density may affect the way BSA adsorbs to surfaces [116]. It can bind reversibly a wide variety of ligands. BSA is the principle carrier of fatty acids and serves as a transport protein, so it has a high affinity for fatty acids [8,117]. In addition, it is the major soluble protein found in the human cornea [118].
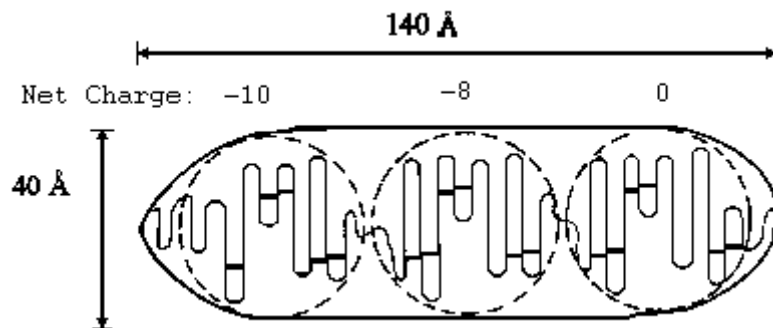
Figure 2.8 2D structure of bovine serum albumin [8].

As can be seen in Figure 2.9, proteins can be immobilized on different surfaces in many different ways but conformation is crucial to sustain their active conformation [113]. The

31

immobilization of BSA onto a glass network did not cause any detectable loss of its bioactivity [113]. Various orientations of BSA on glass or self-assembled monolayer (SAM) surfaces are present because physical interactions and chemical binding are not specific [115]. The reactivity of the protein depends on the orientation and Wadu-Mesthride et al. showed that only 60% of BSA molecules could react with the monoclonal anti-BSA due to different orientations present on the surface.
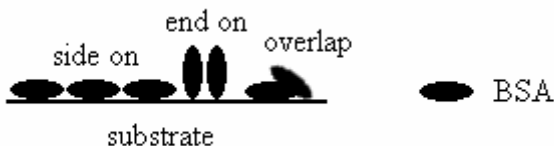
Figure 2.9 Schematic figure showing BSA adsorption
on substrates (Adapted from [9]).

BSA is similar to the albumins from other species, with an average molecular weight of ~ 66 kDa [8,18]. For example, the sequences of BSA and human serum albumin (HSA) are about 80% homologous, their molecular weights differ by less than 1%, and many other properties such as isoelectric points are identical [117,119,120]. HSA is also a globular protein and contains 585 amino acids, with a 65 kDa molecular weight [23,24]. It is the most abundant protein in the circulatory system and makes up about 60% of the total protein in blood serum [23,121,122]. HSA is also composed of three structurally similar globular domains [122]. Its principle function is to transport fatty acids [121] and it has two to three dominant long-chain fatty acid binding sites [122]. Therefore, BSA can be a good representative of human proteins.

2.5.2 Concanavalin A

Concanavalin A (Con A) is one of the important proteins from the lectin family. Lectins are proteins that specifically bind to sugar residues [123]. They are useful probes for studying carbohydrates of cell surfaces [27]. Lectins have been used to demonstrate the presence of particular sugar residues on the surface of bacterial cells [123]. Lectins form cross-links between polysaccharide or glycoprotein molecules in solution. These cross-linking reactions of lectins are inhibited by the sugar ligands for which the lectins are specific [124].

Con A is a plant lectin with a molecular weight of 102 kDa [125,126], which is capable of binding to α-D-mannose and α-D-glucose [127]. Moreover, Con A binds to mannose better than glucose but does not bind to galactose [126]. The Con A tetramer presents two saccharide binding sites on each face, and binds saccharides by forming hydrogen bonds [128]. Its tertiary structure was discovered by Becker et al. [129]. Con A is a tetramer above pH 7 and a dimmer below pH 6 [28]. It has several isoelectric points, which are reported as 4.5 - 5.5 [130], possibly corresponding to different isoforms.

Since lipopolysaccharides are important for adhesion of bacteria, the role of lectins in cell adhesion is of interest of many researchers and AFM is used as a tool to investigate the interactions between Con A and microbial or other types of biological cells [125,131-133]. Lebed et al. showed that the average height of Con A layer was 15 nm from AFM section analysis and it was compared with literature data for single Con A tetramer with

dimensions 6.7 nm x 11.3 nm x 12.2 nm [132,134]. Gad et al. have shown that the binding force between Con A and mannose ranged from 75-200 pN and the ligand-receptor complex was extended up to 500-600 nm (pull-off distance) or even more in some cases [125]. Touhami et al. showed that the adhesion forces between Con A and mannose residues of *S. carlsbergensis* cells were 117 ± 41 pN [133]. Avni et al. showed that *P. aeruginosa* did not bind to fluorescein-conjugated Con A [123].

Several human corneal epithelial proteins provide receptor sites for bacterial binding and the binding is specific and competitive [135]. Wu et al. found that the carbohydrate mannose functions as an integral component of corneal epithelial protein pili binding receptors [135]. Con A recognizes mannose residues and prevented pili binding of *P. aeruginosa* [135]. Con A is capable of inhibiting the adherence of *P. aeruginosa* to injured corneal epithelial cells by competitively binding to the sugar groups on the surface of corneal epithelial cell [127]. Contact lens wear increases the binding of Con A and *P. aeruginosa* to the corneal epithelial cells [136].

2.6 Atomic Force Microscopy

Microscopes are one of the essential instruments for biomedical research. The atomic force microscope (AFM) is a part of the family of scanning probe microscopes, and was discovered by Binning et al. in 1986 [137]. AFM has been used to study interactions between bacteria and different surfaces such as biomaterials [11,14]. For example, AFM can be used to measure the interaction forces between bacteria and surfaces such as soil,

natural organic matter, and organic compounds. AFM provides superior topographic contrast and direct measurements of surface features providing quantitative height information compared with the scanning electron microscope (SEM), for which conductive or dehydrated samples are required [138].

2.6.1 Principles of AFM

In contrast of other forms of microscopy, AFM does not have a lens, and images samples by 'feeling' rather than 'looking' [139]. The force between the tip and sample varies as the sample is scanned. There are three primary modes of AFM: contact mode, non-contact mode and tapping mode. Figure 2.10 illustrates the main features of an AFM contact mode. The first important part of the AFM is the tip which does the probing. The sharp tip is mounted on the end of a cantilever [138,139]. The cantilever allows the tip to move up and down as it probes the sample. Cantilevers usually have a very low spring constant enabling the AFM to control the small forces between the tip and the sample [139]. They can be triangular or rectangular. In general, the cantilever-tip assembly is made of silicon or silicon nitride because these materials are hard, wear resistant and ideal for micro-fabrication [138,139]. Sharpness, measured by radius of curvature, and aspect ratio are the essential parameters for AFM tips [138]. The second crucial feature of the AFM is the scanning mechanism. The scanning is controlled by a piezoelectric transducer in three orthogonal directions, x, y and z [139].
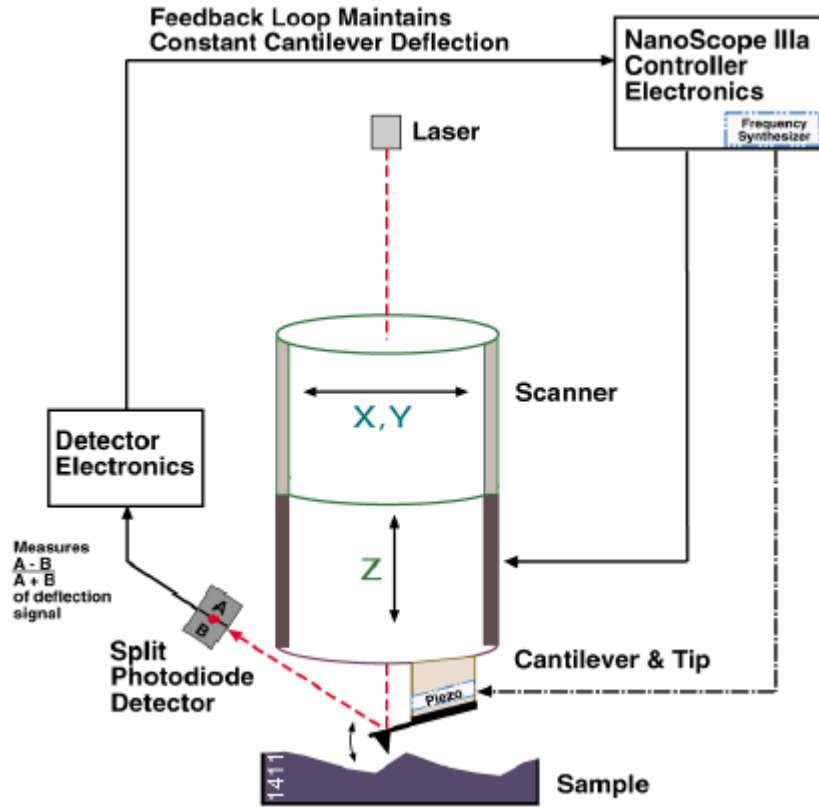
Figure 2.10 Contact mode AFM [10].

The third significant feature of the AFM is the detection mechanism. Laser beam deflection is the most common detection method used in modern AFMs [139]. The laser beam, reflected by the cantilever, is detected by a photo-detector. The photo-detector is usually a simple photodiode which turns light falling on it into an electric signal [139]. The difference between the two photodiode signals indicates the position of the laser spot on the detector and thus the deflection of the cantilever [138]. The feedback control loop is the final important feature of the AFM. Proportional-integral (PI) controllers are commonly used for an AFM control loop [138,139]. The proportional gain responds quickly to small features and integral gain helps maintain a precise set-point. The basic function of the controller is to maintain a predefined set-point. The feedback loop

maintains a constant cantilever deflection in contact mode and constant oscillation amplitude in tapping mode.

2.6.2 Capturing Force Curves and Images with AFM

As the name 'Atomic Force Microscopy' suggests, the important forces are due to one or more interactions such as van der Waals forces, electrostatic and steric interactions. AFM works by bringing a cantilever tip in contact with the surface to be probed. A repulsive force from the surface applied to the tip bends the cantilever upwards and force can be calculated by using the amount of bending which is measured by a laser spot reflected on to a split photodiode detector (Figure 2.11). AFM has also been used to obtain surface topographic images of a variety of biological materials and microbial cells. AFM can capture topographical data with vertical resolution down to the nanometer range, and can examine surfaces either in air or in liquid. Samples can be imaged in liquid environment and nano-scale or pico-scale interaction forces can be captured.

AFM has been used in many biological applications by revealing the nanoscale structure of living microbial cells (bacteria, yeast, fungi), mapping interaction forces at microbial sufaces, and monitoring conformational changes of individual membrane proteins [140,141] and peptide interactions [142]. Touhami et al. investigated the characteristics of *P. aeruginosa* pili and determined the adhesion forces [143] using AFM. Bolshakova et al. compared bacterial surfaces using different modes of AFM [144]. The adhesion of lactic acid bacteria [145] and sulfate-reducing bacteria to Si_3N_4 [146] was also

investigated using AFM. Afrin et al. analyzed the force curves obtained on the live fibroblast cell membrane using chemically modified AFM tips [147]. AFM tips are also modified by bacterial cells and used to probe different substrates such as proteins, epithelial cells and biomaterials [38,43,143,148].
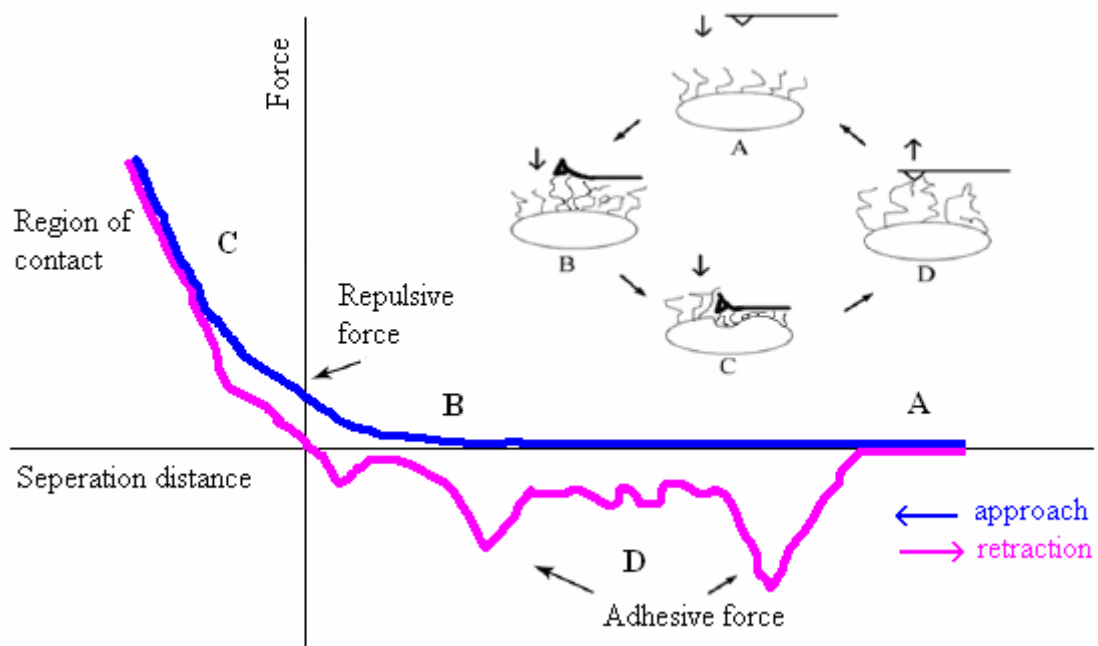
Figure 2.11 Schematic of relative cantilever position in a typical force curve. The cantilever approaches the surface (A), starts interacting with bacterial surface structures (B), contacts the sample and may be deform the surface (C), finally retracts from the sample and attachment and breaking off from the cantilever occurs (D) (Adapted from [11]).

3 - Materials and Methods

3.1 Bacterial Culture Conditions

Two strains of *Pseudomonas aeruginosa*, smooth PAO1 and semi-rough AK1401, were provided by Professor Gerald Pier (Channing Laboratory, Department of Medicine, Brigham and Women's Hospital, Harvard Medical School). Both strains were maintained at 4^oC on Tryptic Soy Agar (TSA, 40 g·L^{-1}) plates. Tryptic Soy Broth (TSB, 30 g·L^{-1}) was used as the liquid growth media. 30 g of TSB powder was dissolved in 1 L of ultrapure water (Milli-Q). The solution was autoclaved at 121^oC for 30 minutes and kept in the refrigerator. *P. aeruginosa* cells were precultured in 10 mL of TSB in 25 mL culture flasks (VWR) on a radially oriented rotator (Cole-Parmer) overnight at 37^oC. 1 mL of preculture was then transferred into 50 mL of TSB and grown at 37^oC in an orbital shaker (Lab-Line) bath at 160 RPM until the absorbance value of the suspension reached 0.9 at 600 nm. Then, bacterial cells were harvested and prepared for attachment on the clean glass slides.

3.2 Bacterial Cell Attachment

Bacterial cells were attached to clean glass slides by using different binding materials. Bacteria coated glass slides were used for AFM experiments.

3.2.1 Glass Slide Cleaning

Micro cover glass slides (VWR) were cleaned with a 4:1 mixture of H_2SO_4 (Fisher) and H_2O_2 (Fisher). They were kept in the acid solution for 25 minutes. Then, they were rinsed with ultrapure water and stored in the refrigerator in fresh ultrapure water.

3.2.2 Attachment of *P. aeruginosa* AK1401

Since the LPS structure of the two *P. aeruginosa* strains were different, one with neutral and one with negatively charged polysaccharides, different procedures were used to attach bacterial cells on the clean glass slides.

P. aeruginosa AK1401 cells were attached to clean glass slides for AFM experiments. The clean glass slides were treated with 100% ethanol (Fisher) for 5 minutes, and followed with 100% methanol (Fisher) treatment for 5 minutes. Then, the glass slides were allowed to stay in the aminosilane solution for 15 minutes. The aminosilane solution was prepared by adding 1 mL of 3-aminopropyl dimethoxysilane (Aldrich) to 9 mL of methanol. Finally, the glass slides were rinsed with at least 50 mL of methanol followed by 25 mL of ultrapure water, and kept in methanol until the bacterial solution was added to the slides.

P. aeruginosa AK1401 was grown in TSB until cells reached an absorbance value of 0.9 at 600 nm, and 18 mL of cell suspension was centrifuged at 1360 xg for 15 minutes. The

supernatant was eluted and the pellet was washed once with ultrapure water and resuspended in an equivalent amount of ultrapure water. The cell suspension was treated with 300 μL of 100 mM 1-Ethyl-3-(3-dimethylaminopropyl) carbodiimide hydrochloride (EDC, Pierce) at pH 5.5 and left to equilibrate for 3 minutes. The treatment with EDC was followed by addition of 300 μL of 40 mM N-hydroxysulfosuccinimide (Sulfo-NHS, Pierce) at pH 7.5 to the mixture. The bacterial suspension with EDC/NHS was left to equilibrate for 10 minutes and added aminosilane treated clean glass slides. Finally, glass slides with bacterial suspension, were agitated for 12 hours on a shaker (Lab-Line) at 70 RPM at room temperature to allow for bacterial cell attachment to the glass slides.

3.2.3 Attachment of *P. aeruginosa* PAO1

P. aeruginosa PAO1 cells were attached to clean glass slides for AFM experiments. *P. aeruginosa* AK1401 was grown in TSB until cells reached an absorbance value of 0.9 at 600 nm and 18 mL of cell suspension was centrifuged at 1360 xg for 15 minutes. The supernatant was eluted and the pellet was washed with ultrapure water once and resuspended in an equivalent amount of ultrapure water. Clean glass slides were soaked in 100 μL of 0.1% w/v poly-l-lysine solution (PLL, Sigma) and the PLL solution was allowed to dry for 2 hours. Then bacterial suspension was added to PLL treated glass slides and kept on the shaker at 70 RPM for 2 hours to allow for bacterial attachment to the glass slides.

3.3 Cell Counting

Bacterial cells were grown in TSB till they reached the selected absorbance values at 37°C. Harvested bacterial cells were centrifuged at 1360 xg for 10 minutes and then washed once with 0.1 M 2-[N-Morpholino]-ethanesulfonic acid (MES) buffer (Sigma). Bacterial suspension was then sonicated for 5 minutes (40 kHz, 130 W; Branson, Model 2510, USA). Approximately 200 µL of bacterial suspension was put into a spermometer (Zander Spermometer^{TM}, Zander Medical Supplies) and imaged using an optical microscope (Eclipse E400, Nikon). The dimensions of the counting chamber are 1mm^2 with 0.01mm depth. The counting chamber has 100 square cells of 0.1 mm x 0.2 mm each. Twenty images were captured for each absorbance value, and Sigma Scan Pro5 was used to count the numbers of cells in each image. Finally, a calibration curve of number of bacteria per mL versus absorbance values in TSB was obtained for each strain of *P. aeruginosa*.

3.4 Optical Microscopy Imaging

P. aeruginosa AK1401 and PAO1 were imaged using an optical microscope (Eclipse E400, Nikon) under FITC wavelengths. Bacterial cells were grown in TSB until they reached an absorbance value of 0.9 at 600 nm and centrifuged at 1360 xg for 15 minutes. The supernatant was eluted and the pellet was resuspended in an equivalent amount of ultrapure water. Two mL of resuspended bacterial cells were stained with 400 µL of 0.1% acridine orange. The suspension was poured onto a 0.2 µm filter (Membrane Filters,

Millipore) and vacuum filtered (Welch Dry Vacuum Pump, Thomas Industries Inc.) after mixing for 10 minutes with the vortexer (Mini Vortexer, Fisher Scientific). Finally, the filter was attached to a glass slide and imaged using the optical microscope. The results were used to determine the shape of *Pseudomonas* cells and for comparison with AFM imaging results.

3.5 Supernatant Preparation for Lowry Protein Assay

Since there were various extrapolymeric substances in the supernatant of *P. aeruginosa,* the amount of protein molecules in the supernatant was measured. Bacterial cells were grown in TSB till they reached absorbance value of 0.9. Ten mL of supernatant was centrifuged at 4350 xg for 15 minutes using the supercentrifuge (Beckman Coulter Inc., Palo Alto, CA, USA) to remove the bacterial cells from the suspension. The pellet was discarded and the supernatant was centrifuged at 12,100 xg for 30 minutes to pellet down the EPS. The supernatant was eluted and the pellet containing EPS was resuspended in an equivalent amount of ultrapure water and centrifuged at 12,100 xg for 30 minutes. This step was repeated one more time to remove all the TSB residue. Finally, the amount of protein in the final solution containing EPS was tested using the Lowry assay.

3.6 Lowry Protein Assay

The Lowry assay is a widely used colorimetric method for estimation of proteins that are already in a solution using the Folin reaction [149]. Due to the reaction of proteins with

copper ion in alkaline solution, the blue color appears. There are four reagents used for the procedure. Reagent A is prepared by dissolving 20 g of Na_2CO_3 in 1 L of 0.1 N NaOH. Reagent B is prepared by dissolving 0.5 g of $CuSO_4 \cdot 5H_2O$ in 100 mL of a 1% (wt/vol) aqueous solution of sodium tartrate. Reagent C is prepared by mixing 50 mL of reagent A and 1 mL of reagent B just before use. Reagent D is diluted Folin reagent. 2 N Folin Ciocalteau phenol reagent (Sigma) is diluted to 1 N with distilled water.

To measure the protein content of the supernatant, 0.5 mL of the sample was added to a clean 10-mL conical tube (Falcon). 2.5 mL of reagent C was added to the sample and mixed well with the vortexer (Mini Vortexer, Fisher Scientific), and allowed to stand for 10 minutes at room temperature. Then, 0.25 mL of reagent D was added to the mixture and mixed immediately at room temperature. After 30 minutes, the absorbance value was measured with the spectrophotometer (ThermoSpectronic, Waltham, MA, USA) at 660 nm. Four readings were taken and averaged for each sample. Bovine serum albumin (BSA, Sigma) was used to prepare the linear standard curve. 1 mg·mL^{-1} BSA solution was used. A series of tubes containing 500, 400, 300, 200, 100, 50, 25, and 0 μg of BSA in 2 mL total volume was prepared. The Lowry procedure was performed for each sample and by comparison with the standard curve, the protein concentration of bacterial supernatants was calculated.

3.7 Contact Angle Measurements

Bacterial cells were grown in TSB until cells reached an absorbance value of 0.9 and centrifuged at 1360 xg for 15 minutes. The supernatant was eluted and the cells were washed once with N-(2-hydroxyethyl)-piperazine-N'-2-ethanesulfonic acid (HEPES, Sigma) buffer and resuspended in HEPES buffer. 50 mM HEPES, 110 mM NaCl, 1 mM DTT is the composition of the buffer solution which is isotonic to human plasma and termed as physiological HEPES buffer (PHB) with the pH of 7.4 [150]. Four mL of the bacterial cell suspension was poured onto a 0.45 μm filter (Membrane Filters, Millipore) and vacuum filtered (Welch Dry Vacuum Pump, Thomas Industries Inc.). Eight filters (containing $> 10^8$ cells$\cdot$m^{-2}) were prepared for each *Pseudomonas* strain and contact angle values were averaged. After the filters reached the drying time, which was the time that the superficial moisture held by the bacterial surface evaporated from the filter and the contact angle values were stable, contact angle measurements were taken at room temperature for water, diiodomethane and formamide using a goniometer (Ramé-Hart Model 100-00, Netcong, NJ). Contact angles were performed by the sessile drop technique and used for surface free energy calculations [47].

3.8 Zeta Potential Measurements

Zetasizer Nano ZS (Malvern Instruments, UK) and disposable folded capillary cells (Malvern Instruments, Southborough, MA, USA) were used to measure the zeta potentials of the protein solutions and bacterial suspensions at room temperature. The

Zetasizer Nano ZS calculates the zeta potentials assuming the Smoluchowski equation (Equation 3.1) [151]:

$$U = \frac{\varepsilon \zeta}{\mu}$$ 3.1

where U is the electrophoretic mobility, ε is the permittivity of vacuum, μ is the viscosity, and ζ is zeta potential. Five mg·mL^{-1} of BSA (Sigma) and Con A (Sigma) solutions were prepared in HEPES buffer. Bacterial cells were grown in TSB until they reached an absorbance value of 0.9 and centrifuged at 1360 xg for 15 minutes. The supernatant was eluted and the cells were washed once with HEPES buffer and resuspended in HEPES buffer at an ionic strength of 0.161 M and pH of 7.4. The same step was repeated using ultrapure water instead of HEPES buffer to be able measure the zeta potentials of the cells in different solutions and see the effect of ionic strength on bacterial surface charge. Six measurements were averaged for each sample solution.

3.9 DLVO Calculations

The interaction energy (E_T, Equation 3.2) between the bacterium and the silicon tip can be described using classical DLVO theory. Classical DLVO theory is the sum of van der Waals (E_V) (Equation 3.3) and electrostatic double layer (E_E) (Equation 3.4) interactions.

$$E_T = E_V + E_E$$ 3.2

$$E_V = -\frac{Aa_m a_p}{6h\left(a_m + a_p\right)\left(1 + 14h/\lambda_c\right)}$$

3.3

and 3.4:

$$E_E = \frac{2\pi a_m a_p n_\infty kT}{(a_m + a_p)\kappa^2}(\varphi_m^2 + \varphi_p^2)\left\{\frac{2\varphi_m\varphi_p}{\varphi_m^2 + \varphi_p^2}\ln\left(\frac{1 + \exp(-\kappa h)}{1 - \exp(-\kappa h)}\right) - \ln[1 + \exp(-2\kappa h]\right\}$$

The properties of the *P. aeruginosa* cells and the AFM tip were taken from experiments.

The size of the bacterial cells was measured by AFM and the volume of the bacterial cells

was approximated to a sphere, and the equivalent bacterial radius (a_m) was calculated.

The tip radius (a_p) of Mikromasch CSC38-B cantilevers is 10 nm. The retardation

coefficient ($\lambda_c = 100$ nm) was taken from literature [2]. The Hamaker constants (A), 5.22

x 10^{-20} J for *P. aeruginosa* PAO1 and 5.56 x 10^{-20} J for *P. aeruginosa* AK1401, were

calculated from an algebraic method of determining the Hamaker constant based on the

apolar component of the microbial surface free energy (Equation 3.5) [44]:

$$A = 24\pi d_0^2 \gamma_M^{LW}$$

3.5

with l_0 being the minimum separation distance between the two contacting bodies. van

Oss also determined that the minimum separation distance fell within a range of 1.57 ±

0.09 Å. The Boltzmann constant (k) is 1.38 x 10^{-23} J·K^{-1}. Temperature (T) is 298 K. n_∞ is

[1000 x molar salt concentration x N$_A$ (Avogadro number)]. Inverse Debye length (κ) is

9.35 x 10^8 m^{-1} for the ionic strength of the media [2]. The normalized surface potentials, φ_m and φ_p are calculated from zeta potential values (ζ) (Equation 3.6) [43,151,152].

$$\varphi_i = \frac{\zeta \cdot electron\ charge}{kT} \qquad\qquad 3.6$$

3.10 AFM Experiments

A Dimension 3100 atomic force microscope (AFM) with Nanoscope IIIa controller (Veeco Metrology Group, Santa Barbara, CA) was used for the experiments. Mikromasch CSC38-B type cantilevers were used for force curve measurements. Mikromasch NSC36-C and Mikromasch CSC38-B type cantilevers were used for imaging.

3.10.1 Spring Constant Measurements

Spring constants of the Mikromasch CSC38-B cantilevers were measured using a thermal method [11] developed by Burnham et al. [153] and applied to the analysis of force curves. Five noise spectra were captured for each cantilever and the spring constants from each image were calculated and averaged before and after the AFM experiments.

3.10.2 Surface Morphology Experiments

Bacterial cells

Bacterial cell cultures were studied to establish cell surface morphologies. Bacterial cells were grown in TSB until they reached an absorbance value of 0.9 and centrifuged at 1360 xg for 15 minutes. The supernatant was eluted and the cells were washed once with ultrapure water and resuspended in ultrapure water. Fifty μL of bacterial suspension was added to clean glass slides and dried at room temperature. Glass slides, containing immobilized bacteria, were affixed to the AFM stage and imaged in air.

Extrapolymeric Substances

Initially, the extrapolymeric substances (EPS) in the supernatant were investigated by AFM. The supernatant of bacterial suspension is poured onto glass slides and dried at room temperature. The bacterial cells were grown in TSB until they reached an absorbance value of 0.9 and centrifuged at 1360 xg for 15 minutes. 100 μL of the supernatant (1st supernatant) was filtered through 0.45 μm syringe filters (Becton Dickinson, Franklin Lakes, NJ) to remove the bacterial cells, and poured onto clean glass slides and dried at room temperature. Then the EPS was imaged in air using AFM.

From the AFM images, it was hard to determine the nature of the molecules present in the supernatant. Thus, the protein content of the supernatant was determined by the

Lowry protein assay. Bacterial cells were grown in TSB until they reached an absorbance value of 0.9 at 600 nm and centrifuged at 4,350 xg for 15 minutes at 18 $^{\circ}$C using the supercentrifuge (Beckman Coulter Inc., Palo Alto, CA, USA) to remove the bacterial cells from the suspension. The pellet was discarded and the supernatant was centrifuged at 12,100 xg for 30 minutes at 18 $^{\circ}$C to concentrate the EPS. The pellet, EPS molecules, was washed once with ultrapure water, resuspended in ultrapure water, and used for the Lowry protein assay. Precentrifuged supernatant, containing the remaining EPS and probably membrane vesicles, was filtered through 0.45 μm syringe filters (Becton Dickinson, Franklin Lakes, NJ) and centrifuged at 260,000 xg for 30 minutes at 18°C using an ultracentrifuge (Beckman Coulter Inc., Palo Alto, CA, USA). The supernatant was eluted and the pellet was resuspended in ultrapure water (4th supernatant). One hundred μL of the 4th supernatant was poured onto clean glass slides and imaged in air using AFM.

Proteins

Proteins were immobilized on clean glass slides and imaged using AFM. Ten mg·mL^{-1} BSA (Sigma) and Con A (Sigma) solutions were each prepared in HEPES buffer at pH 4.5 and poured onto glass slides. The glass slides with protein solution were agitated for 4 hours on a shaker (Lab-Line) at 70 RPM at room temperature to allow protein immobilization. The glass slides, containing immobilized protein molecules, were imaged in HEPES buffer at pH 7.4 using AFM.

3.10.3 Tip Modification

Bacterial cells were immobilized on silicon cantilevers and the glass slides, containing immobilized protein molecules, were probed. The cantilever was treated with 0.1% w/v poly-l-lysine solution (PLL, Sigma) for 30 minutes using a micromanipulator and dried for 10 minutes. The cantilever was soaked in 2 μL of *P. aeruginosa* PAO1 cell suspension (in HEPES buffer, containing ~ 9 x 10^9 cells·mL^{-1}) for 20 minutes and dried for 5 minutes at room temperature. Then the cantilever, containing bacterial cells, was used to probe BSA and Con A molecules and capture interaction forces between strain PAO1 and proteins in HEPES buffer at pH 7.4.

For *P. aeruginosa* AK1401, a slightly different procedure was used. The cantilever was treated with 0.1% w/v poly-l-lysine solution (PLL, Sigma) for 30 minutes using a micromanipulator and dried for 10 minutes. *P. aeruginosa* AK1401 cells were suspended in ultrapure water and vacuum filtered (Welch Dry Vacuum Pump, Thomas Industries Inc.) through a 0.45 μm filter (Membrane Filters, Millipore). The filter was attached to a glass slide using double sided tape and put on the AFM stage. The PLL treated cantilever was lowered onto the filter, containing AK1401 cells, using the piezoactuator of the AFM. The two were allowed to remain in contact for 5 minutes for bacterial attachment. Then, the tip was used to probe BSA and Con A molecules and capture interaction forces between strain AK1401 and proteins in HEPES buffer at pH 7.4. Cantilevers with attached bacterial cells were imaged using a scanning electron microscope (SEM, Jeol JSM-840) to verify placement of bacteria.

3.10.4 Interaction Forces

Interactions of proteins and *P. aeruginosa* strains with silicon cantilevers (Mikromasch CSC38-B), and interactions between proteins and bacterial cells were investigated by AFM force curve analysis. Proteins and bacterial cells were immobilized onto clean glass slides and probed by silicon cantilevers. In addition, proteins were probed by cantilevers containing bacterial cells. The force curves were captured in HEPES buffer at pH 7.4.

The deflection voltage – separation distance curves were converted into force (nN) versus separation (nm) curves using the method of Ducker and Senden [11,154] (Figure 3.1). The raw deflection data were converted to force data using Hooke's law, which describes a linear relationship between force and deflection assuming thermal equilibrium (Equation 3.7).

$$F = k \cdot x \tag{3.7}$$

where F is the interaction force (N), k is the spring constant of the cantilever (N·m^{-1}) and x is the deflection (m) of the cantilever. The constant compliance region was aligned with the vertical axes, and the zero interaction region at large distances was aligned with the horizontal axes (Figure 3.2). First, the retraction curve was aligned according to the peak position. The initial point of first adhesion peak was aligned with the origin, and then the constant compliance region and zero interaction region of the approach curve was aligned on top of retraction curve, assuming thermal equilibrium. Figures 3.3 and 3.4 show representative approach and retraction curves, respectively.
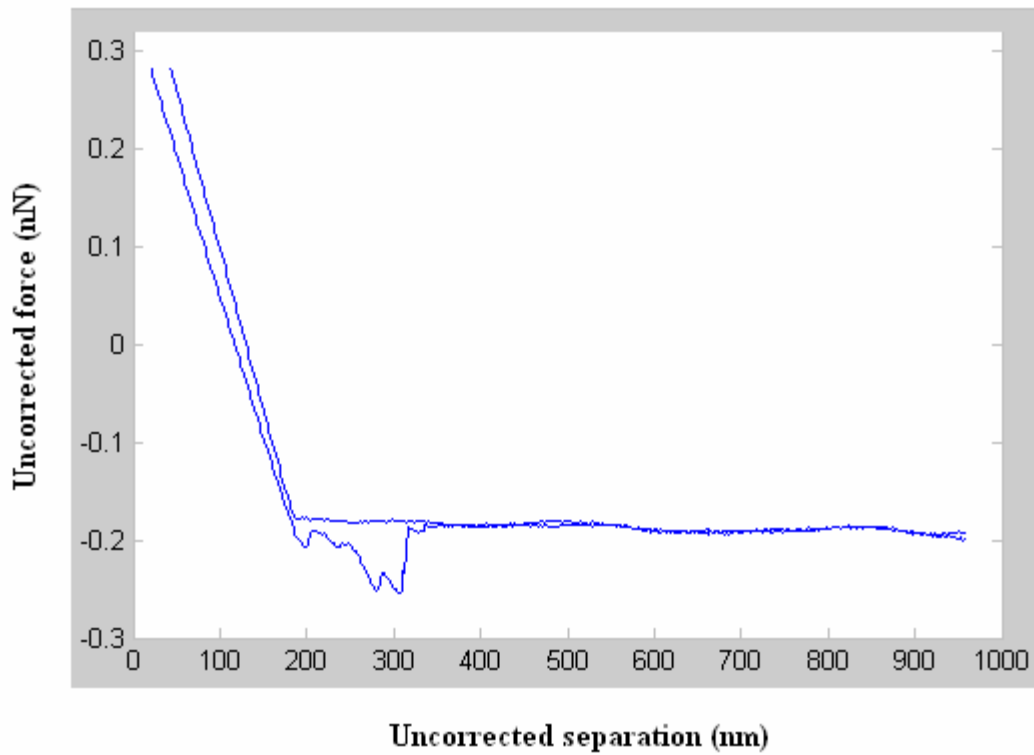
Figure 3.1 Illustration of uncorrected force cycle. The deflection data are transformed to force using Hooke's law.
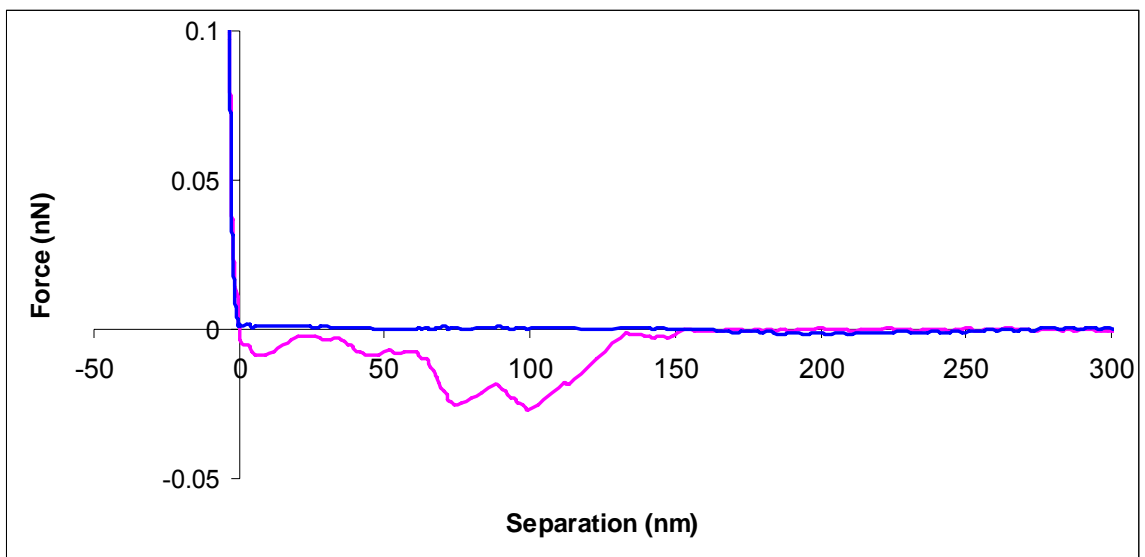
Figure 3.2 Illustration of corrected force cycle. The region of contact and the region of zero interaction are aligned with the axes of the Cartesian plane.
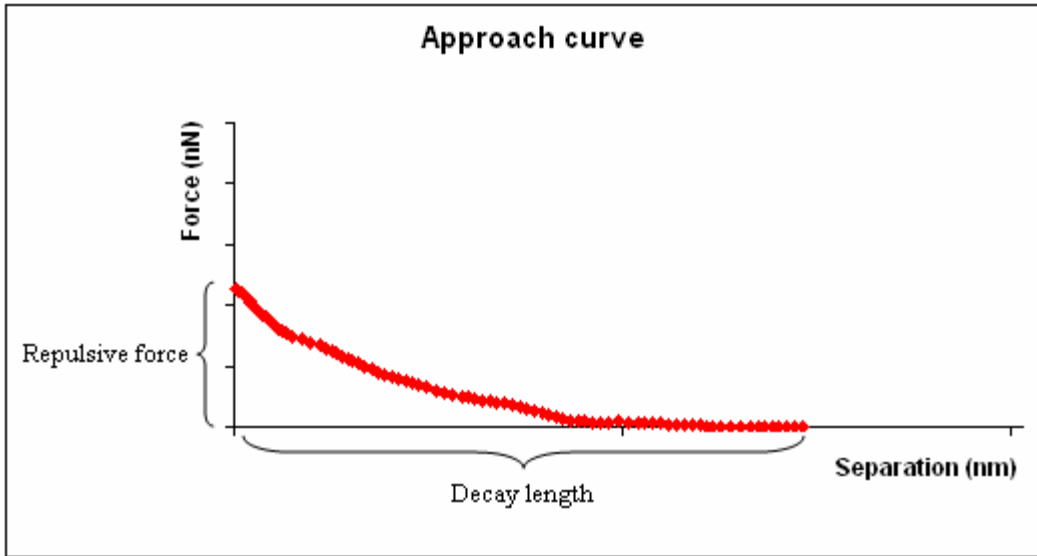
Figure 3.3 Illustration of a typical approach curve.
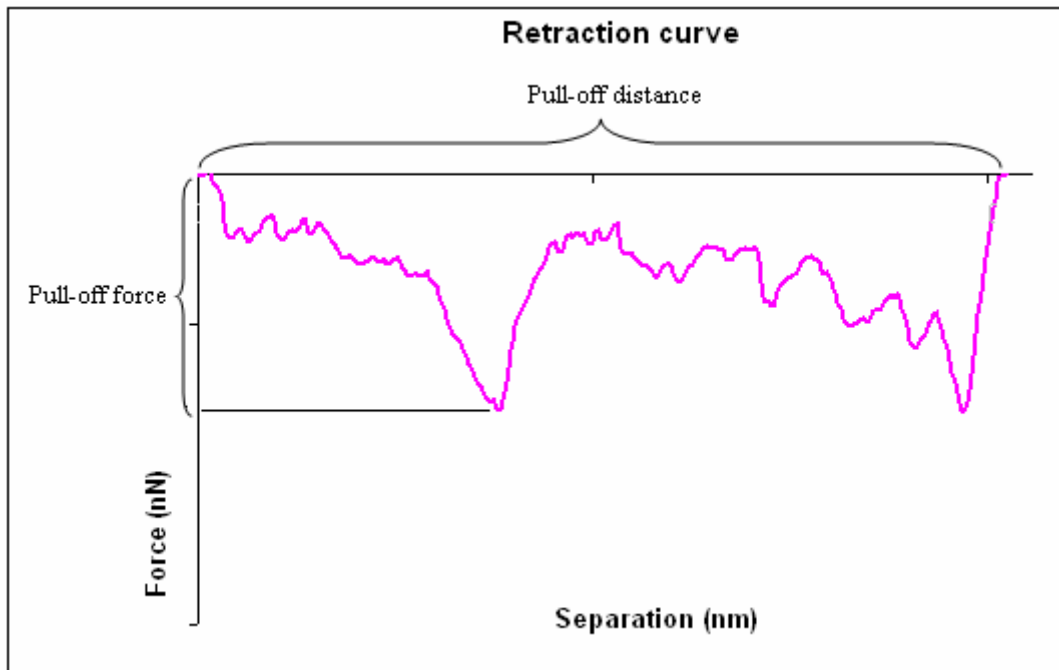
Figure 3.4 Illustration of a typical retraction curve.

4 - Results and Discussion

4.1 Microbial Growth Curves

P. aeruginosa PAO1 and AK1401 were each grown in TSB at 37°C. The absorbance value of the cell suspension was measured with time. Three cultures from different agar plates were grown in different days. As can be seen in Figure 4.1 and Figure 4.2, the growth curves were similar and reproducible for both strains.
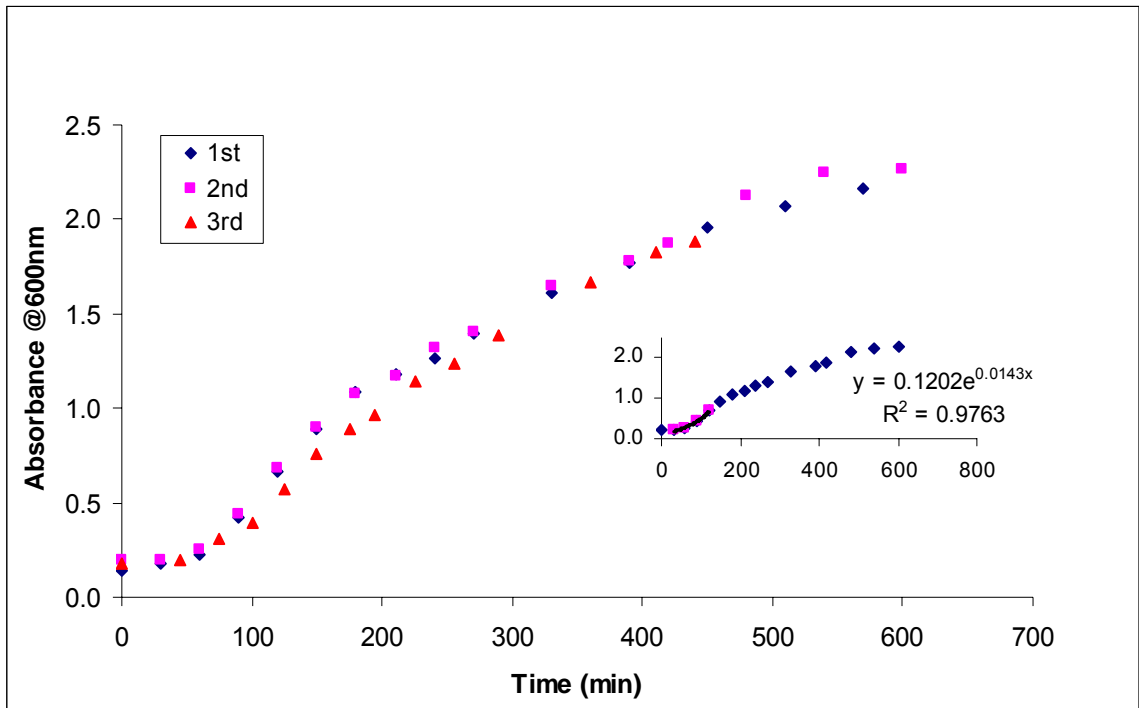
Figure 4.1 Growth curve of *P. aeruginosa* PAO1. Bacterial cells were grown in TSB at 37°C.
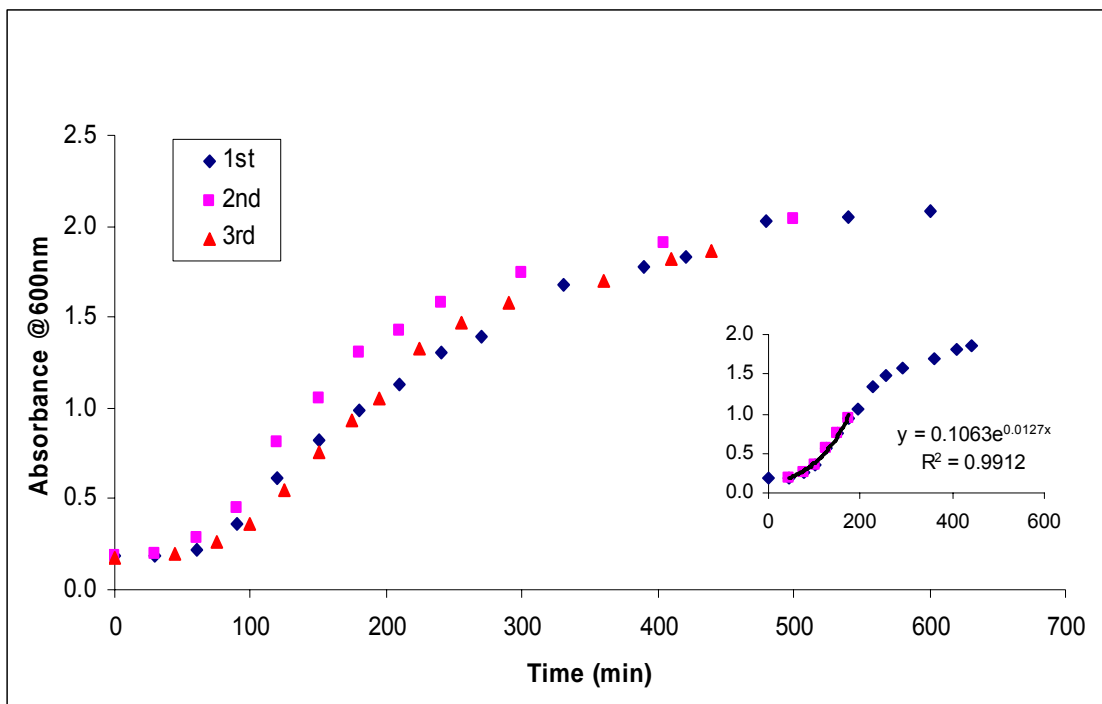
Figure 4.2 Growth curve of *P. aeruginosa* AK1401. Bacterial cells were grown in TSB at 37$^{\text{o}}$C.

An exponentially growing bacterial population doubles at regular intervals. Therefore, the doubling time was calculated when the cells are growing exponentially. Absorbance data were fit using an exponential regression and doubling time was calculated. Doubling time measurements are average values from three different growth curves (Table 4.1).

Table 4.1 Doubling times for *P. aeruginosa.*

P. aeruginosa	Doubling Time (min)
PAO1	52.3 ± 6.5
AK1401	50.3 ± 4.2

The growth curves demonstrated the different phases (lag, exponential, stationary and death phase) of growth and allowed us to choose an absorbance value corresponding to the mid-exponential growth phase. The absorbance value at 600nm of 0.9 was selected for future experiments.

4.2 Cell Counting

The *Pseudomonas aeruginosa* strains, PAO1 and AK1401 were injected in a counting chamber, which had 100 square cells to hold the bacteria, as can be seen in Figure 4.3 The chamber was imaged by optical microscope and the average number of bacteria in 10 cells from phase contrast images was counted for different bacterial cell concentrations to generate a calibration curve (Figure 4.4 and Figure 4.5). The number of bacterial cells corresponding to an absorbance of 0.9 was found to be 9.18×10^9 cells·mL^{-1} for strain PAO1 and 9.28×10^9 cells·mL^{-1} for strain AK1401. These results were used to design further experiments.
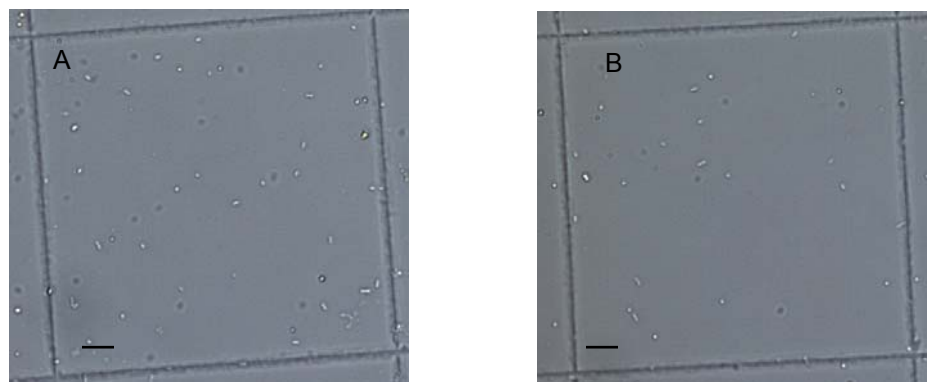
Figure 4.3 One square from counting chamber with *P. aeruginosa* PAO1 (A) and AK1401 (B). Scale bars represent 10 μm.
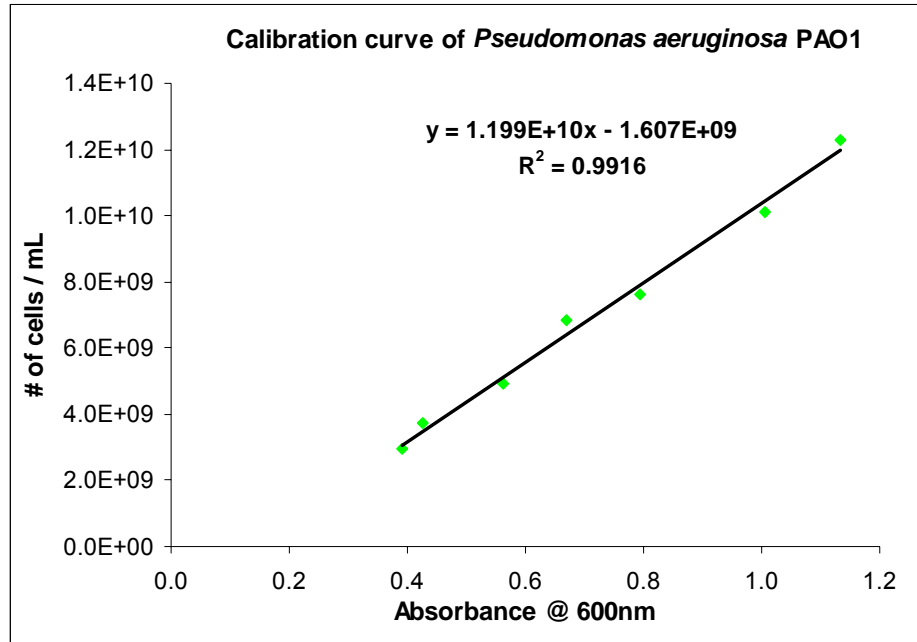
Figure 4.4 Calibration of absorbance with cell number for *P. aeruginosa* PAO1 grown in TSB.
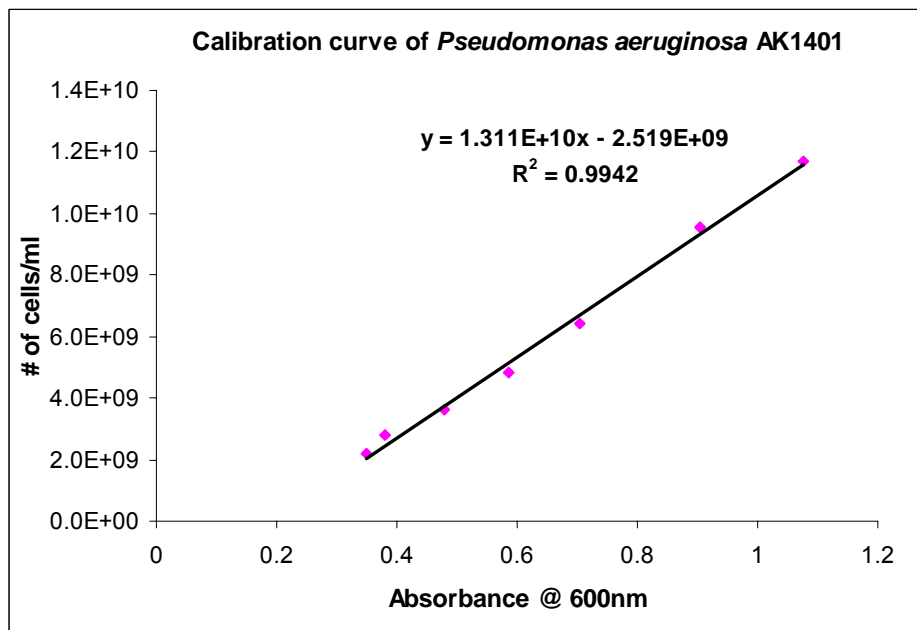
Figure 4.5 Calibration of absorbance with cell number for *P. aeruginosa* AK1401 grown in TSB.

4.3 AFM Studies with Clean Substrates

Some calibration and control experiments were performed before working with bacteria or proteins. For example, the spring constants of cantilevers (CSC38-B) were calculated, and the properties of glass and gold slides were investigated by AFM.

4.3.1 Spring Constant Measurements

Spring constants of CSC38-B cantilevers were measured by using a thermal method [155], which was developed by Burnham et al. [153]. The spring constants were measured before and after the AFM experiments. Most of the average predicted values of spring constants from the noise spectrums of the cantilevers were close to the manufacturer's nominal value, 0.03 N·m^{-1} (Figure 4.6). However, the deviation ranged from 10% to 65%.
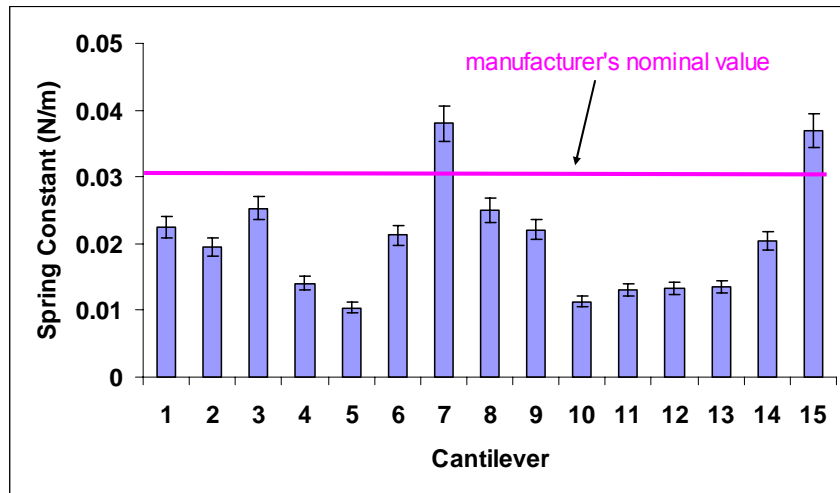
Figure 4.6 Average spring constant of CSC38-B cantilevers measured by using noise spectrums (n = 8). Error bars indicate the standard deviations from the average value for each cantilever.

4.3.2 Clean Glass Slides

New, but uncleaned glass slides were imaged by AFM and their topography was compared with cleaned slides (Figure 4.7 and Figure 4.8). Acid cleaning removes the contaminants that are on the glass slides. The mean roughness of unclean glass slides was 1.124 nm and some particles as large as 10 nm in height were measured in the section analyses.
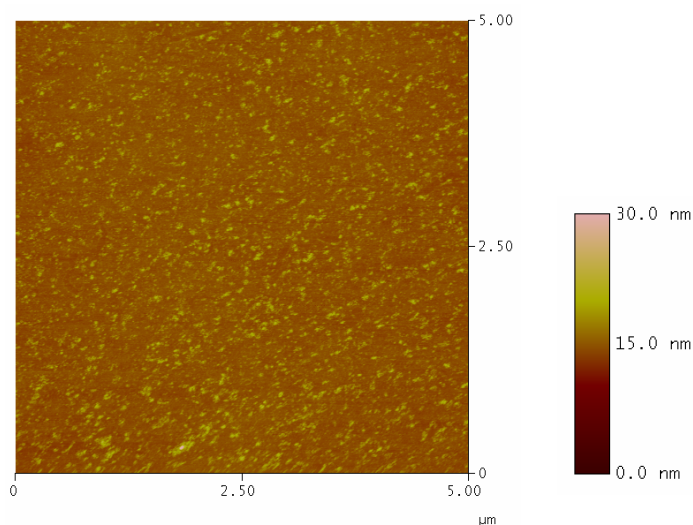
Figure 4.7 2D AFM height image of unclean glass slide (the bar indicates z scale).

No particles were observed on the glass slides after acid cleaning and the mean roughness decreased to 0.251 nm. Section analysis results showed that the vertical height of the features was as small as 0.246 nm. Since the dimensions of proteins and bacteria are in the nano scale, the acid cleaning is necessary in order to use glass slides as a substrate for bacterial cell attachment or protein immobilization for AFM experiments.
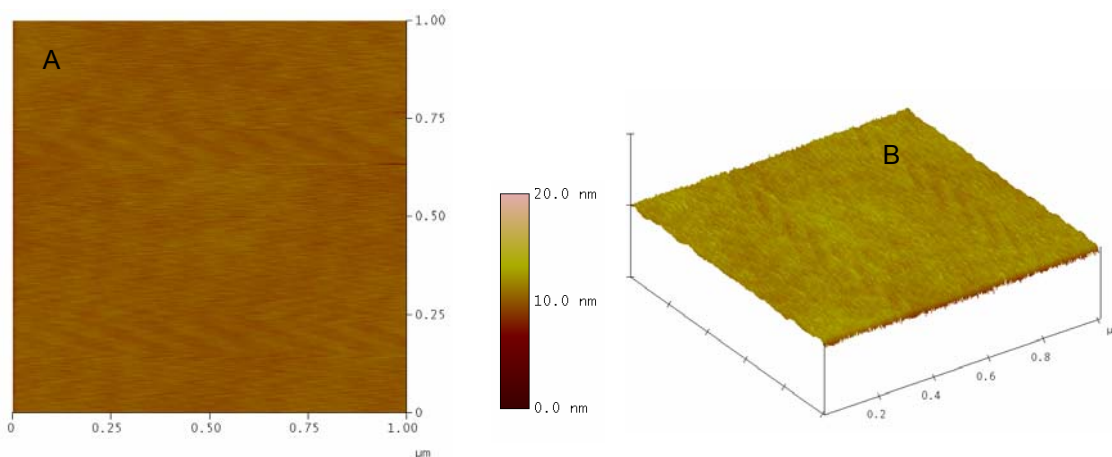
Figure 4.8 2D (A) and 3D (B) AFM height images of a clean micro cover glass slide (the bar indicates z scale).

Force Measurements on Glass

Force curves were captured in ultrapure water at room temperature by AFM. Fifty force curves were analyzed and similar adhesion peaks were observed in each force cycle. Some representative approach and retraction curves can be seen in Figure 4.9 and Figure 4.10. The approach curves showed that there was no repulsion between the silicon AFM tip and the glass slides. Since glass slides are stiff surfaces, there was only one adhesion peak observed in each retraction curve. The magnitude of this adhesive force was found to be less than 0.1 nN.
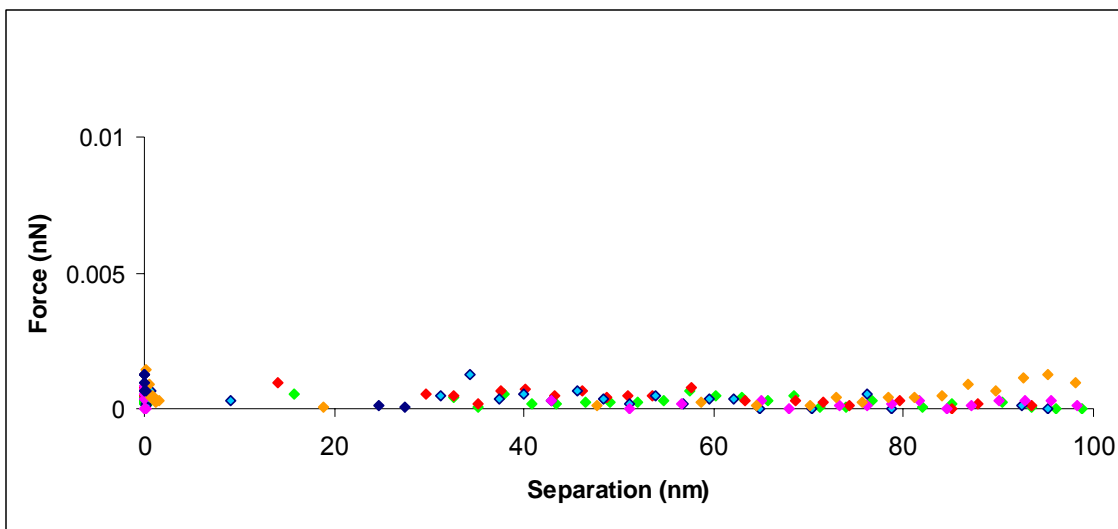
Figure 4.9 Representative approach curves of clean glass slides in water at room temperature. Five examples of fifty curves are shown. The cantilever CSC38-B was used.
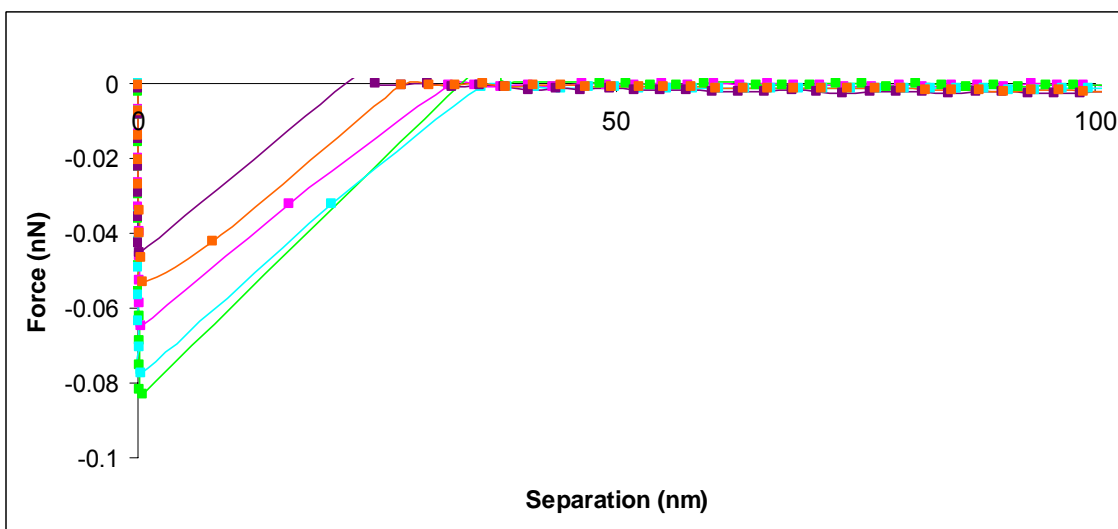
Figure 4.10 Representative retraction curves of clean glass slides in water at room temperature. Five examples of fifty curves are shown. The cantilever CSC38-B was used.

4.3.3 Clean Gold Slides

Gold slides were investigated as a possible alternative substrate for protein and bacteria immobilization (Figure 4.11). Gold slides were cleaned with piranha solution (70% H_2SO_4 and 30% H_2O_2). They were rough compared to clean glass slides, with the mean roughness of clean gold slides equal to 1.083 nm.
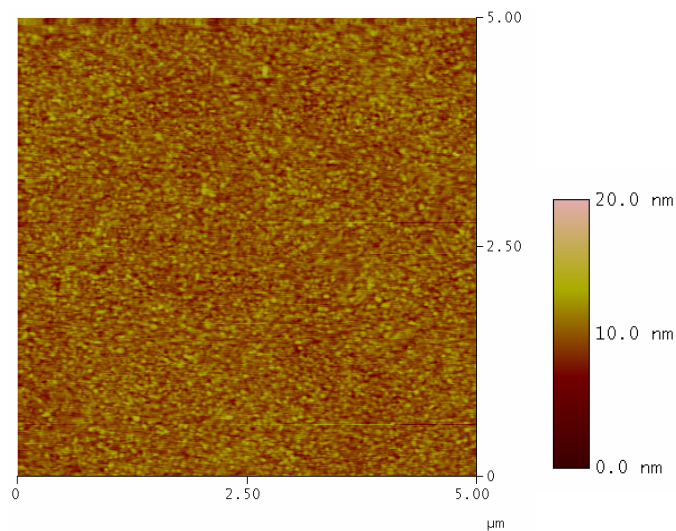
Figure 4.11 A 2D AFM height image of clean gold slide.

Several laboratory protocols are available that allow for biomolecules to be adsorbed to gold, which can facilitate bacterial attachment. However, since the proteins of interest are around 15 nm, these gold slides were not convenient to use because of their roughness. Therefore, we chose to immobilize proteins on glass slides since this process could be more carefully controlled.

4.4 Bacterial Cell Morphologies and Surface Properties

P. aeruginosa AK1401 and PAO1 were imaged using an optical microscope under FITC wavelengths. Figure 4.12 shows the rod shaped *Pseudomonas aeruginosa* cells. Because the bacterial cells were stained with acridine orange, they were green in color under FITC wavelengths. Different dilutions of bacterial suspension were prepared to determine the optimum imaging conditions.
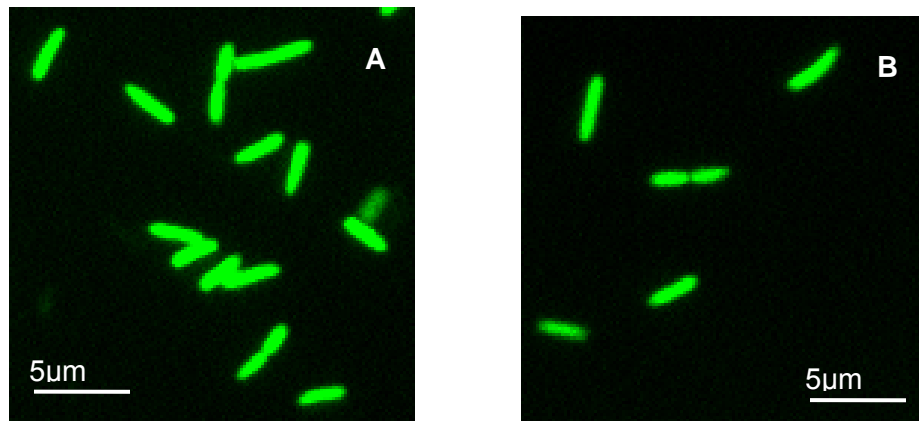
Figure 4.12 Fluorescence microscope images of *P. aeruginosa* AK1401 (A) and PAO1 (B) stained with acridine orange, 1/100 dilution and 1/1000 dilution respectively.

These results were used to determine the shape of *P. aeruginosa* cells and for comparison with AFM imaging results. Topographical images of *P. aeruginosa* were captured using AFM. The AFM images showed that the size and shape of both strains were similar, ranging from 1 to 3 μm (Figure 4.13).
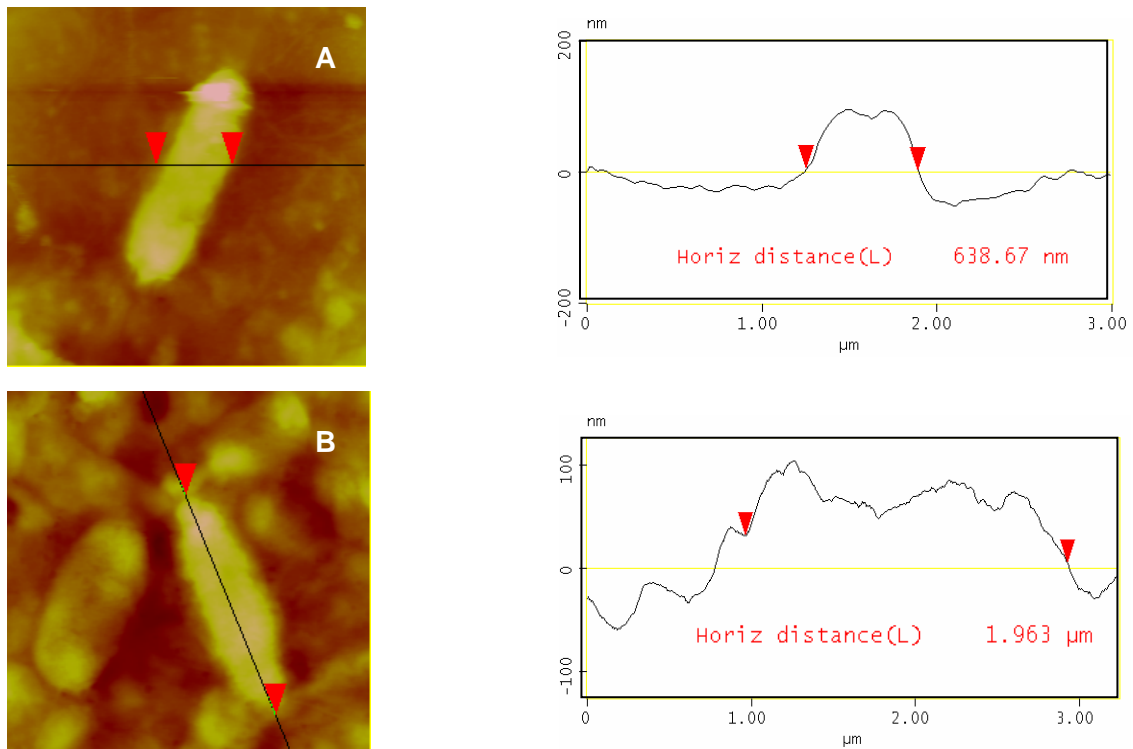
Figure 4.13 AFM images of *P. aeruginosa* AK1401 (A) and PAO1 (B) showing the size of the bacterial cells in air.

When the two *P. aeruginosa* strains were grown on TSA plates, a blue-green color was observed in *P. aeruginosa* PAO1 plates (Figure 4.14), because the strain PAO1 produces a blue-green pigment, pyocyanin. This pigment was shown to be a virulence factor in this organism [85,86].
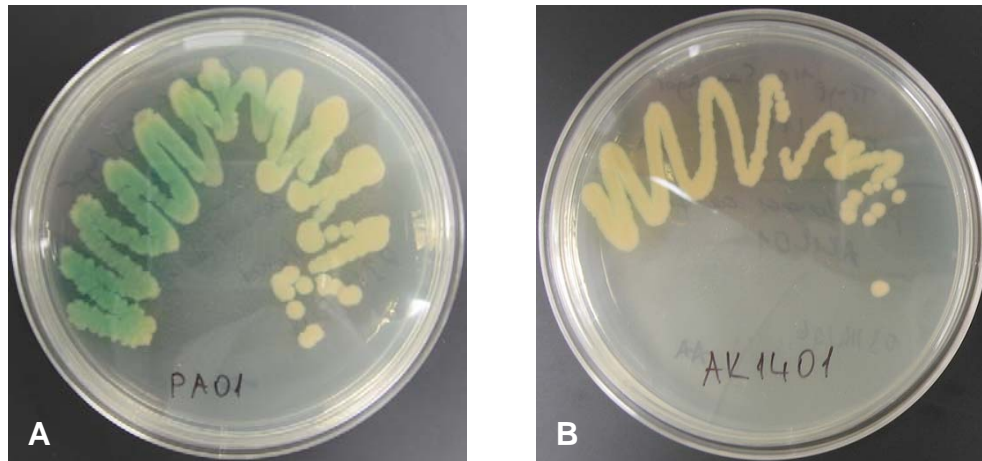
Figure 4.14 *P. aeruginosa* strains, PAO1 (A) and AK1401 (B), grown on TSA plates at 37°C.

The *P. aeruginosa* strains also express flagella and produces EPS and membrane vesicles. AFM images of *P. aeruginosa* PAO1 show the flagella and EPS molecules (Figure 4.15) *P. aeruginosa* is able to pool LPS into small regions on its outer membrane, and release membranous structures which are called membrane vesicle (MVs) [106].
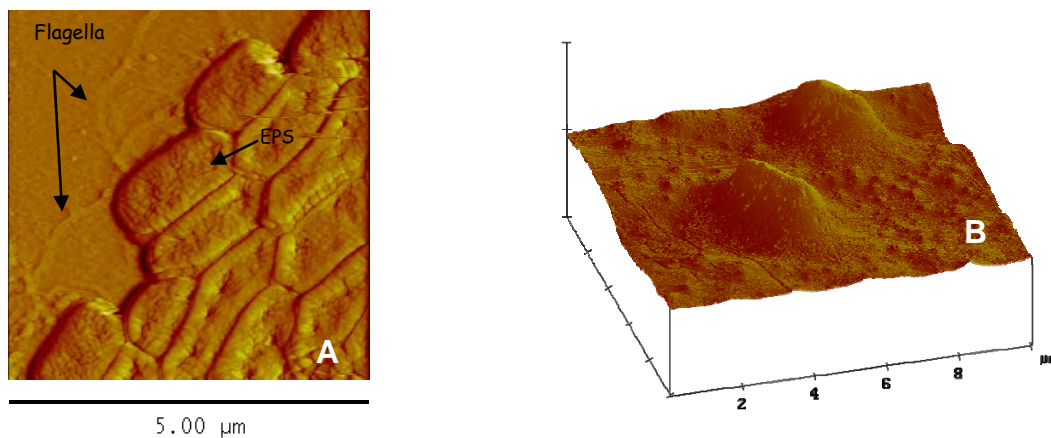
Figure 4.15 2D (A) and 3D (B) AFM images of *P. aeruginosa* PAO1 captured in air at room temperature showing the flagella and EPS.

4.4.1 AFM Force Curve Analysis

Figure 4.16 shows the approach curves of *P. aeruginosa* captured by AFM. The force at zero distance indicates the repulsive force applied by bacterial cell surface molecules to the AFM tip. As can be seen from the decay lengths obtained from AFM approach curves, the length of surface polymers of *P. aeruginosa* PAO1 is longer than that of *P. aeruginosa* AK1401. The repulsive forces at zero distance for strain PAO1 are higher than the ones for strain AK1401 (Figure 4.17). The neutral LPS of AK1401 can be responsible for smaller repulsive forces compared to the negatively charged LPS of PAO1 [103]. The decay length can be related to the length of the surface polymers of bacteria [12,39]. When the repulsion is stronger, the decay length becomes bigger and less representative of the length of the bacterial surface polymers. However, the decay length approximates how long the bacterial surface polymers are.
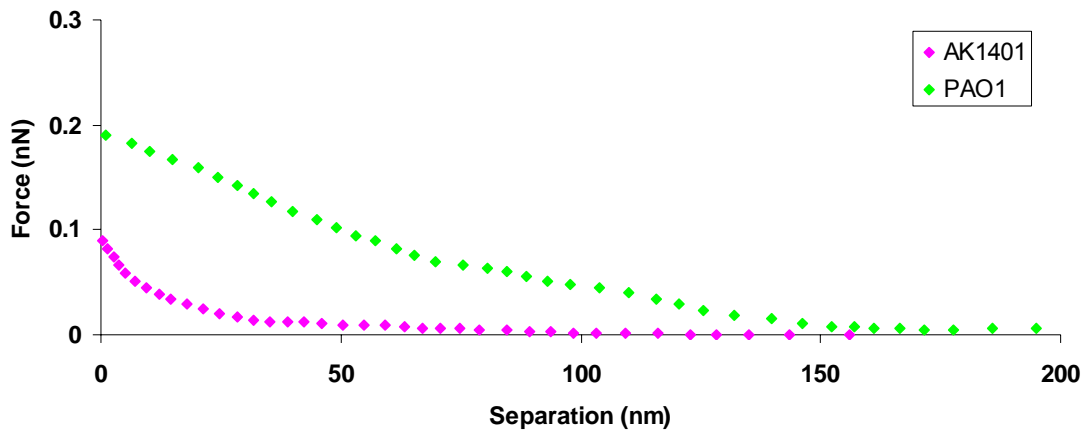
Figure 4.16 Representative approach curves of *P. aeruginosa* strains in water at room temperature. The cantilever CSC38-B was used.
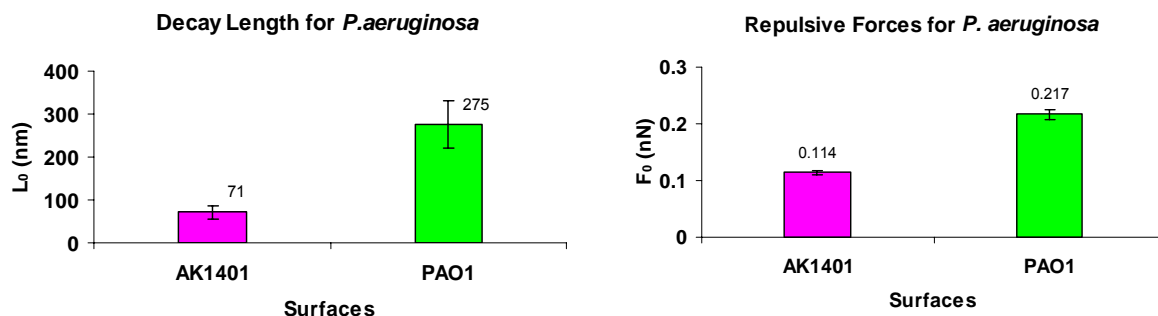
Figure 4.17 The decay length and the repulsive force at zero distance for *P. aeruginosa* strains from AFM approach curves. The *P. aeruginosa* strains are interacting with clean silicon tip in ultrapure water.

Frequently, some polymers from the surface of the bacterium attach to the probe, and their detachment from the probe occurs as the tip is being retracted. Each pull-off event causes a single peak or multiple peaks in the retraction curve, depending on the structure of polymers on the studied surface, and on the number of contact points between the polymers and the probe. We compared the retraction curves of the force cycles (Figure 4.18) for the bacterial cells bound to clean glass slides and probed by a clean silicon cantilever under ultrapure water to investigate the strength of adhesion. The strongest interactions, with an attractive magnitude of ~0.1 nN, occurred at around 300 nm from the surface for strain AK1401, and at around 800 nm from the surface for strain PAO1. Moreover, both of these systems show multiple peaks with different magnitudes in the retraction curves, indicating that multiple polymers have roles in the total interaction. We see a single peak when there is no polymer in the system, such as when probing glass slides.
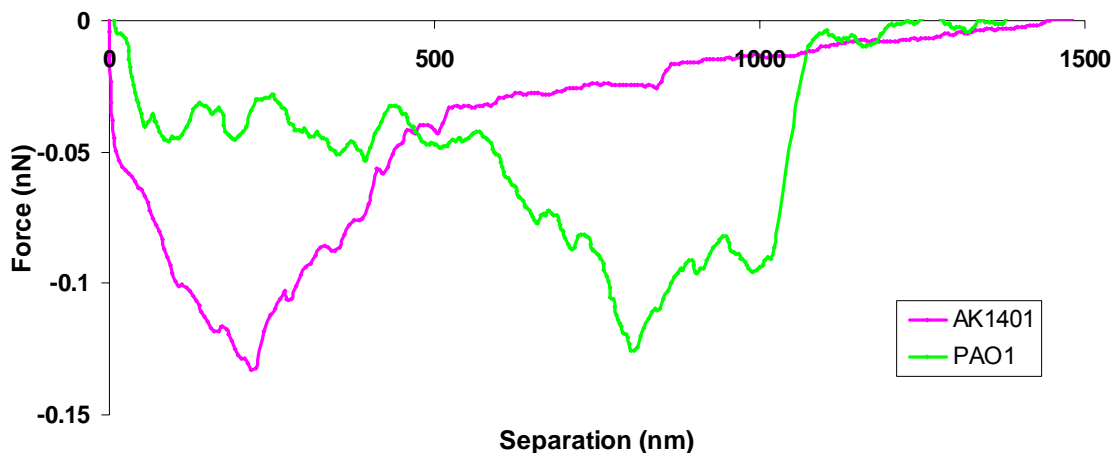
Figure 4.18 Representative retraction curves of *P. aeruginosa* strains probed by a clean AFM tip (CSC38-B) in ultrapure water at room temperature.

The fact that the interaction occurs over such a long range also indicates that the polymers are elastic and might be coiled on the bacterial surface (Figure 4.19). Both of these interactions are almost an order of magnitude stronger than those seen for proteins, BSA and Con A, probed by a clean silicon tip. Figure 4.20 and Figure 4.21 show summaries of the distributions of distance and force, respectively, for *P. aeruginosa* PAO1 and AK1401 interacting with the silicon AFM tip under ultrapure water. The pull-off distance was up to 1000 nm for *P. aeruginosa* PAO1 whereas it was around 500 nm for strain AK1401. Although it is not clear if the pull-off distances are accurate representatives of the length of bacterial surface molecules, the trend suggests that the surface molecules of strain AK1401 are shorter than those of strain PAO1.
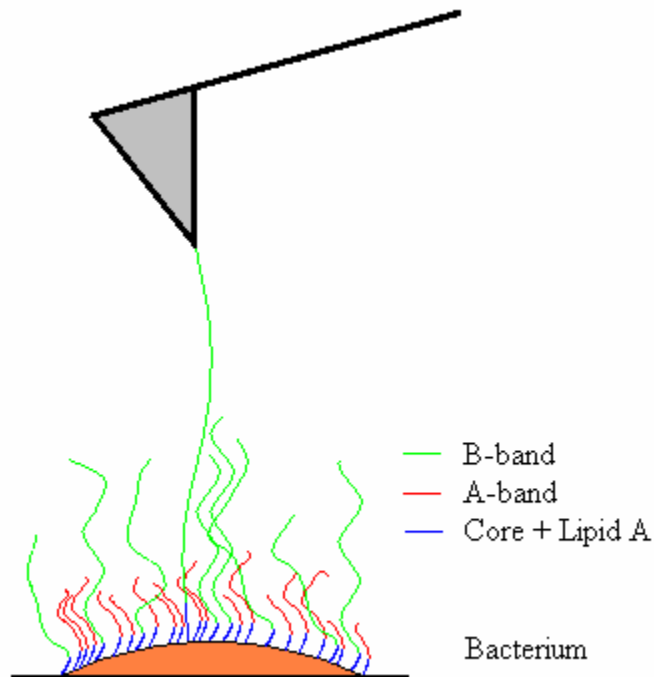
Figure 4.19 Schematic of AFM tip pulling and stretching the LPS molecules.

B-bands contain much longer polysaccharides than A-bands [100]. Lam et al. showed that strain PAO1 expresses 30 to 50 O-repeating units, with an approximate length of 39 to 65 nm, but they were not able to determine if the LPS polymers were coiled or fully extended [103]. Moreover, freeze substitution has shown that B-band LPS can extend up to 40 nm from the outer membrane [103]. A-band, common antigen, is expressed by most of the *P. aeruginosa* strains and is comprised of 10 to 20 repeating α-D-rhamnose units [98,101]. Moreover, *P. aeruginosa* is able to pool B-band LPS into membrane vesicles (MVs) (Kadurugamuwa, 1995), which can be 50 to several hundred nanometers in diameter [19,105]. Therefore, the long range interactions we observed might have been caused by MVs, in addition to LPS.
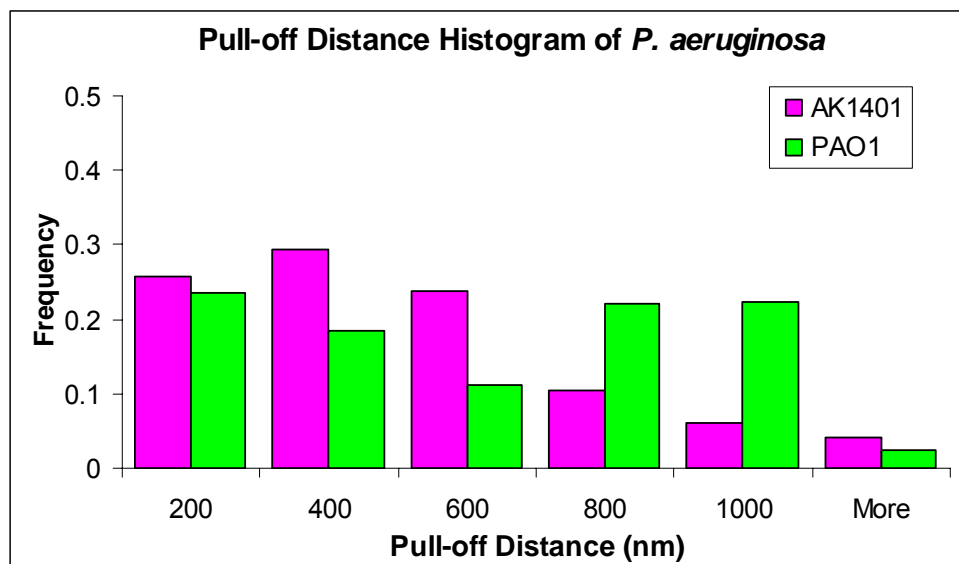
Figure 4.20 Pull-off distance histograms (n=50) of *P. aeruginosa* strains with clean AFM tip (CSC38-B). Measurements were made in ultrapure water at room temperature.
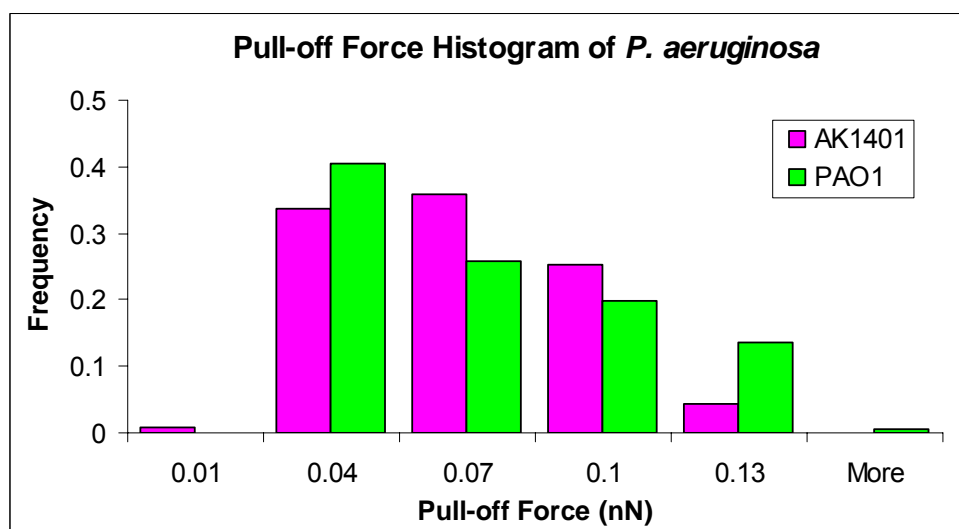
Figure 4.21 Pull-off force histograms (n=50) of *P. aeruginosa* strains with clean AFM tip (CSC38-B). Measurements were made in ultrapure water at room temperature.

There was no statistically significant difference (Mann-Whitney Rank Sum Test, P=<0.001) between the adhesion behavior of the two strains to silicon, which supports the hypothesis that the lipid A and core oligosaccharides are the most important molecules influencing the interaction of *P. aeruginosa* with silicon. Although it is not fully understood, the cells lacking B-band LPS demonstrated the highest surface electronegativity and this result suggests that the main surface charge determining groups are located in the core region of LPS molecule [107]. Langley and Beveridge also proposed that the negatively charged phosphoryl groups in the core-lipid A region of the LPS are the most important sites involved in metal binding by *P. aeruginosa* [50].

4.4.2 Contact Angle and Zeta Potential Results

Total surface free energy and zeta potential values were not significantly different for the two strains. According to water contact angle mesurements, *P. aeruginosa* AK1401, with a water contact angle value of 56.0 ± 1.9, was more hydrophobic than *P. aeruginosa* PAO1 with a water contact angle value of 47.4 ± 3.0 (Table 4.2). Makin and Beveridge have shown that the surface hydrophobicity of *P. aeruginosa* strains, measured by hydrophobic interaction chromatography (HIC), is as follows: $A^+ B^-$ (AK1401) > $A^- B^-$ > $A^+ B^+$ (PAO1) > $A^- B^+$ [107]. Moreover, B-band LPS plays an important role for initial attachment to hydrophilic surfaces since it makes the strains more hydrophilic [40].

The zeta potentials of both strains were similar and they were higher in ultrapure water than buffer, with values of -43.76 ± 0.81 mV for strain PAO1 and -42.84 ± 1.58 for strain

AK1401, compared to the zeta potential values in HEPES/DTT buffer, -16.91 ± 1.14 mV for strain PAO1 and -17.24 ± 1.32 mV for strain AK1401. These results are consistent with the literature because it was shown that the zeta potential of bacterial surface decreases and bacterial surface biopolymers get compressed with increasing salt concentration [39].

Table 4.2 Bacterial surface properties measured at room temperature.

Physicochemical Properties		Bacterium	
		P. aeruginosa PAO1	*P. aeruginosa* AK1401
Contact angles[1] θ (°), n = 8	θ^W	47.4 ± 3.0	56.0 ± 1.9
	θ^D	42.1 ± 2.5	41.0 ± 1.5
	θ^F	63.3 ± 3.9	63.6 ± 3.2
Surface energy components[2] (mJ/m^2)	γ_b^{LW}	28.07	29.91
	γ_b^{+}	0.17	0.12
	γ_b^{-}	57.36	42.29
	γ_b^{AB}	6.28	4.52
	γ_b	34.35	34.44
Zeta Potential (mV), n = 6	in water	-43.76 ± 0.81	-42.84 ± 1.58
	in HEPES	-16.91 ± 1.14	-17.24 ± 1.32

[1] θ^W, θ^D, θ^F are contact angles of water, diiodomethane and formamide on *P.aeruginosa* respectively.
[2] γ_b^{LW}, γ_b^{AB} are Lifshitz - van der Waals and Lewis acid - base surface free energy components of *P. aeruginosa* respectively.

4.4.3 DLVO Calculations

Interaction energy curves for *P. aeruginosa* PAO1 and AK1401 in 0.161 M HEPES/DTT buffer can be seen in Figure 4.22. The van der Waals and electrostatic interactions, and total energies are calculated from DLVO theory. For the DLVO calculations, the Smoluchowski equation (3.1) was used for calculation of microbial surface potentials. *P. aeruginosa* strains show an electrostatic repulsion about 2.48 kT at 0.3 nm using DLVO theory. Both strains show similar repulsive energy values because macroscopic properties were used to calculate interaction energies from DLVO theory. For both *P. aeruginosa* strains, the small repulsions are greatly balanced by van der Waals interactions, showing overall negative interaction energy (attraction) at very small separation distances. Interaction energies for *P. aeruginosa* PAO1 and AK1401 in ultrapure water are also calculated from DLVO theory and can be seen in Figure 4.23. The total energy of the system becomes positive (repulsive) at 5.3 nm, reaches a maximum value of 1.93 kT at 16 nm and decays to zero 150 nm for both strains. These results show that the bacterial cells are more negatively charged when they are in ultrapure water and electrostatic repulsion plays an important role in adhesion behavior.

The decay length obtained from DLVO calculations is much shorter compared to the one obtained from AFM force cycles. Therefore, the DLVO theory does not agree with the behavior seen in AFM force curves in our experiments because it only accounts for van der Waals and electrostatic interactions. Since there are other types of non-specific interactions such as steric and hydrophobic interactions, as well as specific chemical

interactions, they are also important in the overall interactions of the microbes. The DLVO theory is often not sufficient to explain bacterial adhesion due to complexities of biological surfaces [16]. These complexities modify the DLVO forces and add steric, hydrophobic, and bridging effects [12,34]. For example, polymers that are long enough to bridge the distance between cells and the surface may cause adhesion even when the cells do not experience short term attraction [51]. Also, surface roughness may affect bacterial adhesion and is not included in DLVO theory [37,52]. Therefore, the bacterial behavior shown in the AFM force curves must be due to some other physicochemical interactions.
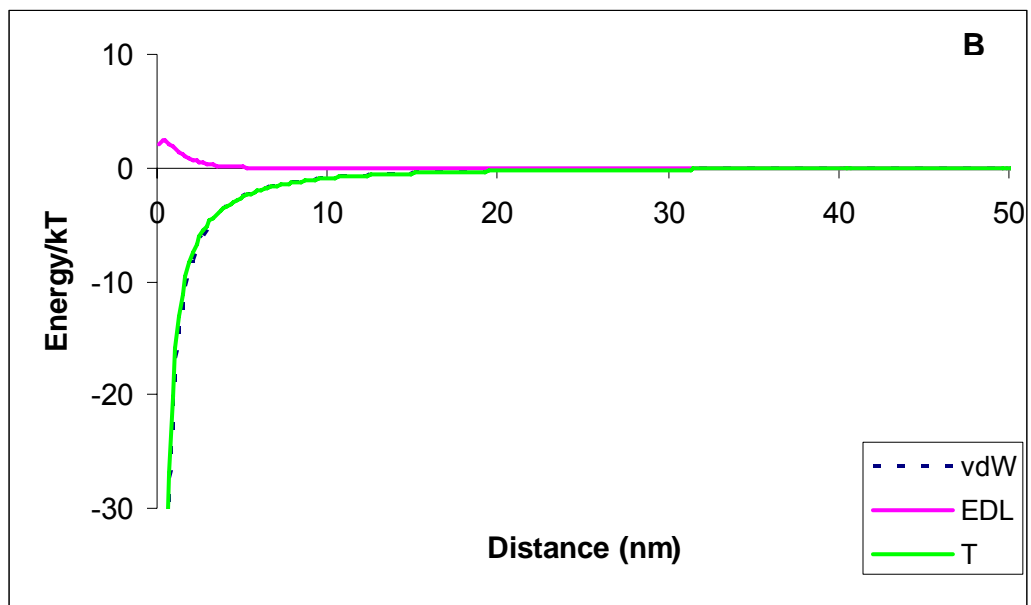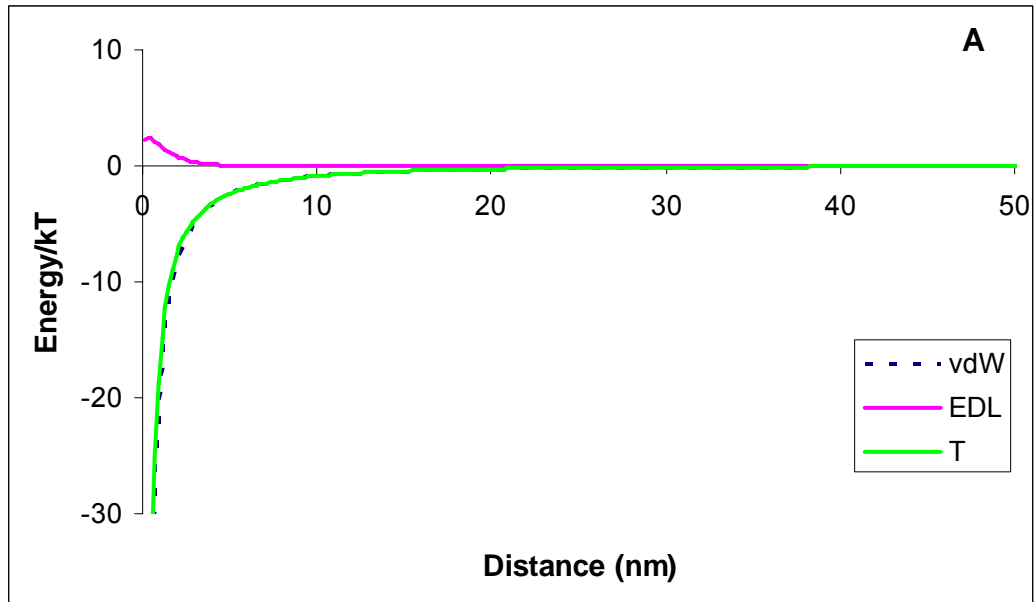
Figure 4.22 Interaction energies for *P. aeruginosa* PAO1 (A) and AK1401 (B in HEPES/DTT buffer (50 mM HEPES, 110 mM NaCl, 1 mM DTT). The total energy and the individual contributions for van der Waals and electrostatic interactions are shown.
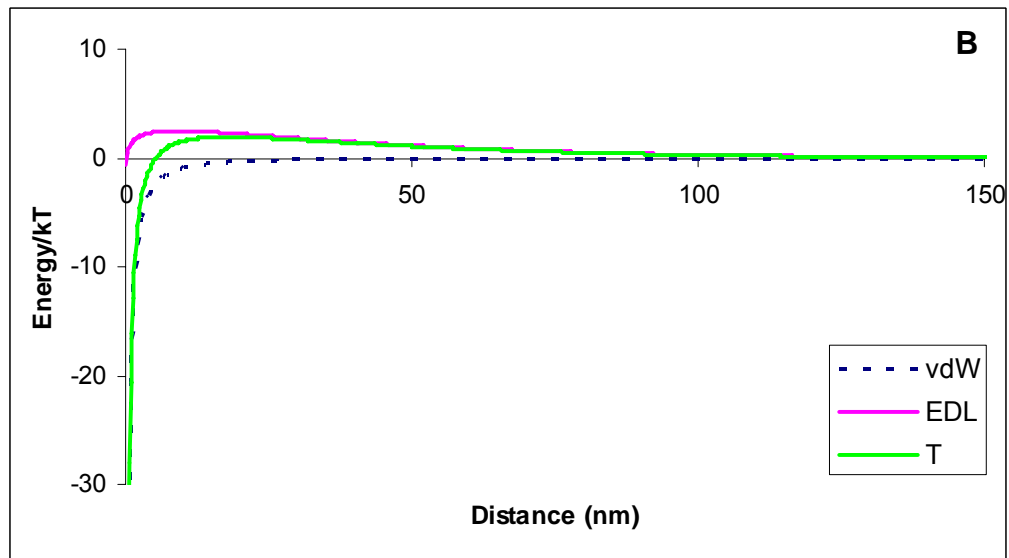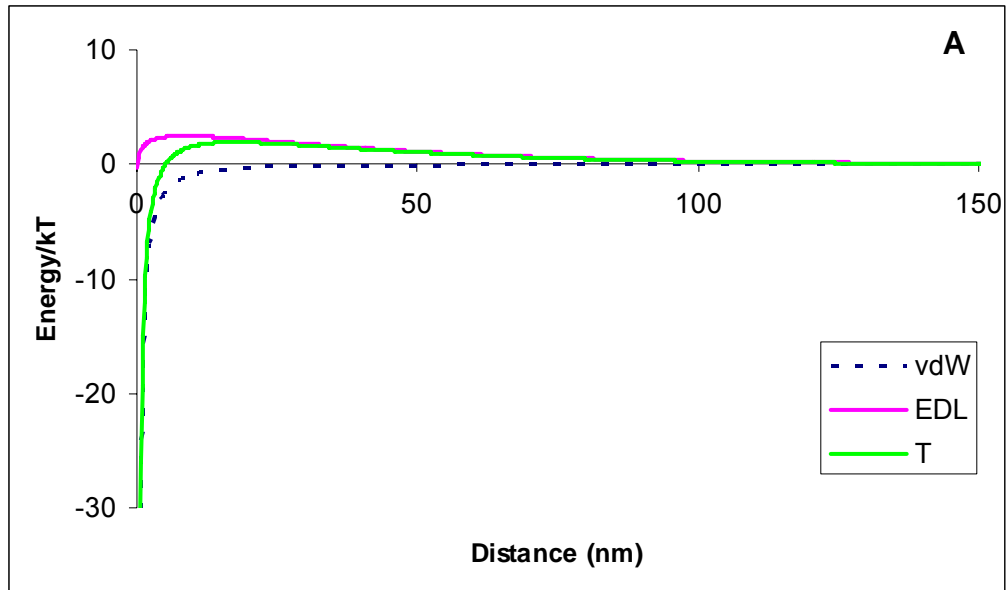
Figure 4.23 Interaction energies for *P. aeruginosa* PAO1 (A) and AK1401 (B) in ultrapure water. The total energy and the individual contributions for van der Waals and electrostatic interactions are shown.

4.4.4 Characterization of *P. aeruginosa* Supernatant Materials

Experiments with bacterial supernatant were performed to help us better explain the properties of the molecules produced and released by these two bacterial strains. The average heights of clusters from dried supernatant of PAO1 are greater than the values for AK1401 (Table 4.3 and Figure 4.24). The average height of the clusters were 23.44 ± 8.14 nm for the first supernatant and 17.76 ± 4.97 nm for the fourth supernatant of strain AK1401 whereas they were 348.37 ± 119.90 nm for the first supernatant and 58.82 ± 15.20 nm for the fourth supernatant of strain AK1401. These results suggest that first supernatants had more EPS molecules that can aggregate and form larger clusters. Since the fourth supernatant was obtained after four centrifugation steps with higher speeds, there were much less EPS or MVs and the height measurements are smaller compared to the ones for the first supernatants. When the two strains are compared, it is clear that *P. aeruginosa* PAO1 EPS forms larger clusters than *P. aeruginosa* AK1401. A and B band LPS were detected in PAO1 MVs whereas AK1401 MVs only had A band LPS [98]. *P. aeruginosa* PAO1 MVs possess outer membrane proteins, LPS and periplasmic constituents, and can be 50 to 250 nm in diameter [19]. MVs of *P. aeruginosa* PAO1 were also studied using contact mode AFM and shown to range in diameter from 25 nm to several hundred nanometers [105].

Table 4.3 Height measurements of *P. aeruginosa* EPS from AFM section analysis.

P. aeruginosa supernatants	Average size of EPS (nm)	
	PAO1	**AK1401**
First (n = 30)	348.37 ± 119.90	23.44 ± 8.14
Fourth (n = 20)	58.82 ± 15.20	17.76 ± 4.97
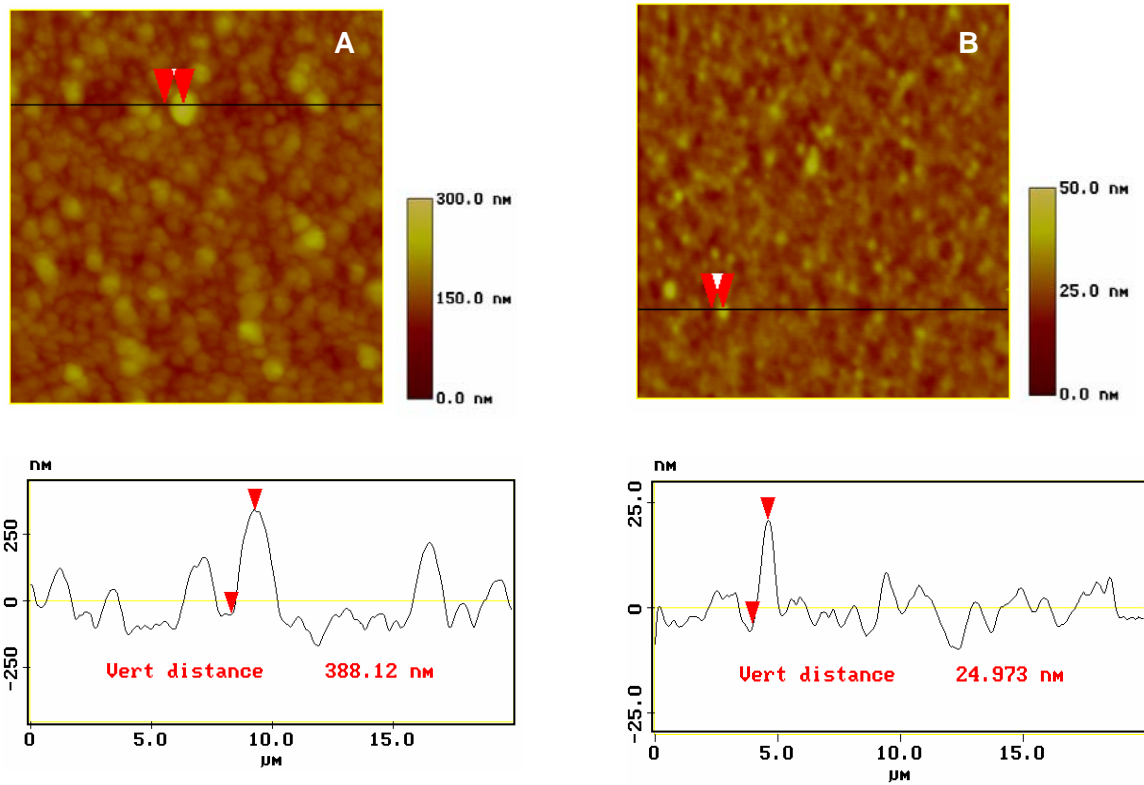
Figure 4.24 The AFM images of first supernatant of *P. aeruginosa* PAO1 (A) and AK1401 (B) filtered through 0.45 μm syringe filter and dried of clean glass slide.

Lowry Protein Assay

Although the AFM analyses provide useful information on the size of bacterial molecules, they can not tell us the composition of such molecules. The total protein content of the supernatant of the *P. aeruginosa* strains was measured using the Lowry protein assay. Protein standards of bovine serum albumin were assayed to develop the Lowry standard curve (Figure 4.25). The measurements were taken at an absorbance value of 660 nm.
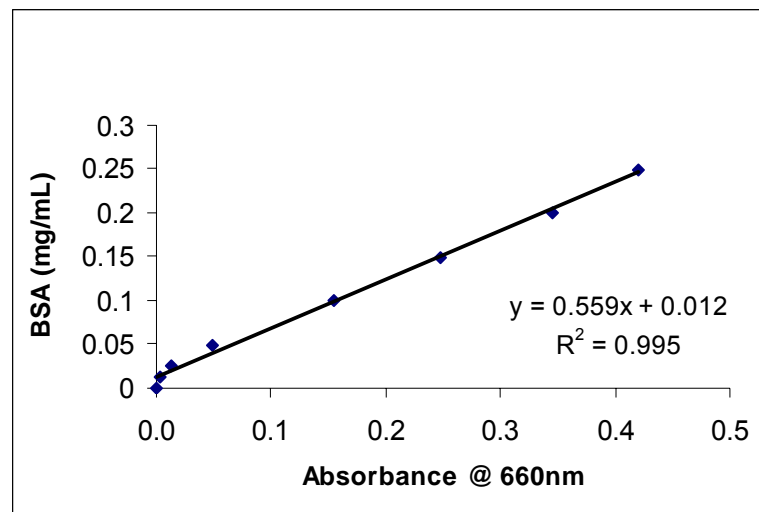
Figure 4.25 Lowry standard curve

The protein content of the supernatant was measured spectrophotometrically and the Lowry standard curve was used to calculate the amount of protein in the solution. Three replicates of each sample were tested and averaged. The EPS from the supernatant of *P. aeruginosa* PAO1 had 0.0056 mg·mL^{-1} protein and *P. aeruginosa* AK1401 had 0.0083 mg·mL^{-1} protein. These results suggest that AK1401 with shorter LPS has more protein

molecules in its EPS. It has been suggested that rough and semi-rough mutants may be associated with higher amounts of protein, not only because of MVs, but also because cellular proteins can leak from the cells into the EPS [98].

4.5 AFM Studies with Proteins

Topographical images and adhesion behaviors of two model proteins were investigated to better understand the protein structures and properties.

4.5.1 BSA

Immobilization of bovine serum albumin (BSA) was studied and optimum conditions for AFM experiments were investigated. Initially, BSA was dissolved in ultrapure water and immobilized on clean glass slides for AFM experiments. The final pH of protein solution was 4.5, the isoelectric point (pI) of BSA, when the protein molecules were fully dissolved in water. Figure 4.26 shows the AFM images of BSA in ultrapure water.
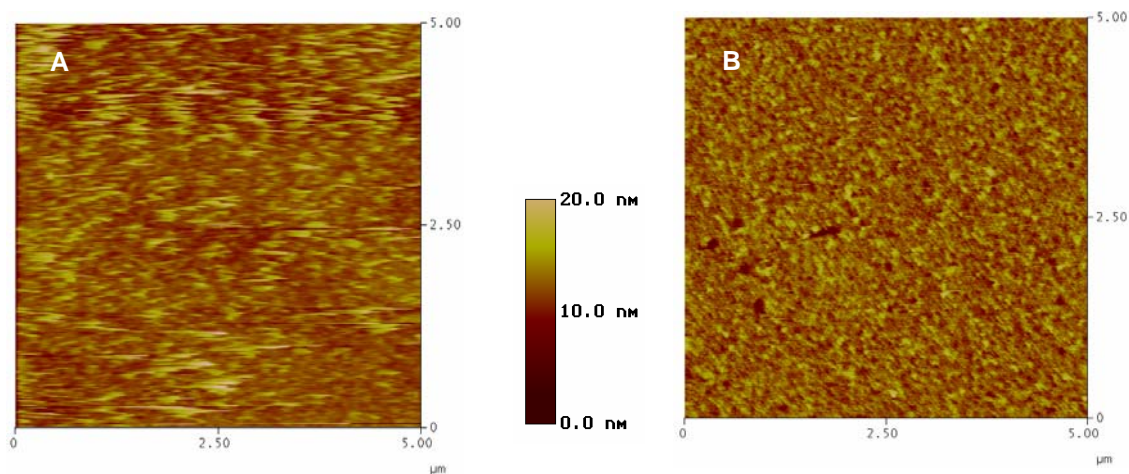
Figure 4.26 2D contact (A) and tapping (B) mode AFM height images of BSA which was dissolved (10mg/mL) and imaged in water (the bar indicates z scale).

Although deposition in water was simple and images could be obtained, we had concerns about the protein's stability. Secondly, HEPES/DTT buffer (50 mM HEPES/DTT, 110 mM NaCl and 1 mM DTT) with different pH values was used to see the effect of pH on protein immobilization. Dithiothreitol (DTT) was added to the buffer to reduce disulfide bonds, promote proteins to unfold, and maximize bonding to the glass slides. The maximum protein immobilization onto glass was obtained when BSA was dissolved in HEPES/DTT buffer and imaged at pH 4.5, as can be seen in Figure 4.27. Since BSA molecules are negatively charged above their isoelectric point, individual BSA molecules repel each other and the glass slide at the same time [115,116]. Therefore, when the protein was dissolved at pH 7.4, the protein molecules did not attach to the glass slide (Figure 4.28). When BSA was dissolved and immobilized in HEPES/DTT buffer at pH 4.5 and imaged by AFM at pH 7.4, BSA formed clusters on the glass slides and immobilization was successful (Figure 4.29). The images are consistent with what others have shown in terms of overall size and morphology [18,156]. Consequently, because physiological conditions are of interest when the proteins interact with bacterial cells, the

proteins were immobilized on glass slides at pH 4.5 and AFM experiments were carried

out in HEPES/DTT buffer at pH 7.4.
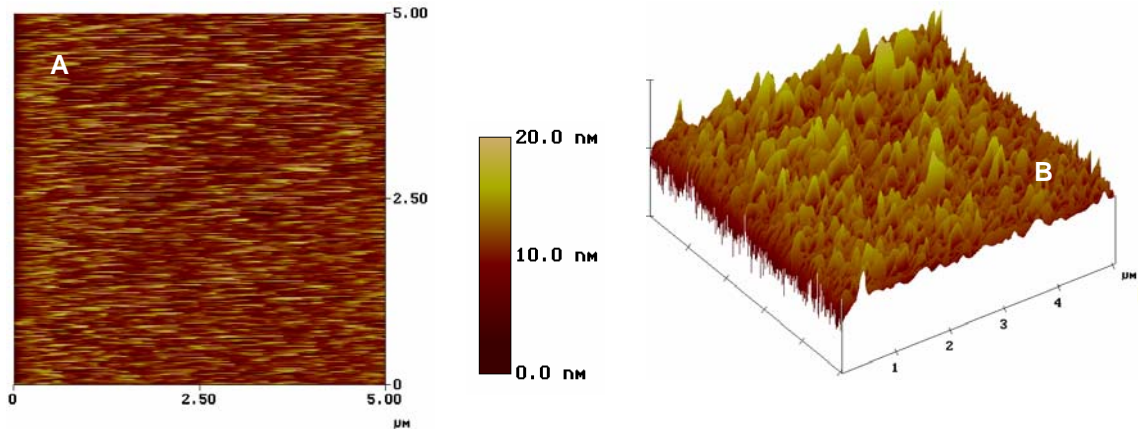
Figure 4.27 2D (A) and 3D (B) AFM height images of BSA, which was dissolved in HEPES/DTT buffer at pH 4.5 and immobilized on glass slides, and imaged in the same buffer (the bar indicates z scale).
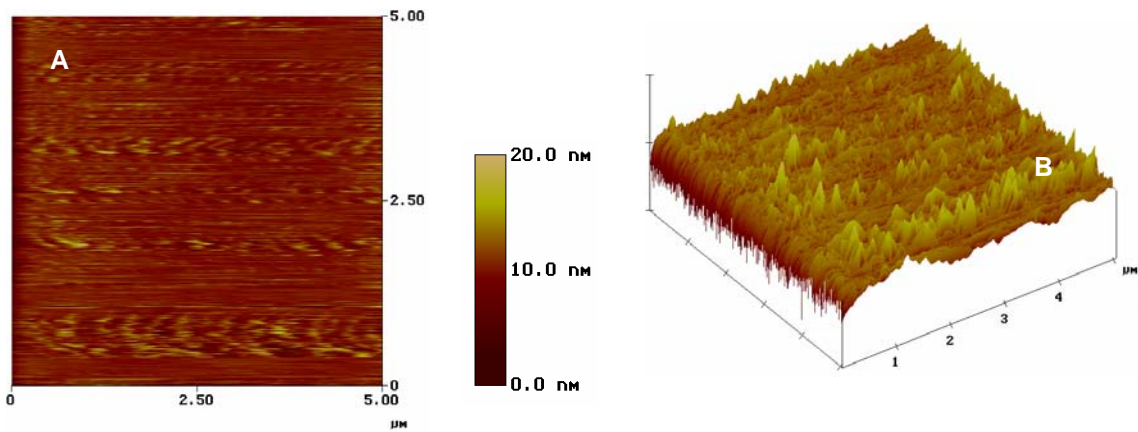
Figure 4.28 2D (A) and 3D (B) AFM height images of BSA, which was dissolved in HEPES/DTT buffer at pH 7.4 and immobilized on glass slides, and imaged in the same buffer (the bar indicates z scale).
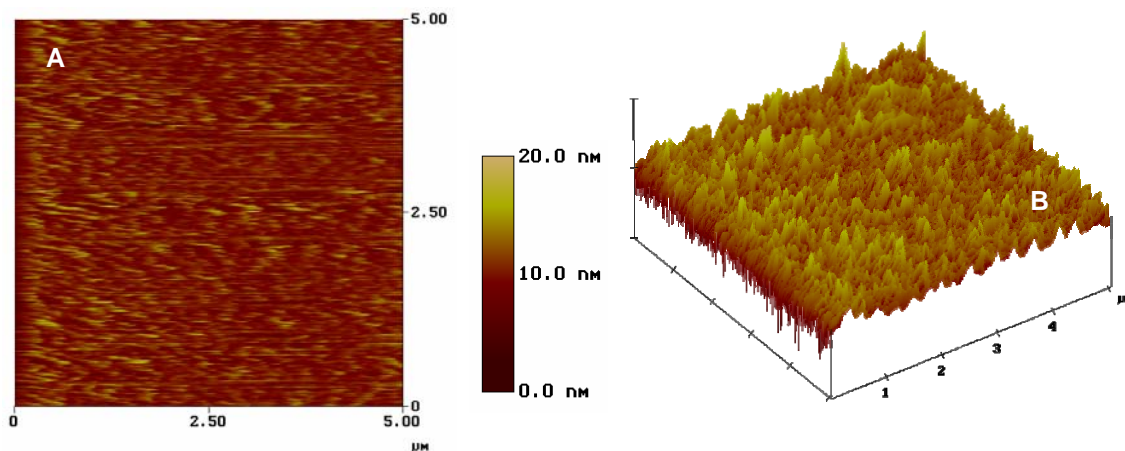
Figure 4.29 2D (A) and 3D (B) AFM height images of BSA, which was dissolved in HEPES/DTT buffer with pH 4.5 and immobilized on glass slides, and imaged in HEPES/DTT buffer with pH 7.4 (the bar indicates z scale).

The immobilization of BSA dissolved in HEPES/DTT buffer was more successful than when water was used. The BSA clusters were 7.55 ± 2.94 nm in HEPES/DTT and 3.95 ± 0.84 nm in water, from section analysis of five different images (n=30). When BSA was dissolved in water, height measurements ranged from 1-3 nm. The smaller height of the BSA clusters in water might be due to the denaturation of BSA during the adsorption process [115]. However, when BSA was dissolved in HEPES/DTT buffer, the range of height measurements was 4-15 nm, which indicates that there are different domains on different locations of the glass slides, and no denaturation. AFM images by other researchers showed that the domain sizes of BSA range from 5-10 nm [18] and various orientations are present, even on surfaces that are hydrophobic (CH_3), hydrophilic but nonionizable (OH), and hydrophilic and ionizable (HOOC) self-assembled monolayers (SAM) surfaces [115]. In our work, the imaging was continued for two hours to see if the BSA molecules were detaching from the glass slides, but there was no indication of BSA detachment after two hours. Others have shown that when the proteins were covalently

bond to the glass slides compared to physically adsorbed, the magnitude of adhesion forces to silicon was the same [18,125,126].

Force Measurements for BSA

Thirty force curve cycles (approach and retraction) were recorded for BSA in HEPES/DTT buffer at pH 7.4. Figure 4.30 shows the reproducibility of the approach curves. Retraction curves were different in each force measurement because the orientation of BSA on the glass slides can vary, and different sites of BSA can be responsible for individual adhesion peaks (Figure 4.31). Compared to the adhesion peaks in ultrapure water, stronger adhesion peaks were observed in HEPES/DTT buffer.
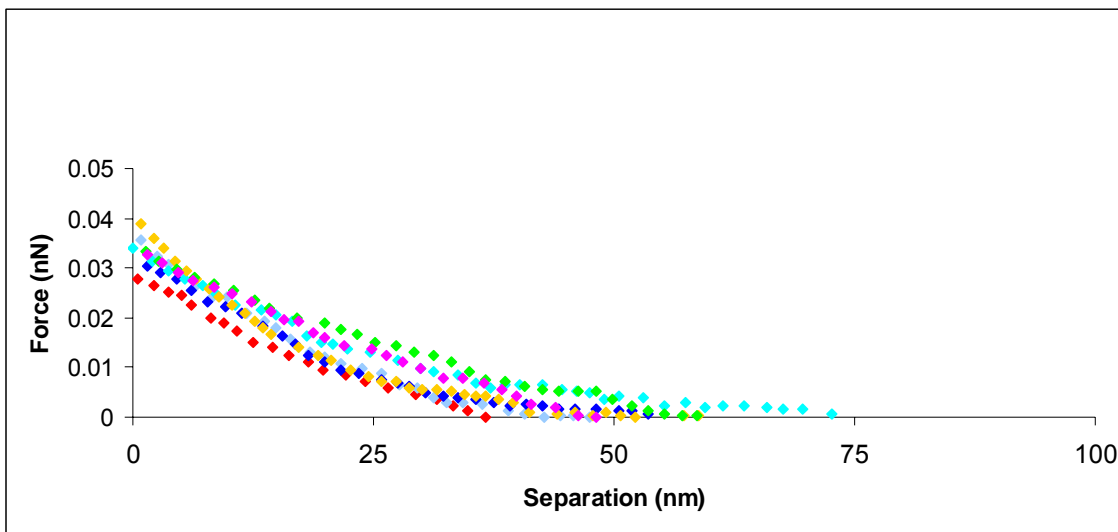
Figure 4.30 Representative approach curves of BSA on glass slides probed by silicon AFM tip in HEPES/DTT buffer at pH 7.4. Five of 30 curves are shown.
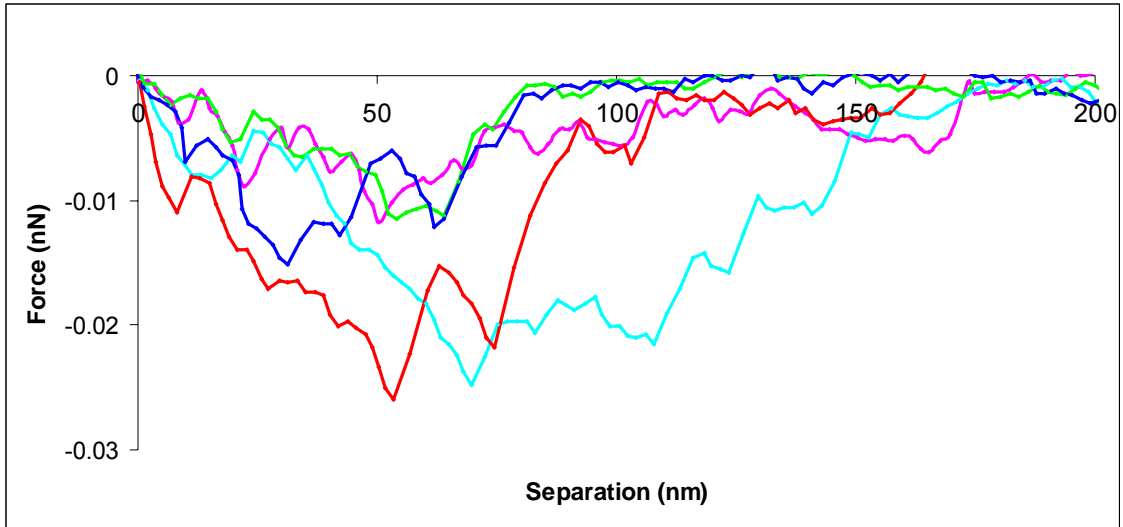
Figure 4.31 Representative retraction curves of BSA on glass slides probed by silicon AFM tip in HEPES/DTT buffer at pH 7.4. Five of 30 curves are shown.

The AFM tip was also coated with BSA molecules and used to probe a clean glass slide. As can be seen from Figure 4.32, there were no repulsive forces captured and results were reproducible. The magnitude of adhesive forces for BSA and glass were similar to the ones for BSA and silicon. However, pull-off distances were shorter when the BSA molecules were on the AFM tip (Figure 4.31 and Figure 4.33).
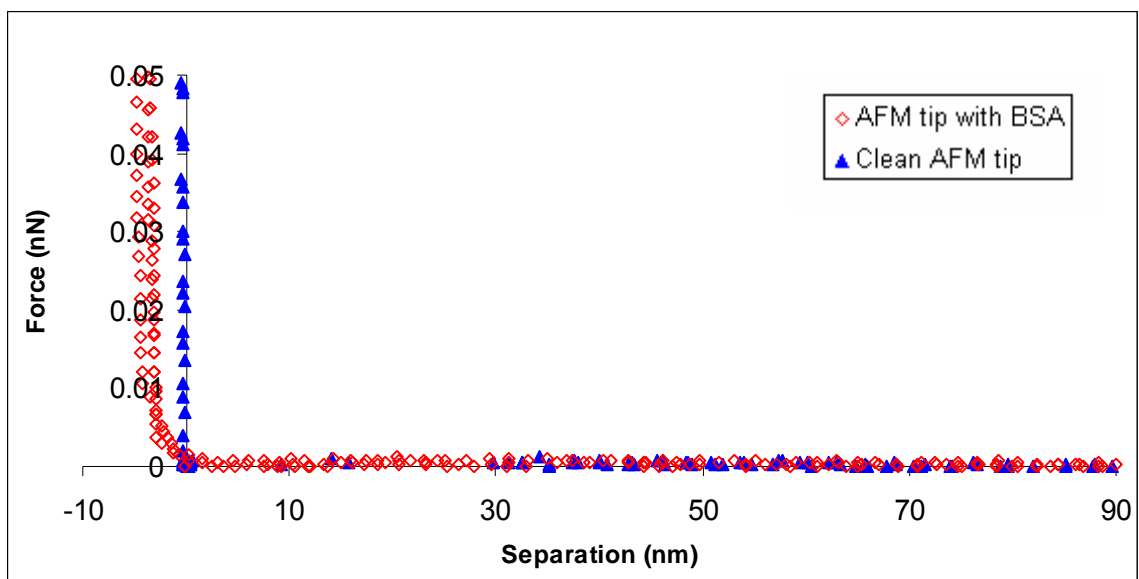
Figure 4.32 Representative approach curves of BSA on AFM tip and clean AFM tip interacting with a clean glass slide in HEPES/DTT at pH 7.4. The interactions below zero can be explained by the compression and the indentation caused by the movement of BSA molecules on the AFM tip.

Since the chemistries of glass and silicon are different, BSA interacts with these surfaces differently. The magnitude of adhesion forces is similar but the pull-off distance is shorter when BSA is interacting with glass. Different geometries might be another reason for different interactions. When BSA-silicon interactions are studied, a clean tip is probing BSA molecules immobilized on the glass slide. However, BSA is immobilized on the AFM tip and probing the glass slide for BSA-glass interactions. Since the tip is approaching to the glass surface, the AFM tip might not be able to detect the repulsion caused by the negatively charged BSA molecules. We do not know the orientation and surface coverage of the AFM tip with BSA molecules, but Figure 4.33 shows that the interactions of the tip are completely different when probing the glass slide, so these

results suggest that the AFM tip certainly has some BSA molecules interacting with the glass.
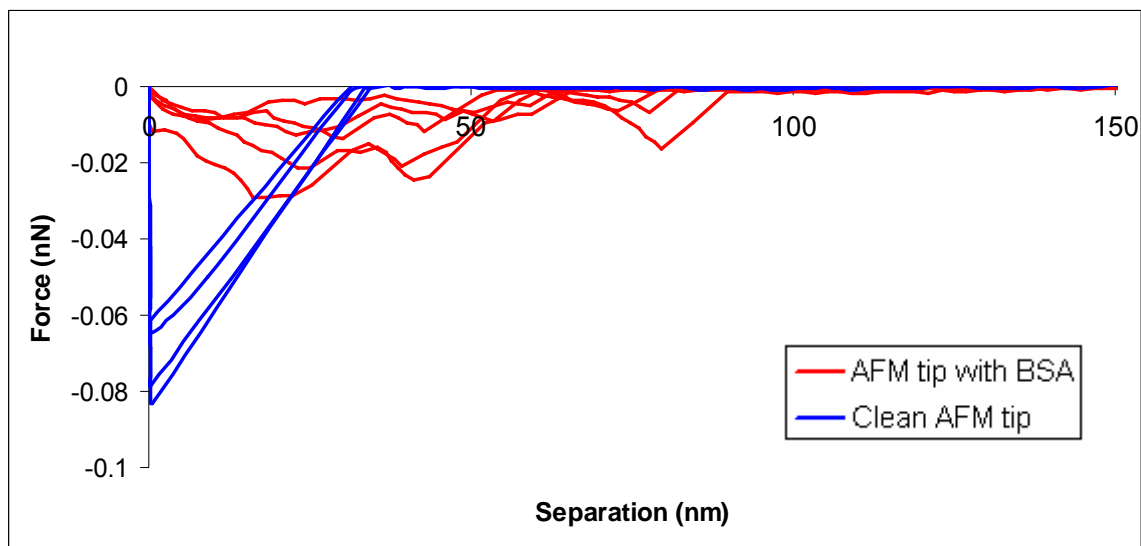
Figure 4.33 Representative retraction curves of BSA on AFM tip and clean AFM tip interacting with a clean glass slide in HEPES/DTT at pH 7.4.

Finally, 1-hexadecanethiol (HDT) was used to see if covalent bonding affects the behavior of BSA and force curves. Glass slides were coated with HDT and soaked in BSA solution. Slides were rinsed with HEPES/DTT buffer solution prior to AFM experiments. The surface coverage, average size of BSA molecules, and magnitude of force curves were the same when no HDT was used (Figure 4.34).
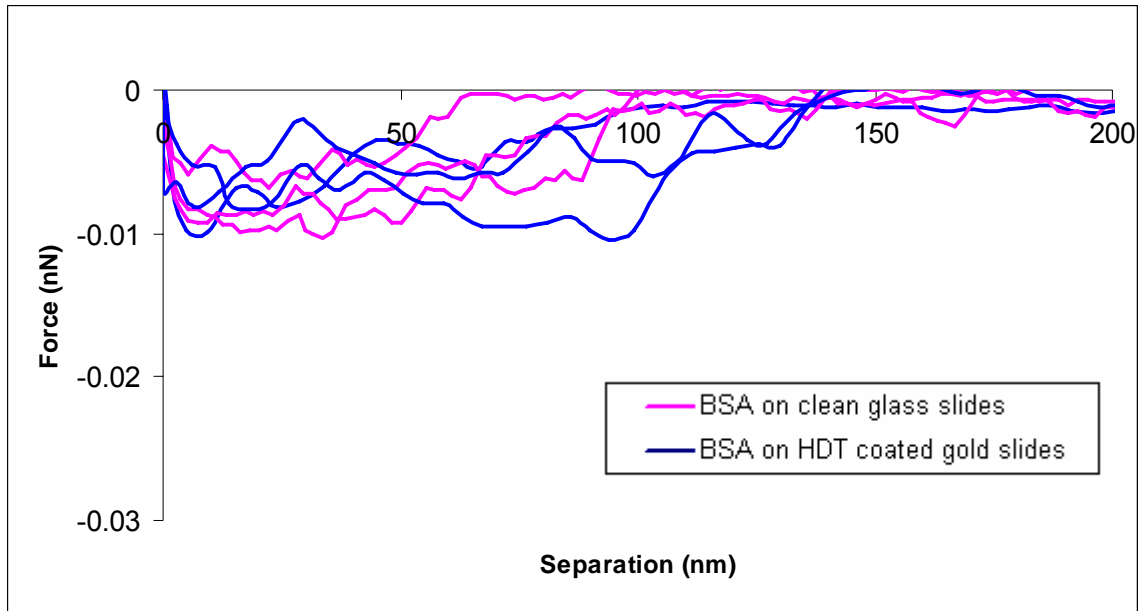
Figure 4.34 Representative retraction curves of BSA on clean glass slide and HDT coated gold slides probed by CSC38-B in ultrapure water.

The BSA molecules were also probed by stiff cantilevers (Mikromasch NSC36-C, k~0.6 N·m^{-1}) to see if cantilever spring constant affects the force measurements. There was no adhesion peak because the interactions were small and the cantilever was not able to capture them. Figure 4.35 shows a representative force cycle (approach and retraction curve) when the BSA was probed by the cantilever NSC36-C. Therefore, softer cantilevers (Mikromasch CSC38-B, k~0.3 N·m^{-1}) are chosen to capture the small interactions of proteins with silicon and bacterial cells.
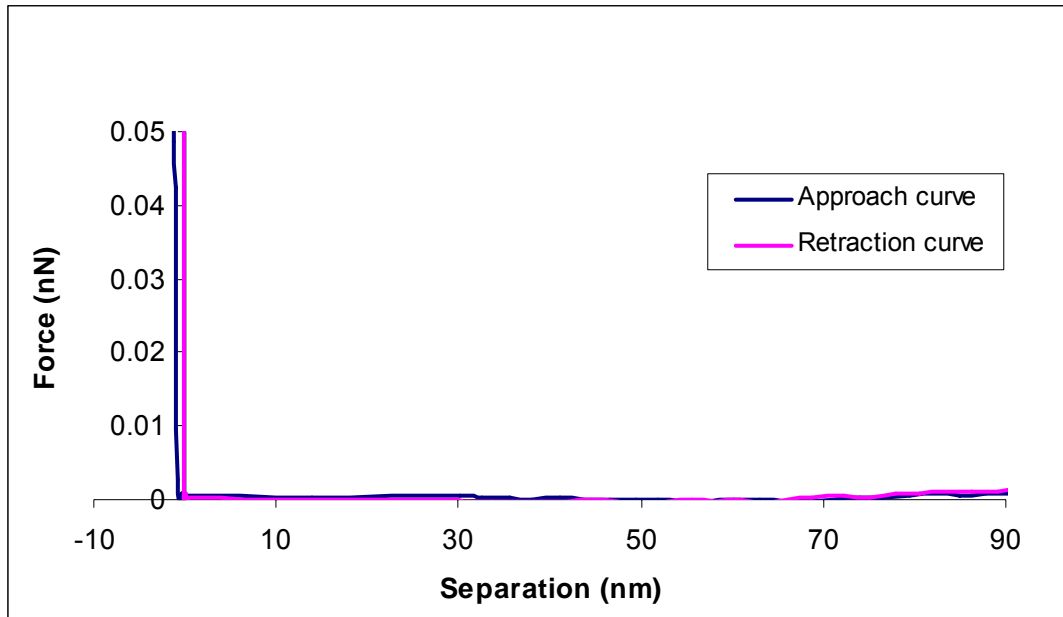
Figure 4.35 Approach and retraction curves of BSA immobilized on a clean glass slide and probed with a stiff cantilever (Mikromasch NSC36-C, k~0.6 N/m) in ultrapure water.

4.5.2 Concanavalin A

Concanavalin A (Con A) is a plant lectin [125,126], which is capable of binding to α-D-mannose and α-D-glucose [127]. Since lipopolysaccharides are important for adhesion of bacteria, the role of lectins in cell adhesion is of interest of many researchers. Con A molecules were immobilized on glass slides at pH 4.5 and AFM experiments were carried out in liquid at pH 7.4. HEPES/DTT buffer (50 mM HEPES, 110 mM NaCl and 1 mM DTT) was used for all experiments. Figure 4.36 shows the AFM image of Con A molecules immobilized on glass slides. The size of Con A clusters was 12.04 ± 3.16 nm (n=30), which is consistent with literature data of single Con A tetramers with

dimensions of 6.7 nm x 11.3 nm x 12.2 nm [132,134]. The observed 12 nm layer from

AFM experiments suggests that there are one or two layers of Con A on the glass surface.
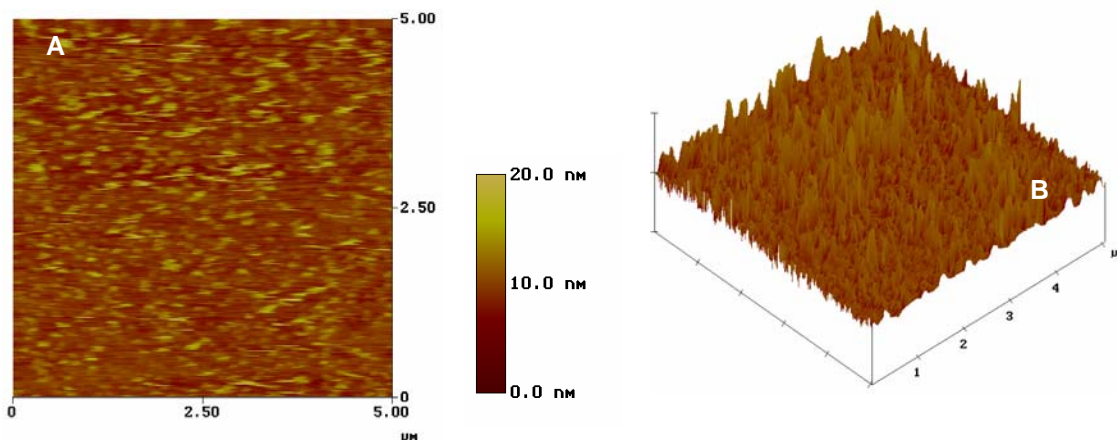
Figure 4.36 2D (A) and 3D (B) AFM height images of Concanavalin A which was dissolved in HEPES/DTT buffer at pH 4.5 and immobilized on glass slides, and imaged in HEPES/DTT buffer at pH 7.4 (the bar indicates z scale).

Force Measurements for Con A

Thirty force curve cycles (approach and retraction) were recorded for Con A in HEPES/DTT buffer at pH 7.4. Figure 4.37 shows the reproducibility of the approach curves. Retraction curves were different in each force measurement because the orientation of Con A on glass slides is not known, and different sites, some of which are specific to certain sugar molecules, of Con A molecules can be responsible for individual adhesion peaks (Figure 4.38).
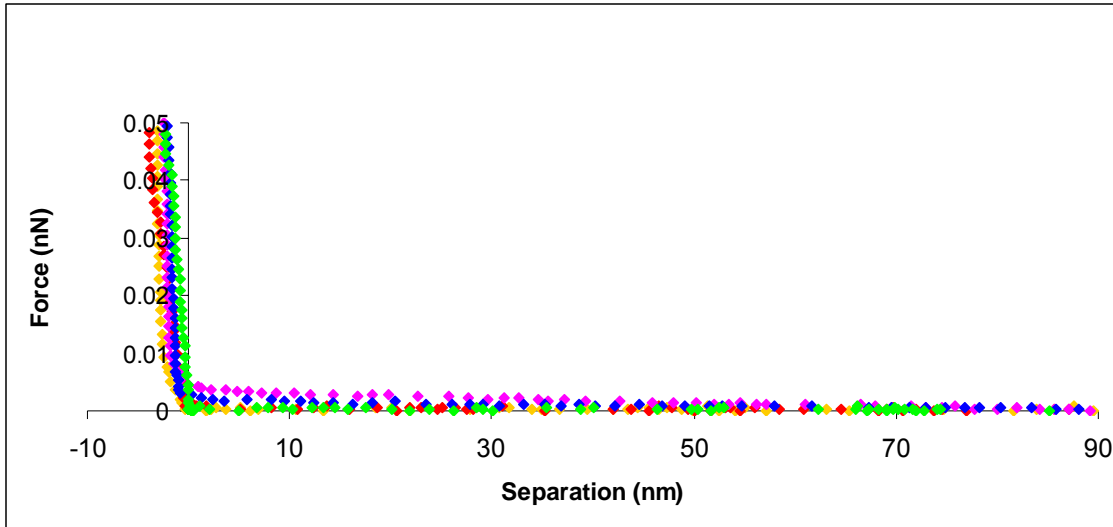
Figure 4.37 Representative approach curves of Con A on glass slides probed by silicon AFM tip in HEPES/DTT buffer with pH 7.4. Five of 50 curves are shown.
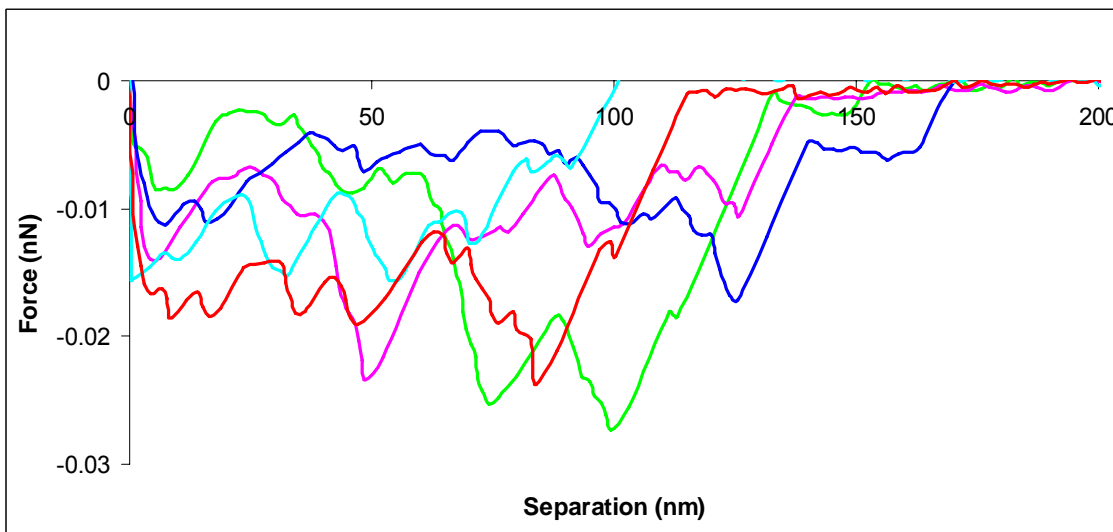
Figure 4.38 Representative retraction curves of Con A on glass slides probed by silicon AFM tip in HEPES/DTT buffer with pH= 7.4. Five of 50 curves are shown.

4.5.3 BSA – Con A Comparison

The properties of BSA and Con A were investigated by zeta potential and AFM experiments. Comparison of results was useful for future experiments and helped to explain the differences between these two proteins.

4.5.3.1 Zeta Potential of Proteins

Proteins are negatively charged above their isoelectric point. The isoelectric points of BSA and Con A are around 4.5 [115,130]. According to zeta potential measurements, BSA and Con A were both negatively charged (Table 4.4) in physiological buffer (pH = 7.4). However, Con A is less negatively charged compared to BSA. The zeta potential values were -8.86 ± 1.12 mV for BSA and -1.46 ± 0.35 mV for Con A at pH 7.4. Xu et al. showed that the zeta potential of BSA was -9.9 mV at pH 7.0 [156] .

Table 4.4 Zeta potentials of proteins in HEPES/DTT buffer at pH 7.4 at room temperature.

Samples	Zeta Potential (mV)
BSA	-8.86 ± 1.12 (n=6)
Con A	-1.46 ± 0.35 (n=6)

4.5.3.2 Comparison of AFM Force Curves of Proteins

Immobilized proteins on glass slides were stable after washing processes by water and HEPES/DTT buffer solution, and sustained the pressure exerted by AFM tips during imaging. The size of protein clusters, determined by AFM section analysis, was 7.55 ± 2.94 nm for BSA and 12.04 ± 3.16 nm for Con A in HEPES/DTT based on five different images (n=30). The fact that Con A clusters were larger than BSA clusters might be explained by 3D protein structure and molecular weight differences since the average molecular weight of Con A (102 kDa) is larger than that of BSA (66 kDa) [18].

According to the approach curves, the repulsive force at zero distance for BSA was higher than that of Con A. Since BSA molecules are more negatively charged in physiological buffer, the repulsion between the silicon tip and BSA molecules is stronger than the repulsion between Con A and the silicon tip. The magnitude of the repulsive forces was 0.003 ± 0.002 nN for Con A and 0.029 ± 0.005 nN for BSA (Figure 4.39). The decay length was 19 ± 5 nm for Con A and 51 ± 14 nm for BSA (Figure 4.40). When the molecules on the glass slide repel the AFM tip, the decay distance is not a good representative of the length of the polymers. For example, AFM images of BSA suggest that the size is 7.55 ± 2.94 nm, but the BSA decay lengths are larger, at 51 ± 14 nm. However, if there is no repulsion, for example Con A-silicon interactions, the decay distance is closer to the size of the clusters and can better represent the length of the polymers on the surface. Twenty force curves were analyzed, and compared by using t-test analysis since the mean values could represent the system. According to t-test

analysis, the difference in the mean values of each pair is greater than would be expected by chance; there is a statistically significant difference between the repulsive forces and decay distance (P = <0.001).
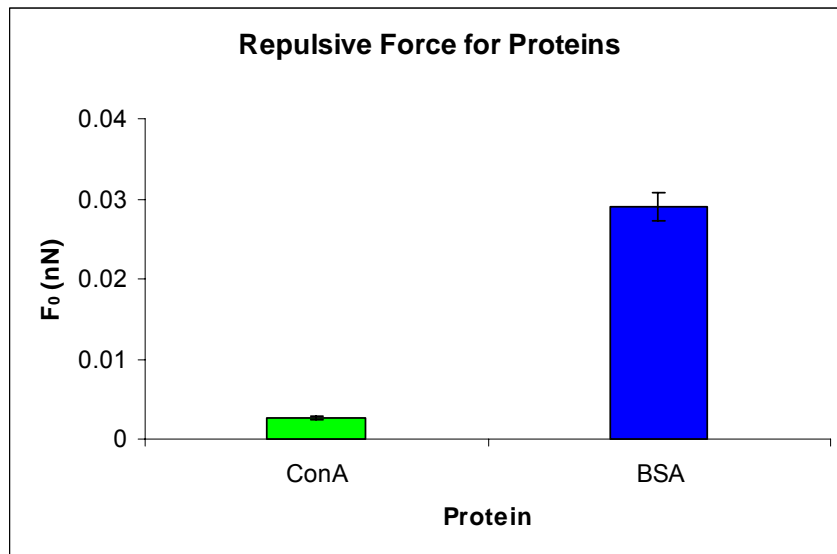
Figure 4.39 Repulsive force at zero distance for proteins from AFM approach curves.
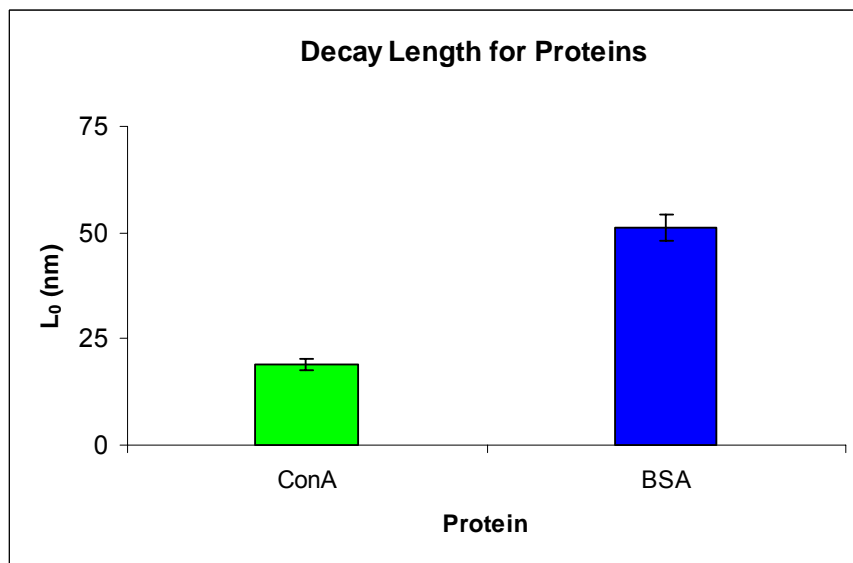
Figure 4.40 Decay length for proteins from AFM approach curves.

Since different locations on the glass slide contain different active sites of protein molecules, the pull-off forces and pull-off distances exhibit a range of values that can be presented in a histogram. Since the population size is large, a-non parametric statistical test can be used to compare two groups. The difference in the median values of pull-off distances of two proteins is greater than would be expected by chance; there is a statistically significant difference (P = <0.001) according to the Mann-Whitney Rank Sum Test (Figure 4.41). In addition, Figure 4.42 shows the difference in the magnitude of pull-off forces, which are also statistically significant when BSA forces is compared to Con A forces (P = <0.001). Since Con A has specific sugar sites and can competitively adhere to corneal epithelial cells and block *P. aeruginosa* adhesion, its structure and adhesion behavior might be similar to the LPS of *P. aeruginosa* [136].
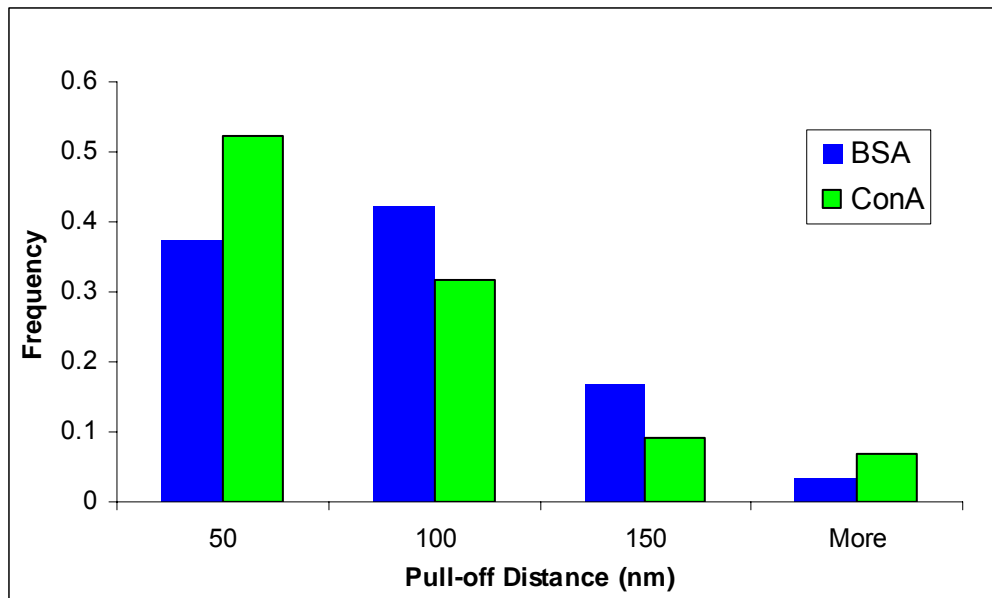
Figure 4.41 Pull-off distance histograms (n=50) of BSA and Con A with silicon AFM tip (CSC38-B), which indicates the separation of AFM tip from the protein surface. Measurements were made in HEPES/DTT buffer at pH 7.4.
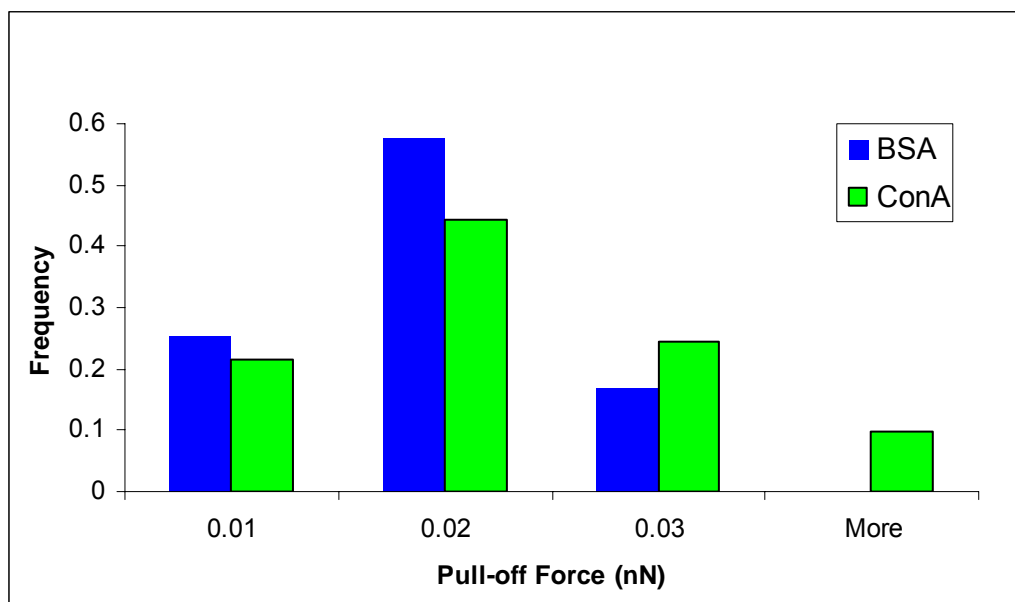
Figure 4.42 Pull-off force histograms (n=50) of BSA and Con A with silicon AFM tip (CSC38-B), which indicates the magnitude of forces occurred when the silicon tip was retracting from the protein surface. Measurements were made in HEPES/DTT buffer at pH 7.4.

4.6. Protein - *Pseudomonas aeruginosa* Interactions

P. aeruginosa strains cause serious infections, especially in immunocompromised patients [20,33]. On the other hand, they are effective isolates in biodegradation of hazardous contaminants in the environment, so they can be used for bioremediation of contaminated soils or wastewater [79,84]. These bacteria find receptors on epithelial cells and use different ligands to attach to various substrates [33]. For example, some proteins on the epithelial cells are found to be responsible for bacterial adhesion to the corneal epithelial cells. Proteins play an important role in bacterial adhesion and recognition of pathogens [27]. Moreover, proteins are one group of recognizable organic matter from the environment, and play an important role in bacterial transport in natural environments

97

[31]. Therefore, it is important to understand the interactions between proteins and bacterial cells. In the present study, bovine serum albumin (BSA) and concanavalin A (Con A) are model proteins chosen to represent protein molecules that might affect adhesion of the two *P. aeruginosa* strains, PAO1 and AK1401.

4.6.1 SEM Imaging

The silicon AFM tips were modified with poly-l-lysine and coated with bacterial cells to probe protein molecules. We verified adhesion of the cells on the cantilevers after preparation of the bacteria coated AFM tips. Examination of the AFM tips with SEM showed the bacterial cells bound to the cantilever with multiple cells present on the tip (Figure 4.43). Since we could only image dry samples with SEM, the cantilevers were dried after probing the protein molecules. In addition to SEM imaging, the AFM force curves are a good indicator of difference between clean tip and bacteria coated tip probing the protein molecules. When the AFM tip is successfully coated with bacterial cells, we can see long range interactions between the probe and the protein molecules. It can also been observed that how long the bacterial cells stay on the surface of the AFM tip and probe the surface. If the bacterial cells detach from the tip, there are no long range interactions between the tip and the protein molecules. This is a good control for the system because the presence of bacterial cells on the AFM tip at the time of the experiment can be verified. Others also used poly-l-lysine (PLL) [143] and different binding materials such as polyethyleneimine (PEI) and glutaraldehyde [148,157], and 1-Hexadecanethiol (HDT) [43] to immobilize microbial cells on different AFM tips.

Velegol and Logan showed that treating bacteria with 2.5% glutaraldehyde stiffens the cell and changes the adhesion behavior of the bacterial cells [14]. Therefore, PLL was chosen over PEI and glutaraldehyde.
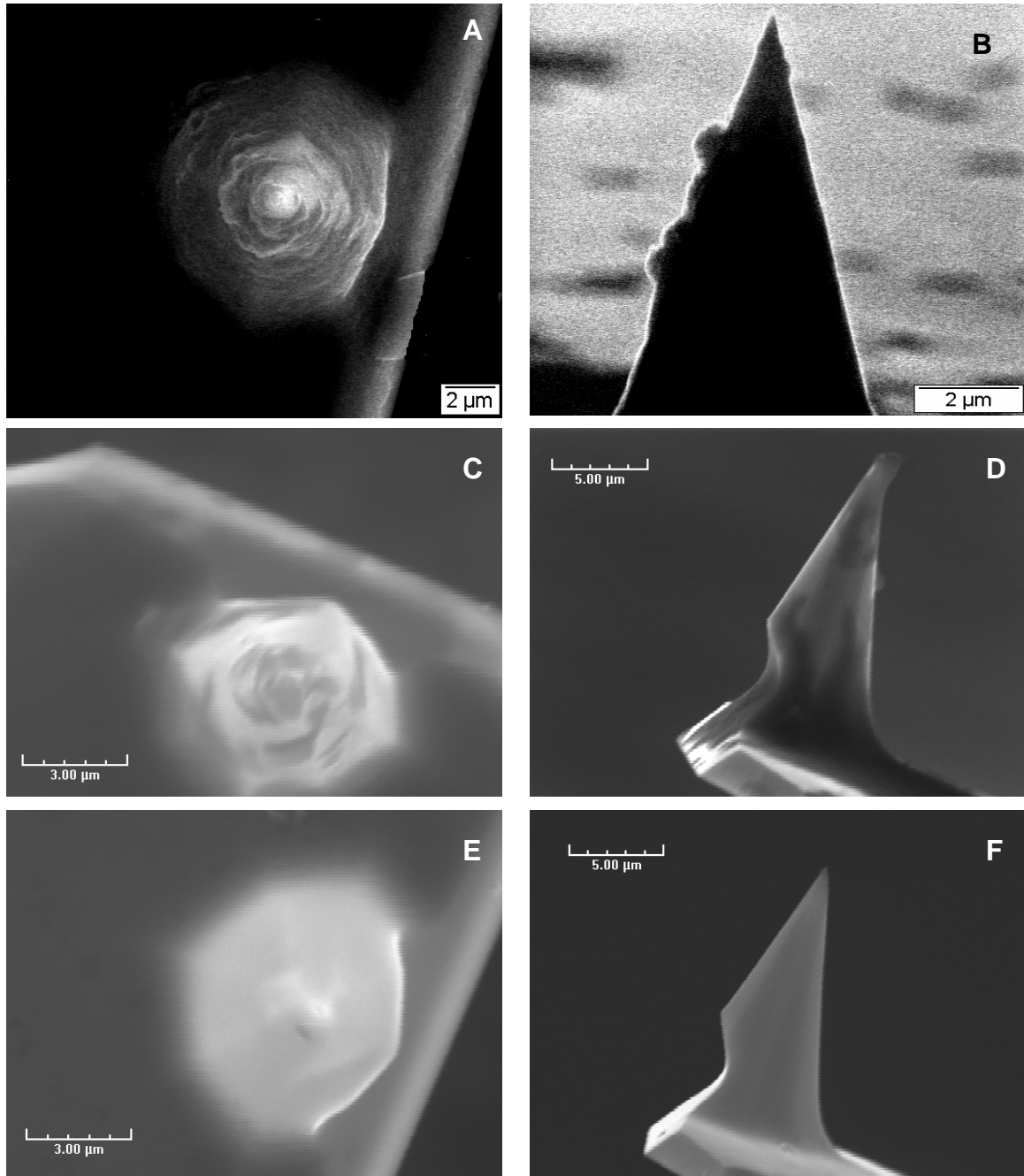
Figure 4.43 SEM images of silicon Mikromasch CSC38-B cantilever coated with *P. aeruginosa* AK1401 (A, B) and PAO1 (C, D), and PLL (E, F).

4.6.2 BSA – *P. aeruginosa* Interactions

The AFM force curves show differences between the clean tip and bacteria coated tip probing the surface. The bacteria coated AFM tip has stronger and longer interactions with BSA molecules compared to the clean silicon AFM tip, suggesting that the bacterial cell surface polymers can interact with the protein molecules (Figure 4.44). Figure 4.45 shows that the pull-off distances for BSA and silicon interactions are between 0 to 200 nm. However, when BSA interacts with *P. aeruginosa* strains, the pull-off distances can extend up to 900 nm. Figure 4.46 shows that the pull-off (adhesive) forces for BSA and silicon interactions are smaller than 0.03 nN. However, when BSA interacts with *P. aeruginosa* strains, the adhesive forces are up to 0.09 nN for PAO1 and 0.2 nN for AK1401. Since there are different orientations of BSA molecules on the glass slides interacting with bacteria, and the bacterial surface is also heterogeneous, the adhesive force and pull-off distance vary over a wide range.
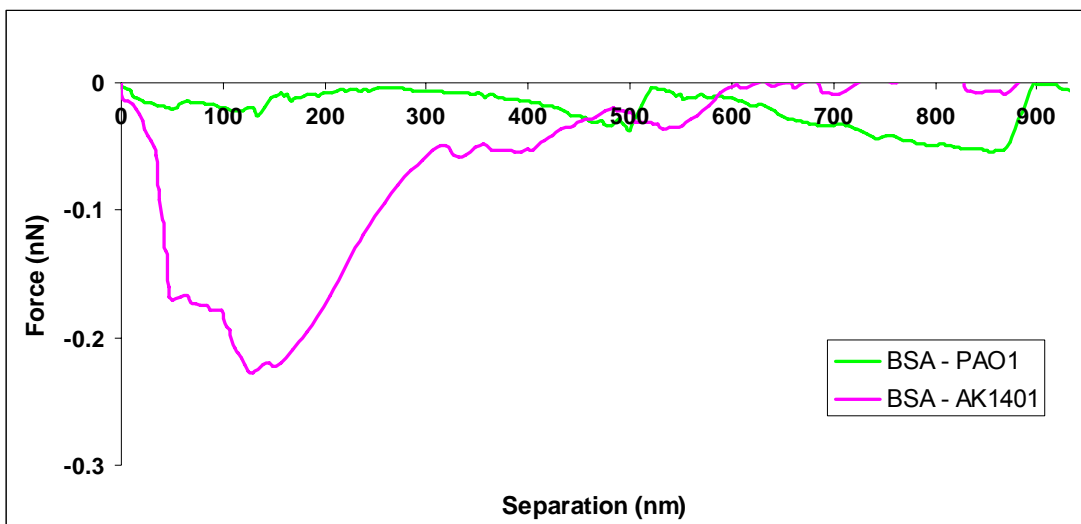
Figure 4.44 Representative retraction curves of BSA on glass slides probed by *P. aeruginosa* strains immobilized on AFM tip in HEPES/DTT buffer at pH 7.4.

The Kruskal-Wallis One Way Analysis of Variance (ANOVA) test was used to check if the adhesion behavior of both *P. aeruginosa* strains was statistically different. According to the results of the test, there was a statistically significant difference (P =< 0.001) between the magnitude of adhesion forces and between the range of pull-off distances for both strains when they interact with BSA molecules. Therefore, different LPS structures of two strains play an important role when they are interacting with BSA. Since PAO1 has longer pull-off distances than AK1401, B-band polymers affect the adhesion behavior and result in weaker interactions than A-band polymers. When each pair from the histogram are compared, the differences in the median values among the treatment groups are greater than would be expected by chance, showing that there is a statistically significant difference (P < 0.05, Dunn's Method).
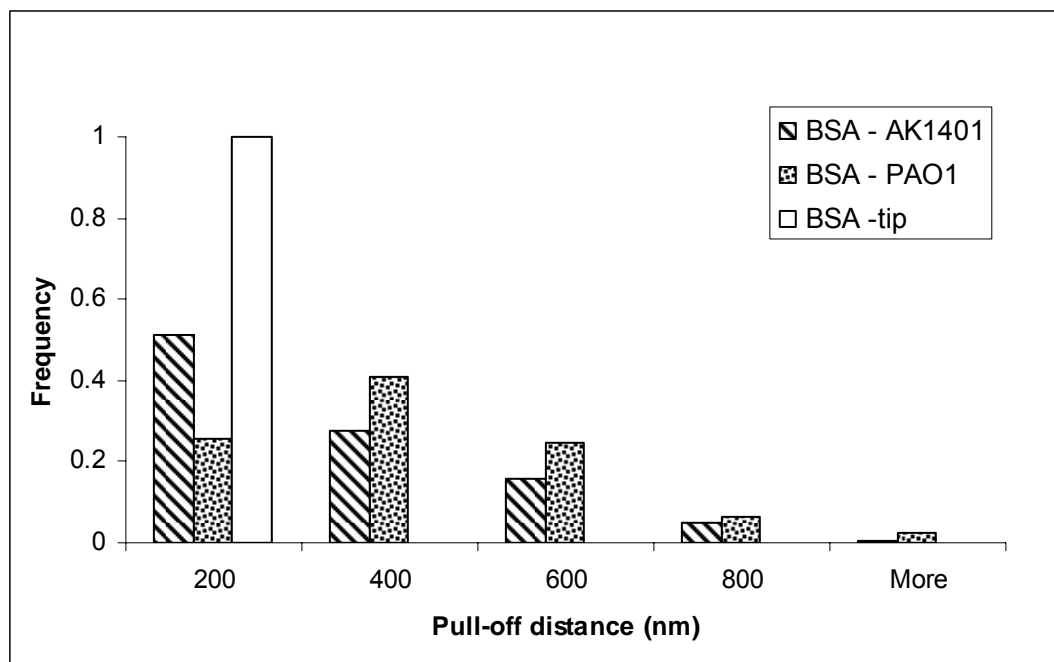
Figure 4.45 Pull-off distance histograms (n=50) of BSA with clean and modified AFM tip (CSC38-B). Measurements were made in HEPES/DTT buffer at pH 7.4.
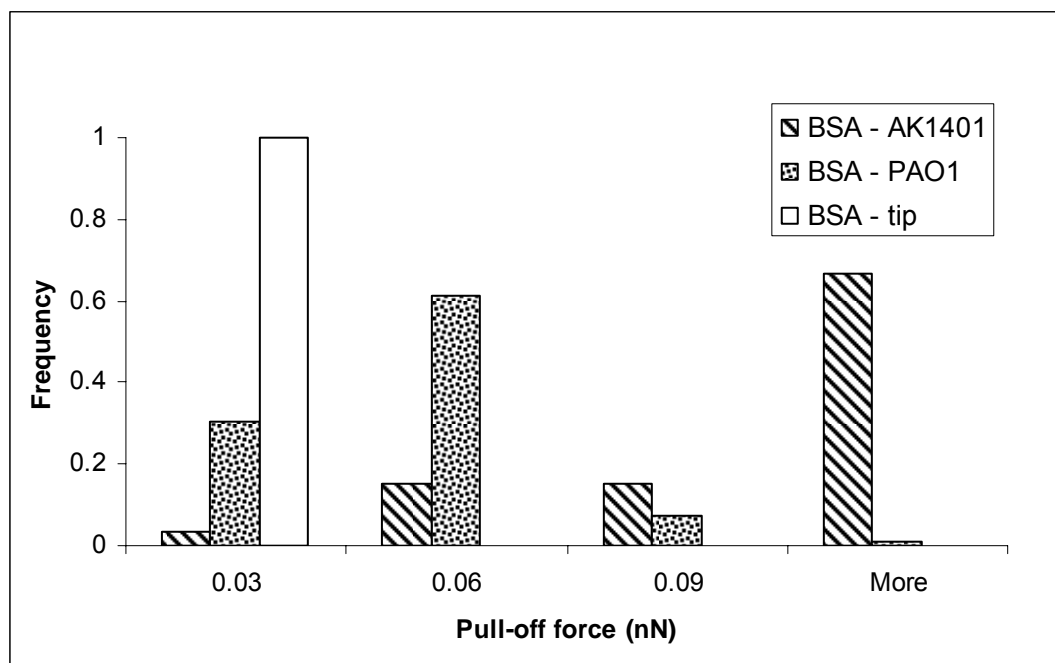
Figure 4.46 Pull-off force histograms (n=50) of BSA with clean and modified AFM tip (CSC38-B). Measurements were made in HEPES/DTT buffer at pH 7.4.

The magnitude of the average adhesive forces for AK1401 was larger than that of PAO1 (Figure 4.47). In other words, the adhesion of AK1401 to BSA molecules was much stronger than the adhesion of PAO1. AK1401 has mostly neutral polysaccharides on its surface, and BSA molecules are negatively charged in physiological pH, our results suggest that the BSA molecules strongly interact with the surface polymers of AK1401 and weakly interact with the negatively charged LPS of PAO1 due to differences in electrostatic repulsion [90,99]. The LPS of PAO1 is more negatively charged and the longer B-band polymers can hinder the exposure of A-band and core-region polysaccharides, the latter which might be the most important molecules for the adhesion of *P. aeruginosa* cells [50].
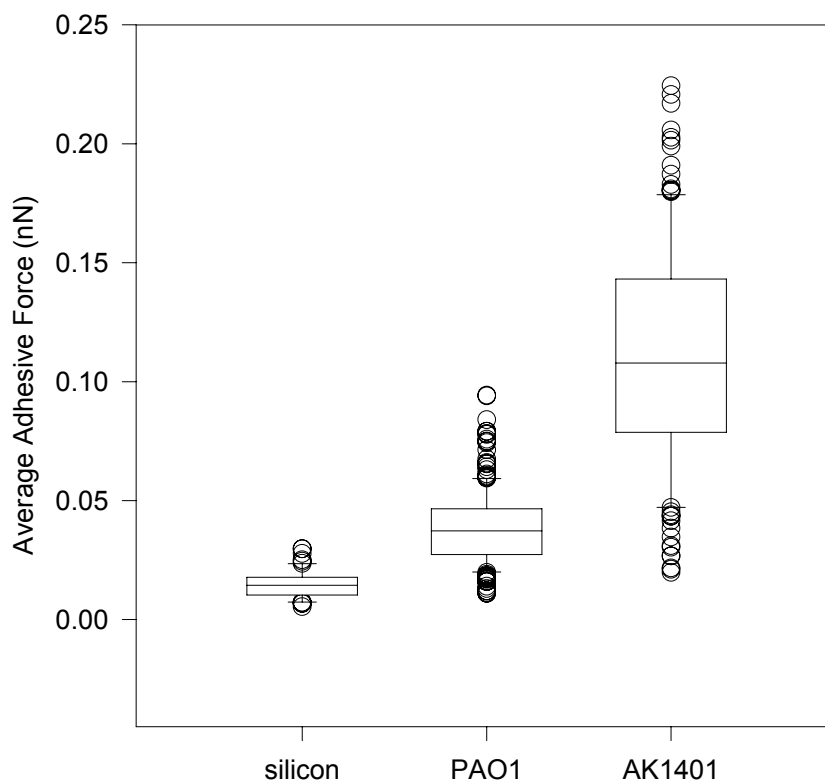
Figure 4.47 A comparison of average adhesive forces of BSA interacting with various probes. Measurements were made in HEPES/DTT buffer at pH 7.4.

4.6.3 Concanavalin A – *P.aeruginosa* Interactions

The AFM force curves show the difference between the clean tip and bacteria coated tip probing the surface. The bacteria coated AFM tip has weaker but long range interactions with the Con A molecules compared to the clean silicon AFM tip, which shows that the bacterial cell surface polymers are interacting with protein molecules (Figure 4.48). We also examined the interaction of the PLL coated AFM tip with the Con A molecules to be certain that the weak interactions were caused by bacterial surface molecules. Figure 4.49 shows that the pull-off distances are between 0 to 200 nm for the Con A - silicon

103

interactions, and between 0 to 100 nm for the Con A – PLL interactions. However, when Con A interacts with *P. aeruginosa* strains, the pull-off distances can extend more than 200 nm. Figure 4.50 shows that the pull-off (adhesive) forces can be up to 0.04 nN for the Con A - silicon interactions and 0.03 nN for the Con A - PLL interactions. Nevertheless, when Con A interacts with *P. aeruginosa* strains, the adhesive forces are smaller than the ones with the clean silicon tip and the PLL coated tip (Figure 4.51). The median value of adhesive forces to Con A is 0.0085 nN for AK1401, and 0.005 nN for PAO1. The wide ranges in force and distance histograms can be explained by the different orientation of the Con A molecules on the glass slides and the heterogeneous bacterial surface.
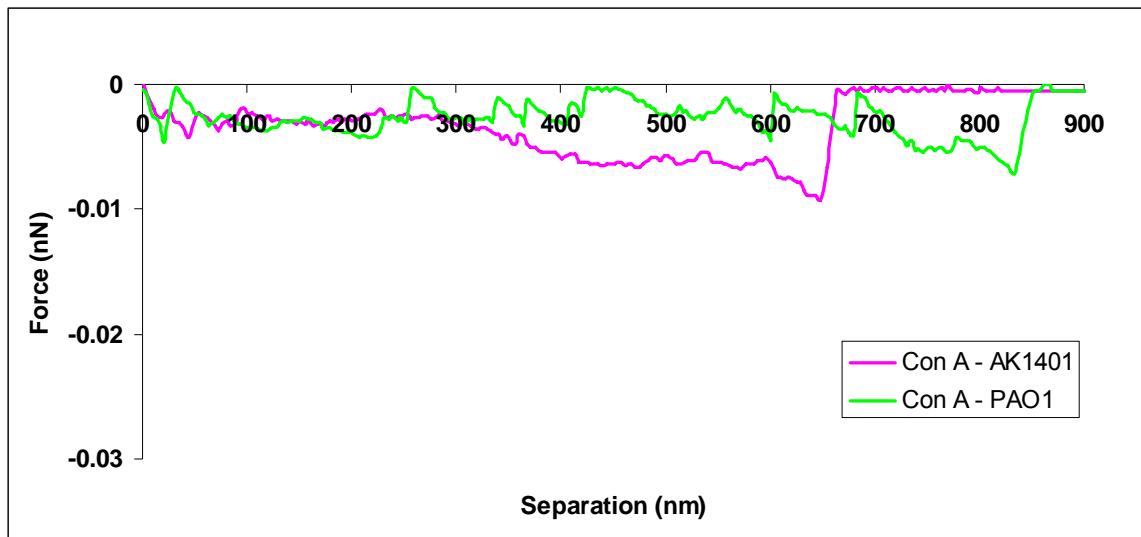
Figure 4.48 Representative retraction curves of Con A on glass slides probed by *P. aeruginosa* strains immobilized on AFM tip in HEPES/DTT buffer at pH 7.4.

The Kruskal-Wallis One Way Analysis of Variance (ANOVA) test was used to check if the adhesion behaviors of the *P. aeruginosa* strains were statistically different. According

to the results of the test, there was a statistically significant difference (P =< 0.001) between the magnitude of adhesion forces when they interact with Con A molecules, but the median values of pull-off distances for the interactions of both strains with Con A molecules were not statistically different (P =< 0.001). Since the interactions are not very strong, the bacterial surface polymers do not become become extended to large distances, so the difference in the length of LPS is not clearly observed by AFM. However, PAO1 still shows longer pull-off distances and weaker pull-off forces than AK1401. Therefore, even though the structure and surface charge of the LPS molecules of the two strains may play an important role on the magnitude of adhesive forces, the length of the LPS does not appear to have a significant role when they are interacting with Con A molecules. The magnitude of average adhesive forces for AK1401 was larger than that of PAO1 (Figure 4.51). In other words, adhesion of AK1401 to Con A molecules was relatively stronger than the adhesion of PAO1 to Con A, which was consistent with the trend of BSA interactions.
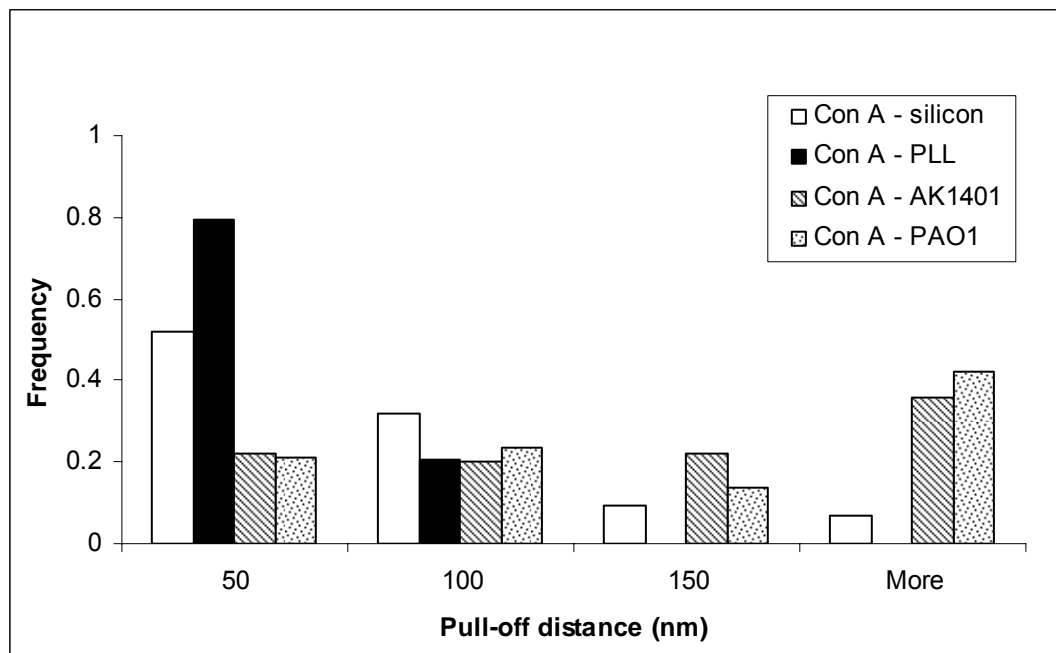
Figure 4.49 Pull-off distance histograms (n=50) of Con A with clean and modified AFM tip. Measurements were made in HEPES/DTT buffer at pH 7.4.
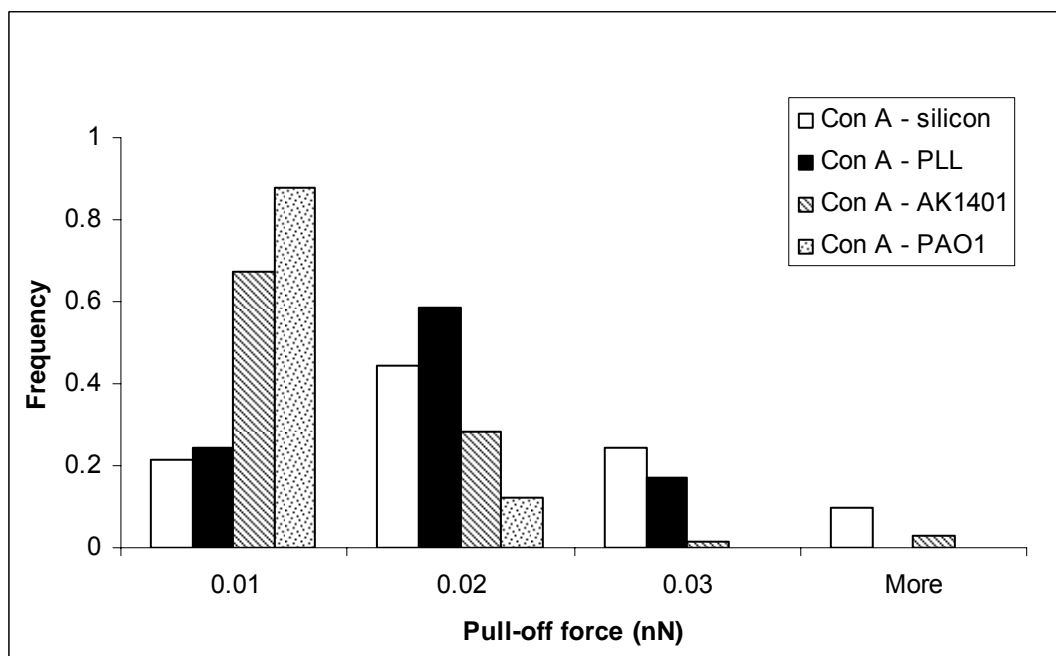
Figure 4.50 Pull-off force histograms (n=50) of Con A with clean and modified AFM tip. Measurements were made in HEPES/DTT buffer at pH 7.4.

Our results show that both two *P. aeruginosa* strains have weak interactions with Con A molecules. Avni et al. also showed that *P. aeruginosa* did not bind to fluorescein-conjugated Con A [123]. Since it was shown that Con A could competitively bind to the receptors of *P. aeruginosa* LPS on epithelial cells and block *P. aeruginosa* attachment [127,135,136], our results are consistent with the literature. Gad et al. have shown that the binding force between Con A and mannose ranged from 75-200 pN [125]. Our results show that the binding force between Con A and LPS of *P. aeruginosa* is up to 40 pN. Therefore, we can suggest that the *P. aeruginosa* strains do not express mannose molecules in their LPS.
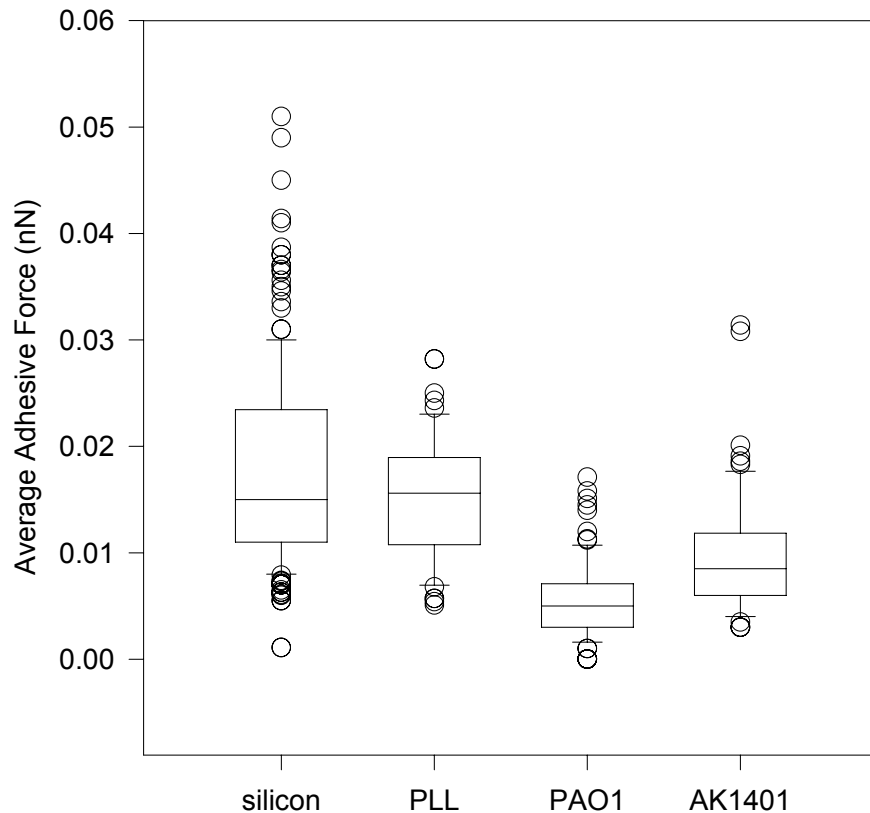
Figure 4.51 A comparison of average adhesive forces of Con A interacting with various probes. Measurements were made in HEPES/DTT buffer at pH 7.4.

4.6.4 Comparison of *P. aeruginosa* Interactions with BSA and Con A

The AFM force curves show the differences between the interactions of two *P. aeruginosa* strains with BSA and Con A molecules. Figure 4.52 shows the AFM retraction curves of AK1401. The adhesive forces of AK1401 for BSA are much stronger than the ones for Con A. The AK1401 coated AFM tip has long range interactions with protein molecules. The median value of the BSA – AK1401 pull-off forces are an order of magnitude greater than that of the Con A – AK1401 pull-off forces. Therefore, *P. aeruginosa* AK1401 has stronger interactions with BSA compared to Con A.
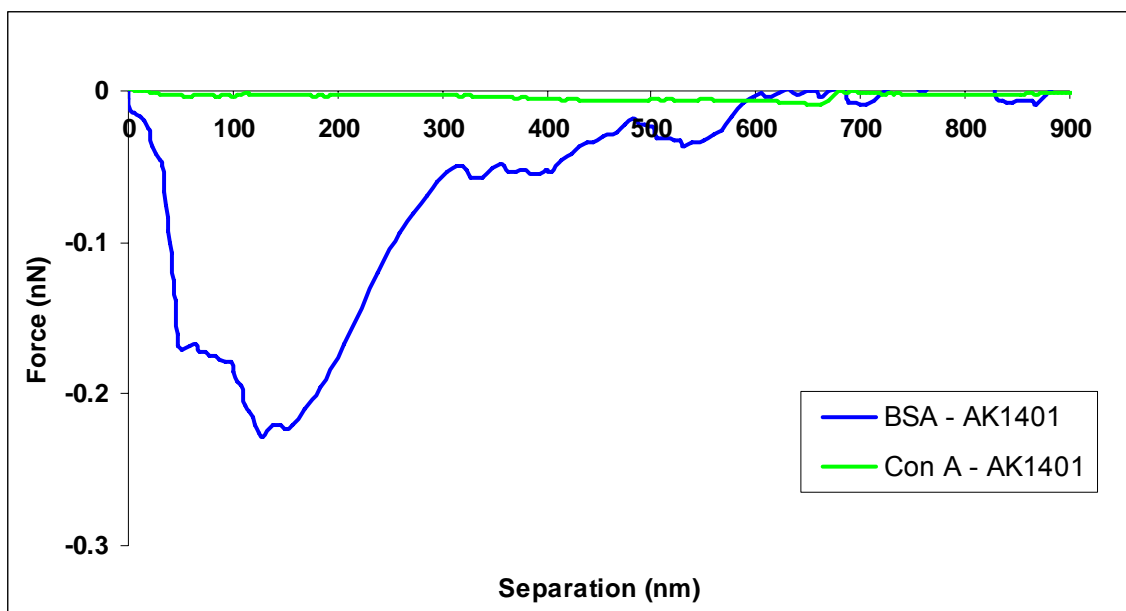
Figure 4.52 Representative retraction curves of Con A and BSA on the glass slides probed by *P. aeruginosa* AK1401 immobilized on AFM tip, in HEPES/DTT buffer at pH 7.4.

Figure 4.53 shows the AFM retraction curves for PAO1 interacting with each protein. The adhesive forces of PAO1 for BSA are much stronger than the ones for Con A. The

PAO1 coated AFM tip has long range interactions with protein molecules. The median

value of the BSA – PAO1 pull-off forces are also an order of magnitude greater than that

of the Con A – PAO1 pull-off forces. Therefore, *P. aeruginosa* PAO1 has stronger

interactions with BSA compared to Con A.
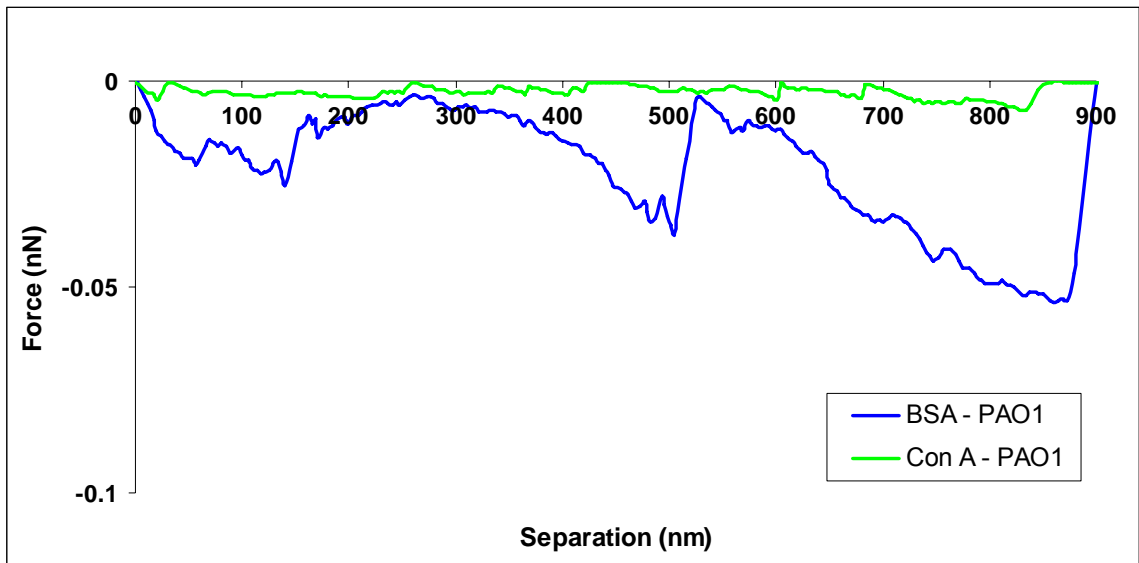
Figure 4.53 Representative retraction curves of Con A and BSA on the glass slides
probed by *P. aeruginosa* PAO1 immobilized on AFM tip, in HEPES/DTT buffer at pH
7.4.

The Kruskal-Wallis One Way Analysis of Variance (ANOVA) test was used to check if

the adhesion behavior of both *P. aeruginosa* strains to protein molecules was statistically

different. There was a statistically significant difference ($P = < 0.05$) between the

magnitude of adhesion forces when both strains interact with BSA molecules, but the

magnitude of adhesion forces for the interactions of both strains with Con A molecules

were not statistically different, although they were different when the sensitivity

increased to $P = < 0.001$. The difference between the pull-off distances of both strains

was statistically significant ($P < 0.05$, Dunn's method) for BSA interactions, but it was

not significant for Con A interactions with either strain. However, PAO1 still shows

longer pull-off distances and weaker pull-off forces than AK1401 while interacting with

Con A (Figure 4.54 and Figure 4.55). Therefore, the length and surface charge of

different LPS molecules of two strains play an important role on the magnitude of

adhesive forces for Con A, but it is difficult to appreciate because of the very weak

interactions between *P. aeruginosa* and Con A. When we compare the interactions of

both strains with BSA, the distributions of forces show different behavior. The

interactions of PAO1 with BSA can be up to 0.1 nN, but the interactions of AK1401 with

BSA can be up to 0.3 nN. Therefore, AK1401 can adhere to BSA molecules three times

more strongly than PAO1.
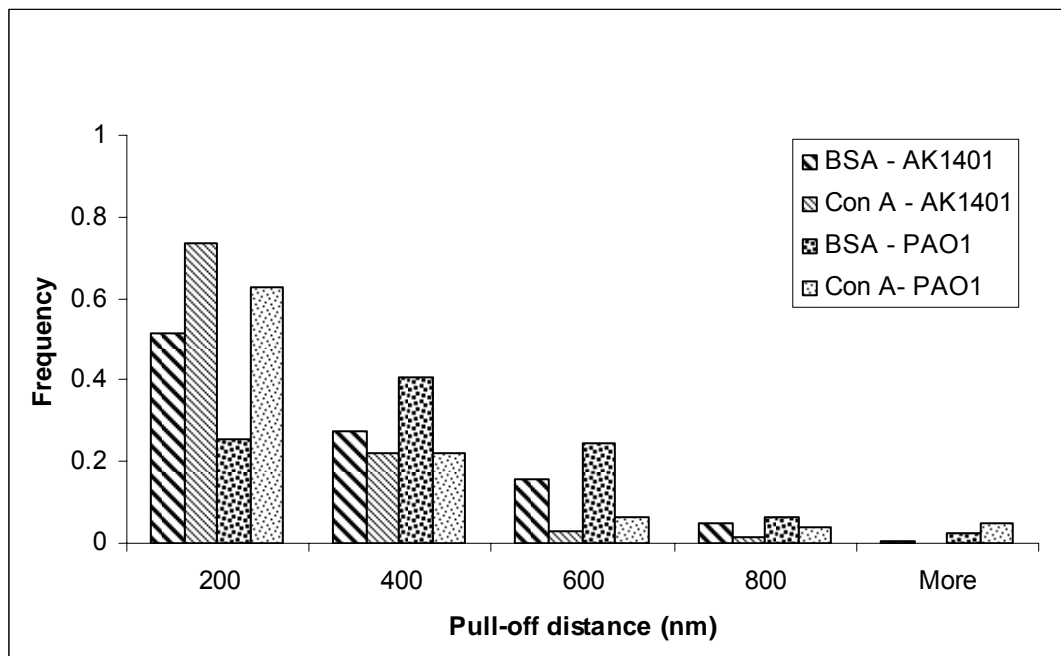
Figure 4.54 Pull-off distance histograms (n=50) of proteins probed by *P. aeruginosa* cells immobilized on the AFM tip (CSC38-B). Measurements were made in HEPES/DTT buffer at pH 7.4.
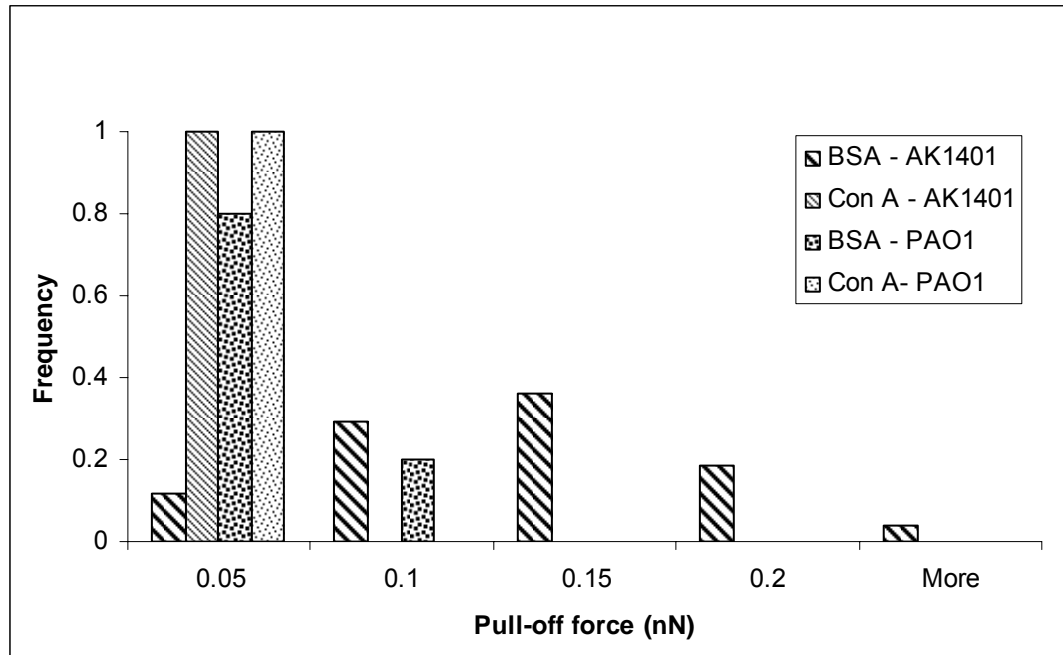
Figure 4.55 Pull-off force histograms (n=50) of proteins probed by *P. aeruginosa* cells immobilized on the AFM tip (CSC38-B). Measurements were made in HEPES/DTT buffer at pH 7.4.

The adhesion of AK1401 to BSA molecules was much stronger than that of PAO1 to BSA (Figure 4.56). Moreover, the adhesion of AK1401 to Con A molecules was relatively stronger than the adhesion of PAO1 to Con A. When we compare the interactions of each *P. aeruginosa* strain with both proteins, AK1401 has higher attraction to both BSA and Con A than PAO1. Overall, the strongest protein interactions are the ones between BSA and AK1401. Therefore, AK1401 adheres to protein molecules stronger than PAO1 does. The neutral surface charge of AK1401 might play an important role in strong adhesion since BSA and Con A are both negatively charged in physiological buffer [90,99,115,116].
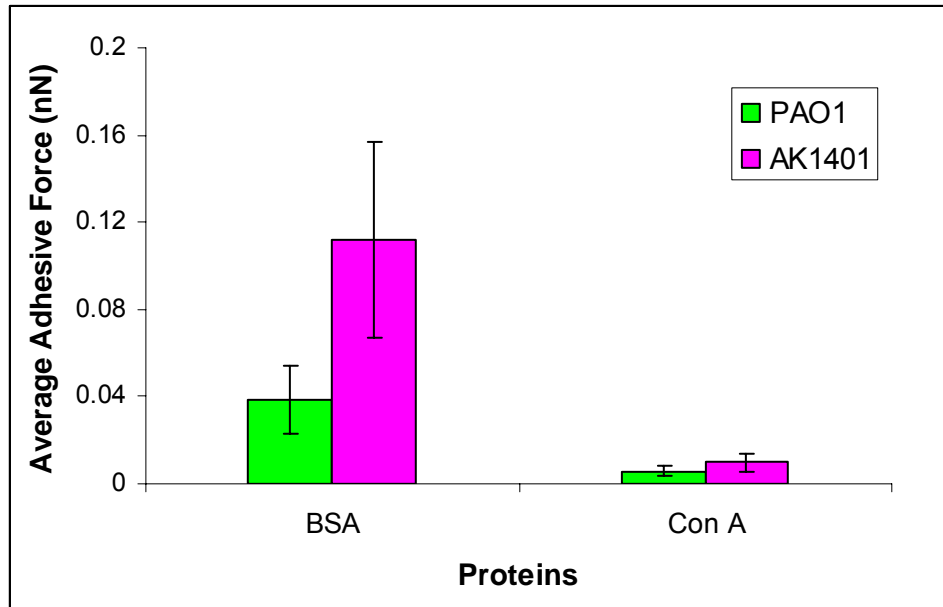
Figure 4.56 A comparison of average adhesive forces of *P. aeruginosa* strains. Measurements were made in HEPES/DTT buffer at pH 7.4.

The infections in CF patients are mostly caused by rough mutants of *P. aeruginosa* [70,108]. Even if the bacterial cells are smooth in the beginning stages, they can mutate and become semi-rough or rough under clinical conditions [40]. Strain AK1401 and clinical CF strains have similar LPS structures, considering O-antigens [99,109]. Recent studies suggest that the CFTR protein may influence *P. aeruginosa* lung infections directly through its role as an epithelial cell receptor for this organism [20]. We found that the ability of semi-rough mutant, AK1401, to attach to protein molecules or protein coated surfaces is much greater than that of the wild type smooth strain, PAO1. Our results suggest that the semi-rough or rough strains can adhere to the protein receptors of the epithelial cells or protein coated implants stronger than the smooth strains, and can cause serious infections.

These results will also impact several environmental applications. The natural organic matters (NOM) such as sediment organic matter (SOM) and dissolved organic matter (DOM) affect bacterial transport through porous media by adhering and increasing the negative surface charge and electrophoretic motility of bacteria, which also alters bacterial retention on the porous media [32]. However, one study found that this magnitude of facilitated transport was considered insufficient for the purpose of enhancing subsurface delivery for bioremediation [32]. Since proteins are also considered as recognizable organic matter, our results can explain the role of proteins on bacterial adhesion and transport. The maximum adhesion force, 300 pN, was obtained between *P. aeruginosa* AK1401 and BSA. The interactions of *P. aeruginosa* PAO1 with BSA were smaller than 100 pN. The interactions of each of the two *P. aeruginosa* strains with Con A were weak, with a maximum value of 50 pN. Overall, the interactions of these two *P. aeruginosa* strains with two model proteins are weaker compared to how the bacteria interact with humic acids [158]. Therefore, the role of protein molecules may be insufficient for the purpose of enhancing subsurface delivery for bioremediation.

5 - Conclusions

We investigated the surface properties of two *P. aeruginosa* strains and their interactions with two model proteins, BSA and Con A. Topographical images were helpful to identify the size and shape of bacterial cells and EPS molecules. AFM force curve analyses were used to understand the adhesion behavior of the bacterial cells. The magnitude of adhesive forces for two *P. aeruginosa* stains was not statistically significant when they interact with silicon. Although it is not clear if the pull-off distances are accurate representatives of the absolute length of bacterial surface molecules, the trend indicates that the surface molecules of strain AK1401 are shorter than those of strain PAO1.

The semi-rough strain AK1401 was more hydrophobic than the smooth strain PAO1, according to the water contact angle measurements. However, surface free energy components and zeta potential values were not significantly different for both strains. Zeta potential of bacterial cells decreased when they were suspended in HEPES/DTT buffer instead of pure water. In other words, the electrostatic double layer was smaller when the bacteria were in HEPES/DTT buffer. Although the macroscopic physicochemical properties show that the two *P. aeruginosa* strains have similar properties, the AFM results demonstrate the importance of nano-scale properties and interactions between bacterial cells and various molecules, such as silicon and proteins.

Interactions between surfaces pre-conditioned with organic matter (i.e. proteins) and bacteria can give clues about the initial steps of bacterial adhesion and biofilm formation.

Studying the specific interactions is important to understand the effect of organic molecules on bacterial adhesion. The AFM results demonstrate the importance of nano-scale interactions between proteins and bacterial cells. Our results show that the lipid A and core oligosaccharides are the most important molecules influencing the interactions of *P. aeruginosa* with protein molecules.

The interactions of *P. aeruginosa* with model proteins in our study were weaker than the interactions previously observed with humic acids. Therefore, the role of protein molecules may be inadequate for the purpose of enhancing subsurface delivery for bioremediation. We found that the ability of semi-rough mutant, AK1401, to attach to protein molecules or protein coated surfaces is much greater than that of the wild type smooth strain, PAO1. Our results suggest that the semi-rough or rough strains can adhere to the protein receptors of the epithelial cells or protein coated implants stronger than the smooth strains, and therefore can cause serious infections. Additional experimentation with a controlled orientation of protein molecules can be useful to identify the adhesion of bacteria to different sites of protein molecules.

6 - Future Work

Interactions between bacteria and sugar molecules, organic acids such as DNA and humic acids can be investigated in the future to understand the role of NOM on the adhesion of bacterial cells. Since the orientation of protein molecules on the glass slides and orientation of bacterial surface polymers are not clearly known, computer simulations (i.e. molecular dynamics) may help to obtain more information on the conformation of bacterial polymers and give a deeper insight into polymer adsorption. Moreover, it is hard to determine the contribution of a certain class of surface polymers to bacterial adhesion since steric influences of different polymers interfere with each other. Contribution of different polymers can be better understood by performing both the AFM experiments and computer simulations with isolated cell surface polymers.

P. aeruginosa strains produce membrane vesicle and capsules, which may play an important role in bacterial adhesion. Therefore, these molecules can be examined by using appropriate staining techniques. Identifying the size and contents of the capsules and membrane vesicles might be used to explain the long range interactions of *Pseudomonas* strains. Vaccines used against pathogenic Gram-negative bacteria consist of a mixture of O-antigens from different serotypes of the same species. Therefore, better understanding of O-side chains can be helpful for vaccine development against *P. aeruginosa* infections.

References

1. van Loosdrecht, M. C., Lyklema, J., Norde, W., Schraa, G. & Zehnder, A. J. The role of bacterial cell wall hydrophobicity in adhesion. *Applied Environmental Microbiology* **53**, 1893-7 (1987).

2. Israelachvili, J. *Intermolecular and Surface Forces.*ed. 2nd. Academic Press Limited, London, 1992.

3. Delden, C. V. & Iglewski, B. H. Cell-to-cell signaling and *Pseudomonas aeruginosa* infections. *Emerging Infectious Diseases* **4**, 551-560 (1998).

4. Davies, D. G., Parsek, M. R., Pearson, J. P., Iglewski, B. H., Costerton, J. W. & Greenberg, E. P. The involvement of cell-to-cell signals in the development of a bacterial biofilm. *Science* **280**, 295-8 (1998).

5. Caroff, M. & Karibian, D. Structure of bacterial lipopolysaccharides. *Carbohydrate Research* **338**, 2431-47 (2003).

6. Walker, S. L., Redman, J. A. & Elimelech, M. Role of Cell Surface Lipopolysaccharides in *Escherichia coli* K12 adhesion and transport. *Langmuir* **20**, 7736-46 (2004).

7. Proteins. *http://web.mit.edu/esgbio/www/lm/proteins/aa/aminoacids.html* (2006).

8. Friedli, G.-L. *Interaction of SWP with Bovine Serum Albumin (BSA).* PhD Dissertation, University of Surrey, (1996).

9. Ying, P., Yu, Y., Jin, G. & Tao, Z. Competitive protein adsorption studied with atomic force microscopy and imaging ellipsometry. *Colloids and Surfaces B: Biointerfaces* **32**, 1-10 (2003).

10. Scanning Probe Microscopy Training Notebook; Digital Instruments, Veeco Metrology Group. 39-40 (1998).

11. Emerson IV, R. J. *A Nanoscale Investigation of Pathogenic Microbial Adhesion in Biomaterial Systems.* PhD Dissertation, Chemical Engineering, Worcester Polytechnic Institute, (2006).

12. Camesano, T. A. & Logan, B. Probing bacterial electrosteric interactions using atomic force microscopy. *Environmental Science and Technology* **34**, 3354-3362 (2000).

13. Li, B. & Logan, B. E. Bacterial adhesion to glass and metal-oxide surfaces. *Colloids and Surfaces B: Biointerfaces* **36**, 81-90 (2004).

14. Velegol, S. B. & Logan, B. E. Contributions of bacterial surface polymers, electrostatics, and cell elasticity to the shape of AFM force curves. *Langmuir* **18**, 5256-5262 (2002).

15. Camesano, T. A., Unice, K. M. & E., L. B. Blocking and ripening of colloids in porous media and their implications for bacterial transport. *Colloids and Surfaces, A: Physicochemical and Engineering Aspects* **160**, 291-308 (1999).

16. Parent, M. E. & Velegol, D. *E. coli* adhesion to silica in the presence of humic acid. *Colloids and Surfaces B: Biointerfaces* **39**, 45-51 (2004).

17. An, Y. H. & Friedman, R. J. Concise review of mechanisms of bacterial adhesion to biomaterial surfaces. *Journal of Biomedical Materials Research: Applied Biomaterials* **43**, 338-48 (1998).

18. Xu, L. C. & Logan, B. E. Adhesion forces between functionalized latex microspheres and protein-coated surfaces evaluated using colloid probe atomic force microscopy. *Colloids and Surfaces B: Biointerfaces* **48**, 84-94 (2006).

19. Beveridge, T. J. Structures of gram-negative cell walls and their derived membrane vesicles. *Journal of Bacteriology* **181**, 4725-33 (1999).

20. Lyczak, J. B., Cannon, C. L. & Pier, G. B. Establisment of *Pseudomonas aeruginosa* infection: lessons from a versatile opportunist. *Microbes and Infection* **2**, 1051-1060 (2000).

21. Parsek, M. R. & Fuqua, C. Biofilms 2003: emerging themes and challenges in studies of surface-associated microbial life. *Journal of Bacteriology* **186**, 4427-40 (2004).

22. Vaudaux, P. E., Francois, P., Proctor, R. A., McDevitt, D., Foster, T. J., Albrecht, R. M., Lew, D. P., Wabers, H. & Cooper, S. L. Use of adhesion-defective mutants of *Staphylococcus aureus* to define the role of specific plasma proteins in promoting bacterial adhesion to canine arteriovenous shunts. *Infection and Immunity* **63**, 585-90 (1995).

23. Cha, M. K. & Kim, I. H. Glutathione-linked thiol peroxidase activity of human serum albumin: a possible antioxidant role of serum albumin in blood plasma. *Biochemical and Biophysical Research Communications* **222**, 619-25 (1996).

24. Kragh-Hansen, U. Structure and ligand binding properties of human serum albumin. *Danish Medical Bulletin* **37**, 57-84 (1990).

25. Murga, R., Miller, J. M. & Donlan, R. M. Biofilm formation by gram-negative bacteria on central venous catheter connectors: effect of conditioning films in a laboratory model. *Journal of Clinical Microbiology* **39**, 2294-7 (2001).

26.   Schulz, G. E. & Schirmer, R. H. *Principles of Protein Structure.* Springer-Verlag, New York, 1979.

27.   Castro, L. B., Kappl, M. & Petri, D. F. Adhesion forces between hybrid colloidal particles and concanavalin A. *Langmuir* **22**, 3757-62 (2006).

28.   Gupta, D., Dam, T. K., Oscarson, S. & Brewer, C. F. Thermodynamics of lectin-carbohydrate interactions. Binding of the core trimannoside of asparagine-linked carbohydrates and deoxy analogs to concanavalin A. *Journal of Biological Chemistry* **272**, 6388-92 (1997).

29.   Martin, R. E., Bouwer, E. J. & Hanna, L. M. Application of clean-bed filtration theory to bacterial deposition in porous media. *Environmental Science and Technology* **26**, 1053-1058 (1992).

30.   Crawford, R. L. & Crawford, D. L. *Bioremediation: Principles and Applications.* ed. Lynch, J. Press Syndicate of the University of Cambridge, 1996.

31.   Fabiano, M., Marrale, D. & Misic, C. Bacteria and organic matter dynamics during a bioremediation treatment of organic-rich harbour sediments. *Marine Pollution Bulletin* **46**, 1164-73 (2003).

32.   Johnson, W. P. & Amy, G. L. Facilitated transport and enhanced desorpsion of polycyclic aromatic hydrocarbons by natural organic matter in aquifer sediments. *Environmental Science and Technology* **29**, 807-817 (1995).

33.   Fletcher, M. *Bacterial adhesion: molecular and ecological diversity.* Wiley, New York, 1996.

34.   Ong, Y. L., Razatos, A., Georgiou, G. & Sharma, M. M. Adhesion forces between *E. coli* bacteria and biomaterial surfaces. *Langmuir* **15**, 2719-2725 (1999).

35.   Schmidt, L. M., Delfino, J. J., Preston III, J. F. & St Laurent III, G. Biodegradation of low aqueous concentration pentachlorophenol (PCP) contaminated groundwater. *Chemosphere* **38**, 2897-912 (1999).

36.   Dunne, W. M., Jr. Bacterial adhesion: seen any good biofilms lately? *Clinical Microbiology Reviews* **15**, 155-66 (2002).

37.   Li, Q. & Logan, B. E. Enhancing bacterial transport for bioaugmentation of aquifers using low ionic strength solution and surfactants. *Water Resources* **33**, 1090-1100 (1999).

38.   Vadillo-Rodriguez, V. *Macroscopic and Microscopic Approaches Toward Bacterial Adhesion.* Doctoral dissertation, Institute of Biomedical Materials Science and Applications, University of Groningen, Groningen, The Netherlands, (2004).

39. Abu-Lail, N. I. & Camesano, T. A. Role of ionic strength on the relationship of biopolymer conformation, DLVO contributions, and steric interactions to bioadhesion of *Pseudomonas putida* KT2442. *Biomacromolecules* **4**, 1000-12 (2003).

40. Sabra, W., Lunsdorf, H. & Zeng, A. P. Alterations in the formation of lipopolysaccharide and membrane vesicles on the surface of *Pseudomonas aeruginosa* PAO1 under oxygen stress conditions. *Microbiology* **149**, 2789-95 (2003).

41. van der Mei, H. C., Bos, R. & Busscher, H. J. A reference guide to microbial cell surface hydrophobicity based on contact angles. *Colloids and Surfaces B: Biointerfaces* **11**, 213-221 (1998).

42. Vanhaecke, E., Remon, J. P., Moors, M., Raes, F., De Rudder, D. & Van Peteghem, A. Kinetics of *Pseudomonas aeruginosa* adhesion to 304 and 316-L stainless steel: role of cell surface hydrophobicity. *Applied Environmental Microbiology* **56**, 788-95 (1990).

43. Emerson IV, R. J. & Camesano, T. A. Nanoscale investigation of pathogenic microbial adhesion to a biomaterial. *Applied Environmental Microbiology* **70**, 6012-22 (2004).

44. van Oss, C. J. *Interfacial Forces in Aqueous Media.* Marcel Dekker, New York, 1994.

45. Madigan, M. T., Martinko, J. M. & Parker, J. *Brock Biology of Microorganisms.* Prentice Hall, New Jersey, 1997.

46. Verwey, E. J. W. & Overbeek, J. T. G. *Theory of Stability of Lyophobic Colloids.* Elsevier, Amsterdam, 1948.

47. Busscher, H. J., Weerkamp, A. H., van der Mei, H. C., van Pelt, A. W., de Jong, H. P. & Arends, J. Measurement of the surface free energy of bacterial cell surfaces and its relevance for adhesion. *Applied Environmental Microbiology* **48**, 980-3 (1984).

48. van Loosdrecht, M. C., Lyklema, J., Norde, W. & Zehnder, A. J. Influence of interfaces on microbial activity. *Microbiology Reviews* **54**, 75-87 (1990).

49. Jucker, B. A., Zehnder, A. J. B. & Harms, H. Quantification of polymer interactions in bacterial adhesion. *Environmental Science and Technology* **32**, 2909-2915 (1998).

50. Langley, S. & Beveridge, T. J. Effect of O-side-chain-lipopolysaccharide chemistry on metal binding. *Applied Environmental Microbiology* **65**, 489-98 (1999).

51.	Jucker, B. A., Harms, H. & Zehnder, A. J. B. Polymer interactions between five gram-negative bacteria and glass investigated using LPS micelles and vesicles as model systems. *Colloids and Surfaces B: Biointerfaces* **11**, 33-45 (1998).

52.	Shellenberger, K. & Logan, B. E. Effect of molecular scale roughness of glass beads on colloidal and bacterial deposition. *Environmental Science and Technology* **36**, 184-9 (2002).

53.	Smith, A. W. Biofilms and antibiotic therapy: is there a role for combating bacterial resistance by the use of novel drug delivery systems? *Advanced Drug Delivery Reviews* **57**, 1539-50 (2005).

54.	Donlan, R. M. Biofilms: microbial life on surfaces. *Emerging Infectious Diseases* **8** (2002).

55.	Drenkard, E. & Ausubel, F. M. *Pseudomonas* biofilm formation and antibiotic resistance are linked to phenotypic variation. *Nature* **416**, 740-3 (2002).

56.	O'Toole, G., Kaplan, H. B. & Kotler, R. Biofilm formation as microbial development. *Annual Review of Microbiology* **54**, 49-79 (2000).

57.	Wozniak, D. J., Wyckoff, T. J., Starkey, M., Keyser, R., Azadi, P., O'Toole, G. A. & Parsek, M. R. Alginate is not a significant component of the extracellular polysaccharide matrix of PA14 and PAO1 *Pseudomonas aeruginosa* biofilms. *Proceedings of the National Academy of Sciences (USA)* **100**, 7907-12 (2003).

58.	Donlan, R. M. Role of biofilms in antimicrobial resistance. *Asaio Journal* **46**, S47-52 (2000).

59.	Lewis, K. Riddle of biofilm resistance. *Antimicrobial Agents and Chemotheraphy* **45**, 999-1007 (2001).

60.	Drenkard, E. Antimicrobial resistance of *Pseudomonas aeruginosa* biofilms. *Microbes and Infections* **5**, 1213-9 (2003).

61.	Heurlier, K., Denervaud, V., Pessi, G., Reimmann, C. & Haas, D. Negative control of quorum sensing by RpoN (sigma54) in *Pseudomonas aeruginosa* PAO1. *Journal of Bacteriology* **185**, 2227-35 (2003).

62.	Latifi, A., Winson, M. K., Foglino, M., Bycroft, B. W., Stewart, G. S., Lazdunski, A. & Williams, P. Multiple homologues of LuxR and LuxI control expression of virulence determinants and secondary metabolites through quorum sensing in *Pseudomonas aeruginosa* PAO1. *Molecular Microbiology* **17**, 333-43 (1995).

63.	Whiteley, M., Parsek, M. R. & Greenberg, E. P. Regulation of quorum sensing by RpoS in *Pseudomonas aeruginosa*. *Journal of Bacteriology* **182**, 4356-60 (2000).

64. Albus, A. M., Pesci, E. C., Runyen-Janecky, L. J., West, S. E. & Iglewski, B. H. Vfr controls quorum sensing in *Pseudomonas aeruginosa*. *Journal of Bacteriology* **179**, 3928-35 (1997).

65. Sperandio, V., Torres, A. G. & Kaper, J. B. Quorum sensing *Escherichia coli* regulators B and C (QseBC): a novel two-component regulatory system involved in the regulation of flagella and motility by quorum sensing in *E. coli. Molecular Microbiology* **43**, 809-21 (2002).

66. Kahraman, H. & Geckil, H. Degradation of benzene, toluene and xylene by *Pseudomonas aeruginosa* engineered with the *Vitreoscilla* hemoglobin gene. *Engineering in Life Science* **5** (2005).

67. Welsh, M. J. & Fick, R. B. Cystic fibrosis. *The Journal of Clinical Investigation* **80**, 1523-6 (1987).

68. Ramsey, M. M. & Whiteley, M. *Pseudomonas aeruginosa* attachment and biofilm development in dynamic environments. *Molecular Microbiology* **53**, 41075-1087 (2004).

69. Kolter, R. & Losick, R. One for all and all for one. *Science* **280**, 226-227 (1998).

70. Bush, A. Decision facing the cyctic fibrosis clinician at first isolation of *Pseudomonas aeruginosa*. *Paediatric Respiratory Reviews* **3**, 82-88 (2002).

71. Branda, S. S., Vik, S., Friedman, L. & Kolter, R. Biofilms: the matrix revisited. *Trends in Microbiology* **13**, 20-6 (2005).

72. Schaefer, F., Bruttin, O., Zografos, L. & Guex-Crosier, Y. Bacterial keratitis: a prospective clinical and microbiological study. *British Journal of Ophthalmology* **85**, 842-7 (2001).

73. Shovlin, J. P., Schneider, J. W. & Chandoha, H. J. Assessment and management of bacterial keratitis in contact lens wearers. *http://www.opt.pacificu.edu/ce/catalog/11412-AS/ShovBactKer.html* (2006).

74. Rudner, X. L., Zheng, Z., Berk, R. S., Irvin, R. T. & Hazlett, L. D. Corneal epithelial glycoproteins exhibit *Pseudomonas aeruginosa* pilus binding activity. *Investigative Ophthalmology and Visual Science* **33**, 2185-93 (1992).

75. Fleiszig, S. M. & Evans, D. J. The pathogenesis of bacterial keratitis: Studies with *Pseudomonas aeruginosa*. *Clinical and Experimental Optometry* **85**, 271-278 (2002).

76. Bruinsma, G. M., Abbing, M. R., de Vries, J., Stegenga, B., van der Mei, H. C., van der Linden, M. L., Hooymans, J. M. M. & Busscher, H. J. Influence of wear and overwear on surface properties of etafilcon A contact censes and adhesion of

Pseudomonas aeruginosa. Investigative Ophthalmology & Visual Science **43**, 3646-3653 (2002).

77. Bruinsma, G. M., Abbing, M. R., van der Mei, H. C. & Busscher, H. J. Effects of cell surface damage on surface properties and adhesion of *Pseudomonas aeruginosa. Journal of Microbiological Methods* **45**, 95-101 (2001).

78. Head, I. M. & Swannell, R. P. Bioremediation of petroleum hydrocarbon contaminants in marine habitats. *Current Opinion in Biotechnology* **10**, 234-239 (1999).

79. Ojumu, T. V., Bello, O. O., Sonibare, J. A. & Solomon, B. O. Evaluation of microbial systems for bioremediation of petroleum refinery effluents in Nigera. *African Journal of Biotechnology* **4**, 31-35 (2005).

80. Holliger, C., Gaspard, S., Glod, G., Heijman, C., Schumacher, W., Schwarzenbach, R. P. & Vazquez, F. Contaminated environments in the subsurface and bioremediation:organic contaminants. *FEMS Microbial Reviews* **20**, 517-523 (1997).

81. Apel, W. A. & Turick, C. E. *Mineral Bioprocessing: Bioremediation of Hexavalent Chromium by Bacterial Reduction*. Engineering Foundation Conference, San Francisco, CA, 376-387, 1991.

82. Ganguli, A. & Tripathi, A. K. Bioremediation of toxic chromium from electroplating effluent by chromate-reducing *Pseudomonas aeruginosa* A2Chr in two bioreactors. *Applied Microbiology and Biotechnology* **58**, 416-420 (2002).

83. Manal, M. A., El-Naggar, S., El-Aasar, A. & Barakat Khlood, I. Bioremediation of crystal violet using air bubble bioreactor packed with *Pseudomonas aeruginosa. Water Resources* **39**, 5045-54 (2005).

84. Chayabutra, C. & Ju, L. K. Degradation of n-hexadecane and its metabolites by *Pseudomonas aeruginosa* under microaerobic and anaerobic denitrifying conditions. *Applied Environmental Microbiology* **66**, 493-8 (2000).

85. Cox, C. D. Role of pyocyanin in the acquisition of iron from transferrin. *Infection and Immunity* **52**, 263-70 (1986).

86. Evans, K., Passador, L., Srikumar, R., Tsang, E., Nezezon, J. & Poole, K. Influence of the MexAB-OprM multidrug efflux system on quorum sensing in *Pseudomonas aeruginosa. Journal of Bacteriology* **180**, 5443-7 (1998).

87. Stover, C. K., Pham, X. Q., Erwin, A. L., Mizoguchi, S. D., Warrener, P., Hickey, M. J., Brinkman, F. S., Hufnagle, W. O., Kowalik, D. J., Lagrou, M., Garber, R. L., Goltry, L., Tolentino, E., Westbrock-Wadman, S., Yuan, Y., Brody, L. L., Coulter, S. N., Folger, K. R., Kas, A., Larbig, K., Lim, R., Smith, K., Spencer, D., Wong, G. K., Wu, Z., Paulsen, I. T., Reizer, J., Saier, M. H., Hancock, R. E.,

Lory, S. & Olson, M. V. Complete genome sequence of *Pseudomonas aeruginosa* PAO1, an opportunistic pathogen. *Nature* **406**, 959-64 (2000).

88. Kropinski, A. M., Lewis, V. & Berry, D. Effect of growth temperature on the lipids, outer membrane proteins, and lipopolysaccharides of *Pseudomonas aeruginosa* PAO. *Journal of Bacteriology* **169**, 1960-6 (1987).

89. Makin, S. A. & Beveridge, T. J. *Pseudomonas aeruginosa* PAO1 ceases to express serotype-specific lipopolysaccharide at 45 degrees C. *Journal of Bacteriology* **178**, 3350-2 (1996).

90. Hatano, K., Goldberg, J. B. & Pier, G. B. Biologic activities of antibodies to the neutral-polysaccharide component of the *Pseudomonas aeruginosa* lipopolysaccharide are blocked by O side chains and mucoid exopolysaccharide (alginate). *Infection and Immunity* **63**, 21-6 (1995).

91. Todar, K. *Todar's Online Textbook of Bacteriology*. http://www.textbookofbacteriology.net/pathogenesis.html, University of Wisconsin-Madison Department of Bacteriology, 2006.

92. Rocchetta, H. L., Burrows, L. L. & Lam, J. S. Genetics of O-antigen biosynthesis in *Pseudomonas aeruginosa*. *Microbiology and Molecular Biology Reviews* **63**, 523-53 (1999).

93. Kadurugamuwa, J. L., Lam, J. S. & Beveridge, T. J. Interaction of gentamicin with the A band and B band lipopolysaccharides of *Pseudomonas aeruginosa* and its possible lethal effect. *Antimicrobial Agents and Chemotherapy* **37**, 715-21 (1993).

94. Peterson, A. A., Hancock, R. E. & McGroarty, E. J. Binding of polycationic antibiotics and polyamines to lipopolysaccharides of *Pseudomonas aeruginosa*. *Journal of Bacteriology* **164**, 1256-61 (1985).

95. Berry, D. & Kropinski, A. M. Effect of lipopolysaccharide mutations and temperature on plasmid transformation efficiency in *Pseudomonas aeruginosa*. *Canadian Journal of Microbiology* **32**, 436-8 (1986).

96. Lightfoot, J. & Lam, J. S. Molecular cloning of genes involved with expression of A-band lipopolysaccharide, an antigenically conserved form, in *Pseudomonas aeruginosa*. *Journal of Bacteriology* **173**, 5624-30 (1991).

97. Sadovskaya, I., Brisson, J. R., Lam, J. S., Richards, J. C. & Altman, E. Structural elucidation of the lipopolysaccharide core regions of the wild-type strain PAO1 and O-chain-deficient mutant strains AK1401 and AK1012 from *Pseudomonas aeruginosa* serotype O5. *European Journal of Biochemistry* **255**, 673-84 (1998).

98.   Nguyen, T. T., Saxena, A. & Beveridge, T. J. Effect of surface lipopolysaccharide on the nature of membrane vesicles liberated from the Gram-negative bacterium *Pseudomonas aeruginosa*. *Journal of Electron Microscopy* **52**, 465-9 (2003).

99.   Rivera, M., Bryan, L. E., Hancock, R. E. & McGroarty, E. J. Heterogeneity of lipopolysaccharides from *Pseudomonas aeruginosa*: analysis of lipopolysaccharide chain length. *Journal of Bacteriology* **170**, 512-21 (1988).

100.   Rivera, M. & McGroarty, E. J. Analysis of a common-antigen lipopolysaccharide from *Pseudomonas aeruginosa*. *Journal of Bacteriology* **171**, 2244-8 (1989).

101.   Burrows, L. L., Charter, D. F. & Lam, J. S. Molecular characterization of the *Pseudomonas aeruginosa* serotype O5 (PAO1) B-band lipopolysaccharide gene cluster. *Molecular Microbiology* **22**, 481-495 (1996).

102.   Arsenault, T. L., Hughes, D. W., MacLean, D. B., Szarek, W. A., Kropinski, A. M. B. & Lam, J. S. Structural studies on the polysaccharide portion of A-band lipopolysaccharide from a mutant (AK1401) of *Pseudomonas aeruginosa* strain PAO1. *Canadian Journal of Chemistry* **69**, 1273-1280 (1991).

103.   Lam, J. S., Graham, L. L., Lightfoot, J., Dasgupta, T. & Beveridge, T. J. Ultrastructural examination of the lipopolysaccharides of *Pseudomonas aeruginosa* strains and their isogenic rough mutants by freeze-substitution. *Journal of Bacteriology* **174**, 7159-67 (1992).

104.   Knirel, Y. A., Vinogradov, E. V., Kocharova, N. A., Paramonov, R. A., Kochetkov, N. K., Dmitriev, B. A., Stanislavsky, E. S. & Lanyi, B. The structure of O-specific polysaccharide and serological classification of *Pseudomonas aeruginosa*. *Acta Microbiologica Hungarica* **35**, 3-24 (1988).

105.   Stoica, O., Tuanyok, A., Yao, X., Jericho, M. H., Pink, D. & Beveridge, T. J. Elasticity of membrane vesicles isolated from *Pseudomonas aeruginosa*. *Langmuir* **19**, 10916-10924 (2003).

106.   Kadurugamuwa, J. L. & Beveridge, T. J. Virulence factors are released from *Pseudomonas aeruginosa* in association with membrane vesicles during normal growth and exposure to gentamicin: a novel mechanism of enzyme secretion. *Journal of Bacteriology* **177**, 3998-4008 (1995).

107.   Makin, S. A. & Beveridge, T. J. The influence of A-band and B-band lipopolysaccharide on the surface characteristics and adhesion of *Pseudomonas aeruginosa* to surfaces. *Microbiology* **142**, 299-307 (1996).

108.   Lam, M. Y., McGroarty, E. J., Kropinski, A. M., MacDonald, L. A., Pedersen, S. S., Hoiby, N. & Lam, J. S. Occurrence of a common lipopolysaccharide antigen in standard and clinical strains of *Pseudomonas aeruginosa*. *Journal of Clinical Microbiology* **27**, 962-7 (1989).

109. Knirel, Y. A., Bystrova, O. V., Shashkov, A. S., Lindner, B., Kocharova, N. A., Senchenkova, S. N., Moll, H., Zahringer, U., Hatano, K. & Pier, G. B. Structural analysis of the lipopolysaccharide core of rough, cyctic fibrosis isolate of *Pseudomonas aeruginosa. Europian Journal of Biochemistry* **268**, 4708-4719 (2001).

110. Bryan, L. E., O'Hara, K. & Wong, S. Lipopolysaccharide changes in impermeability-type aminoglycoside resistance in Pseudomonas aeruginosa. *Antimicrobial Agents and Chemotherapy* **26**, 250-5 (1984).

111. Darby, N. J. & Creighton, T. E. *Protein Structure*. IRL Press at Oxford University Press, Oxford; New York, 1993.

112. Branden, C. & Tooze, J. *Introduction to Protein Structure*. Garland Pub, New York, 1999.

113. Mansur, H. S., Lobato, Z. P., Orefice, R. L., Vasconcelos, W. L., Oliveira, C. & Machado, L. J. Surface functionalization of porous glass networks: effects on bovine serum albumin and porcine insulin immobilization. *Biomacromolecules* **1**, 789-97 (2000).

114. Peters, T. J. *All about Albumin: Biochemistry, Genetics and Medical Applications*. Academic Press Inc., Orlando, 1996.

115. Wadu-Mesthrige, K., Amro, N. A. & Liu, G. Y. Immobilization of proteins on self-assembled monolayers. *Scanning* **22**, 380-8 (2000).

116. McClellan, S. J. & Franses, E. I. Effect of concentration and denaturation on adsoption and surface tension of bovine serum albumin. *Colloids and Surfaces B: Biointerfaces* **28**, 63-75 (2003).

117. Grdadolnik, J. Conformation of bovine serum albumin as a function of hydration monitored by infrared spectroscopy. *Internet Journal of Vibrational Spectroscopy* **6**, 6 (2002).

118. King, G. & Holmes, R. Human ocular aldehyde dehydrogenase isozymes: distribution and properties as major soluble proteins in cornea and lens. *Journal of Experimental Zoology* **282**, 12-7 (1998).

119. Carter, D. C., He, X. M., Munson, S. H., Twigg, P. D., Gernert, K. M., Broom, M. B. & Miller, T. Y. Three-dimensional structure of human serum albumin. *Science* **244**, 1195-8 (1989).

120. Kurrat, R., Prenosil, J. E. & Ramsden, J. J. Kinetics of human and bovine serum albumin adsorption at silica-titania surfaces. *Journal of Colloid and Interface Science* **185**, 1-8 (1997).

121. Curry, S., Mandelkow, H., Brick, P. & Franks, N. Crystal structure of human serum albumin complexed with fatty acid reveals an asymmetric distribution of binding sites. *Nature Structural Biology* **5**, 827-35 (1998).

122. Dockal, M., Carter, D. C. & Ruker, F. The three recombinant domains of human serum albumin. Structural characterization and ligand binding properties. *Journal of Biological Chemistry* **274**, 29303-10 (1999).

123. Avni, I., Arffa, R. C., Robin, J. B. & Rao, N. A. Lectins for the identification of ocular bacterial pathogens. *Metabolic, Pediatric and Systemic Ophthalmology* **10**, 45-7 (1987).

124. Lis, H. & Sharon, N. Lectins: carbohydrate-specific proteins that mediate cellular recognition. *Chemical Reviews* **98**, 637-674 (1998).

125. Gad, M., Itoh, A. & Ikai, A. Mapping cell wall polysaccharides of living microbial cells using atomic force microscopy. *Cell Biology International Reports* **21**, 697-706 (1997).

126. Lin, C. C., Yeh, Y. C., Yang, C. Y., Chen, G. F., Chen, Y. C., Wu, Y. C. & Chen, C. C. Quantitative analysis of multivalent interactions of carbohydrate-encapsulated gold nanoparticles with concanavalin A. *Chemical Communications (Camb)*, 2920-1 (2003).

127. Blaylock, W. K., Yue, B. Y. & Robin, J. B. The use of concanavalin A to competitively inhibit *Pseudomonas aeruginosa* adherence to rabbit corneal epithelium. *Clao Journal* **16**, 223-7 (1990).

128. Derewenda, Z., Yariv, J., HelliweII, J. R., Kalb, A. J. G., Dodson, E. J., Papiz, M. Z., Wan, T. & Campbell, J. The structure of the saccharide-binding site of concanavalin A. *The EMBO Journal* **8**, 2189-2193 (1989).

129. Becker, J. W., Reeke, G. N., Jr., Cunningham, B. A. & Edelman, G. M. New evidence on the location of the saccharide-binding site of concanavalin A. *Nature* **259**, 406-9 (1976).

130. Entlicher, G., Kostir, J. V. & Kocourek, J. Studies on phytohemagglutinins. 8. Isoelectric point and multiplicity of purified concanavalin A. *Biochimica et Biophysica Acta* **236**, 795-7 (1971).

131. Chen, A. & Moy, V. T. Cross-linking of cell surface receptors enhances cooperativity of molecular adhesion. *Biophysical Journal* **78**, 2814-20 (2000).

132. Lebed, K., Pyka-Fosciak, G., Raczkowska, J., Lekka, M. & Styczen, J. Binding activity of patterned concanavalin A studied by atomic force microscopy. *Journal of Physics: Condensed Matter* **17**, 1447-1458 (2005).

133. Touhami, A., Hoffmann, B., Vasella, A., Denis, F. A. & Dufrêne, Y. F. Aggregation of yeast cells: direct measurement of discrete lectin-carbohydrate interactions. *Microbiology* **149**, 2873-8 (2003).

134. Bouckaert, J., Poortmans, F., Wyns, L. & Loris, R. Sequential structural changes upon zinc and calcium binding to metal-free concanavalin A. *Journal of Biological Chemistry* **271**, 16144-50 (1996).

135. Wu, X., Gupta, S. K. & Hazlett, L. D. Characterization of *P. aeruginosa* pili binding human corneal epithelial proteins. *Current Eye Research* **14**, 969-77 (1995).

136. Klotz, S. A., Misra, R. P. & Butrus, S. I. Contact lens wear enhances adherence of *Pseudomonas aeruginosa* and binding of lectins to the cornea. *Cornea* **9**, 266-70 (1990).

137. Binnig, G., Quate, C. F. & Gerber, C. Atomic force microscope. *Physical Review Letters* **56**, 930-933 (1986).

138. Braga, P. C. & Ricci, D. *Atomic Force Microscopy: biomedical methods and applications.*ed. Walker, J. M. Humana Press Inc., Totowa, NJ, 2004.

139. Morris, V. J., Kirby, A. R. & Gunning, A. P. *Atomic Force Microscopy for Biologists.* London: Imperial College Press, River Edge, NJ, 1999.

140. Dufrêne, Y. F. Application of atomic force microscopy to microbial surfaces: from reconstituted cell surface layers to living cells. *Micron* **32**, 153-65 (2001).

141. Dufrêne, Y. F., Boonaert, C. J. P., van der Mei, H. C., Busscher, H. J. & Rouxhet, P. G. Probing molecular interactions and mechanical properties of microbial cell surfaces by atomic force microscopy. *Ultramicroscopy* **86**, 113-20 (2001).

142. Nakamura, C., Takeda, S., Kageshima, M., Ito, M., Sugimoto, N., Sekizawa, K. & Miyake, J. Mechanical force analysis of peptide interactions using atomic force microscopy. *Biopolymers* **76**, 48-54 (2004).

143. Touhami, A., Jericho, M. H., Boyd, J. M. & Beveridge, T. J. Nanoscale characterization and determination of adhesion forces of *Pseudomonas aeruginosa* pili by using atomic force microscopy. *Journal of Bacteriology* **188**, 370-7 (2006).

144. Bolshakova, A. V., Kiselyova, O. I., Filonov, A. S., Frolova, O. Y., Lyubchenko, Y. L. & Yaminsky, I. V. Comparative studies of bacteria with an atomic force microscopy operating in different modes. *Ultramicroscopy* **86**, 121-8 (2001).

145. Schaer-Zammaretti, P. & Ubbink, J. Imaging of lactic acid bacteria with AFM--elasticity and adhesion maps and their relationship to biological and structural data. *Ultramicroscopy* **97**, 199-208 (2003).

146. Fang, H. H., Chan, K. Y. & Xu, L. C. Quantification of bacterial adhesion forces using atomic force microscopy (AFM). *Journal of Microbiological Methods* **40**, 89-97 (2000).

147. Afrin, R., Yamada, T. & Ikai, A. Analysis of force curves obtained on the live cell membrane using chemically modified AFM probes. *Ultramicroscopy* **100**, 187-95 (2004).

148. Razatos, A., Ong, Y. L., Sharma, M. M. & Georgiou, G. Molecular determinants of bacterial adhesion monitored by atomic force microscopy. *Proceedings of the National Academy of Sciences (USA)* **95**, 11059-64 (1998).

149. Gerhardt, P., Murray, R. G. E., Wood, W. A. & Krieg, N. R. *Methods for General and Molecular Bacteriology*. Washington, D.C.: American Society for Microbiology, 1994.

150. Lang, W. & Zander, R. Physiological HEPES buffer proposed as a calibrator for pH measurement in human blood. *Clinical Chemistry and Laboratory Medicine* **37**, 563-71 (1999).

151. Elimelech, M., Gregory, J., Jia, X. & Williams, R. A. *Particle Deposition and Aggregation: Measuring, Modelling and Simulation*.ed. Williams, R. A. Butterworth-Heinemann, Wouburn, 1998.

152. Emerson IV, R. J. *Microbial Adhesion to Medical Implant Materials: an Atomic Force Microscopy Study*. Master's thesis, Chemical Engineering, Worcester Polytechnic Institute, (2004).

153. Burnham, N. A., Chen, X., Hodges, C. S., Matei, G. A., Thoreson, E. J., Roberts, C. J., Davies, M. C. & Tendler, S. J. B. Comparison of calibration methods for atomic-force microscopy cantilevers. *Nanotechnology* **14**, 1-6 (2003).

154. Ducker, W. A. & Senden, T. J. Measurement of forces in liquids using a force microscope. *Langmuir* **8**, 1831-1836 (1992).

155. Emerson IV, R. J. & Camesano, T. A. On the importance of precise calibration techniques for an atomic force microscope. *Ultramicroscopy* **106**, 413-22 (2006).

156. Xu, L. C., Vadillo-Rodriguez, V. & Logan, B. E. Residence time, loading force, pH, and ionic strength affect adhesion forces between colloids and biopolymer-coated surfaces. *Langmuir* **21**, 7491-500 (2005).

157. Hanna, A., Berg, M., Stout, V. & Razatos, A. Role of capsular colanic acid in adhesion of uropathogenic *Escherichia coli*. *Applied Environmental Microbiology* **69**, 4474-81 (2003).

158. Abu-Lail, L. I. *An Atomic Force Microscopy Study of Bacterial Adhesion to Natural Organic Matter-Coated Surfaces in the Environment.* Master's thesis, Civil & Environmental Engineering, Worcester Polytechnic Institute, (2006).